Negative Thermal Expansion of Organic Compounds

Guillaume Hermanus Greyling

**Thesis presented in partial fulfilment of the requirements for the degree
of Master of Science in Chemistry at the University of Stellenbosch**

Supervisor: Prof. L. J. Barbour

Declaration

I, the undersigned, hereby declare that the work contained in this thesis is my own original work and that I have not previously in its entirety or in part, submitted it at any university for a degree.

_____

Signature

Guillaume Hermanus Greyling

Name in full

_____/_____/2011

Date

Abstract

The primary objective of the work was to investigate the negative thermal expansion of organic materials and to determine the mechanisms governing this phenomenon by using the principles of crystal engineering. To this end, the following three compounds were studied in detail:

- 4,4'-Diiodobiphenyl
- 4-Iodobenzoic acid
- Methyl Paraben

The rationale behind this work was to determine the mechanisms responsible for the observed negative thermal expansion and to uncover the structural factors that induce negative thermal expansion. Single-crystal X-ray diffraction was employed as the primary analytical tool, owing to the unique information it can provide regarding intermolecular interactions in the solid state.

A total of twenty organic compounds were analysed, of which three exhibited negative thermal expansion. Each compound employs a specific mechanism for negative thermal expansion, two of which are closely related and the third distinct.

Opsomming

Die hoof doel van hierdie studie was om ondersoek in te stel in die verskynsel van 'negative thermal expansion' in organiese materiale en gevolglik die meganisme vas te stel deur die beginsels van kristalmanipulsie ('crystal engineering') te gebruik. Gevolglik was drie organise stowwe ondersoek:

- 4,4'-Diiodobiphenyl /4,4'-Diiodobifeniel
- 4-Iodobenzoic acid /4-Iodobensoësuur
- Methyl Paraben

Die redenasie hieragter is om die meganisme verantwoordelik vir die 'negative thermal expansion' vas te stel en die verskillende faktore wat bydra tot dit te bevestig. Enkel-kristal diffraksie word benut as die primêre analitiese tegniek as gevolg van die unieke inligting wat verkry kan word met betrekking tot die intermolekulêre interaksies.

'n Totaal van twintig stowwe is geanaliseer waarvan drie die spesifieke termisie eienskap besit. Elk van die drie stowwe het 'n ander meganisme te vore laat kom waarvan twee baie ooreenstem en die derde verskil.

Acknowledgements

Firstly, I would like to thank my supervisor Prof. Len Barbour for giving me the opportunity and freedom to explore the field of supramolecular chemistry. I am very grateful for the opportunities that I have been given to broaden my scientific knowledge. I appreciate your advice, infinite supply of patience and enthusiasm, insight and guidance.

I would like to thank Dr. Vincent Smith for his help. I am grateful for all the effort you put into assisting the 'new kids on the block'. Thank you for helping me with this thesis. I appreciate your ideas, enthusiasm and willingness to help.

I would like to thank the entire supramolecular group, thank you so much for creating such a wonderful working environment with fun conversations and jokes.
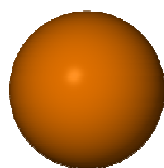
I would like to thank my parents for all of the love and encouragement.

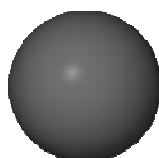I would like to thank the National Research Foundation for financial support

Abbreviations

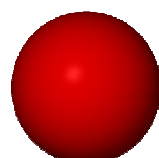|	
α	Linear thermal expansion coefficient
ASU	Asymmetric Unit
CSD	Cambridge Structural Database
δ	In-plane tilt angle
ε	Out-of-plane tilt angle
e.s.d	Estimated standard deviation
L	Length of an axis
L_0	The length of the material or axis at some initial temperature
σ	Herringbone angle
SCD	Single-Crystal X-ray Diffraction
τ	Torsion angle
T	Temperature
T_0	Initial temperature

Atomic colour key

Bromine

Carbon
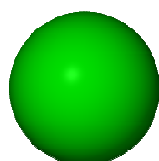
Chlorine
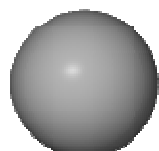
Hydrogen
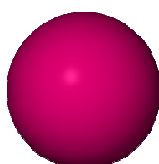
Iodine

Oxygen

Table of Contents

Chapter 1: Introduction

Chapter 2: Intrumentation and Analytical Techniques

Chapter 3: Results

List of Figures

List of Tables

Chapter 1
Introduction

This chapter presents and explains the key concepts of supramolecular chemistry and crystal engineering which are relevant to this study.

1.1 Supramolecular Chemistry

The term "supramolecular chemistry" (Latin: *supra* = "above, beyond") was introduced in 1978 by J.-M. Lehn and was defined as "the chemistry of molecular ensembles and intermolecular associates".[1, 2] The idea of individual molecules aggregating to form a distinct supramolecular assembly with novel and unique physico-chemical properties dates back to the early 19th century with the discovery of the chlorine hydrate by Davy and the subsequent correct assignment of its chemical formulae by Faraday.[3] Traditionally, phrases such as "chemistry beyond the molecule" and "the chemistry of non-covalent bonds" were used to describe this research. In the beginning supramolecules were considered to mainly consist of two components, a host molecule and a guest molecule, which interact with each other in a non-covalent fashion.

Supramolecular chemistry rapidly expanded to include molecular devices and molecular assemblies. More recently, Lehn added a further functional definition: "Supramolecular chemistry aims at developing highly complex chemical systems from components interacting by non-covalent intermolecular forces".[3] Therefore, the focus of supramolecular chemistry has shifted towards increasing complexity and sophisticated functionality in order to obtain the information stored in molecular components, which allows complexity to be achieved. Essentially, supramolecular chemistry concerns the mutual interaction of molecules or molecular entities with discrete properties.[3]

Supramolecular chemistry is a relatively young branch of chemistry which has undergone its primary development in the last quarter of the 20th century.[3] The main reasons for this late growth is that a thorough understanding of synthetic methods is needed to enable the design of large supramolecular systems while powerful analytical techniques are required for the determination of supramolecular structures. This enables the study of the physico-chemical and dynamic properties of supramolecular assemblies.[4]

Techniques that are successfully employed for the analysis of supramolecular entities include UV-visible-, fluorescence- and infra-red spectrophotometry, nuclear magnetic resonance spectroscopy, thermal analysis, powder X-ray diffraction and single crystal X-ray diffraction.

According to Dunitz, crystals can be described as "one of the finest examples of a supermolecule" and a "supermolecule par excellence".[5] Studying crystals by means of X-ray diffraction has led to the greatest improvement in the understanding of the forces that direct supramolecular assembly. Dunitz further noted that only through the successful control of intermolecular interactions could one design property-specific supramolecular entities.[5] There are various diverse areas where property-specific materials could be very useful; these include studies of biomolecular substrate binding and recognition, reactivity and catalysis, development of improved detergents, the petrochemical industry, and the synthesis of novel nonlinear optical and ferroelectric materials and many others.[6]

The intermolecular interactions that hold supramolecular entities together are weak interactions which were poorly understood until recently.[7] The weak intermolecular interactions that are found to hold supramolecules together are referred to as non-covalent bonding interactions. The term "non-covalent" includes a vast range of attractive and repulsive forces. The most important of these, along with their approximate energies, are listed in Table 1.[3]

Table 1. Energies of non-covalent interactions.

Interaction	Strength (kJ mol^{-1})
Ion-dipole	50 - 200
Dipole-Dipole	5 - 50
Hydrogen bond	4 - 120
Cation-π	5 - 80
π-π	0 - 50
van der Waals	< 5

In supramolecular chemistry it has been found that size, shape and the geometric arrangement of molecules, rather than their reactivity, play a dominant role in the formation of supramolecular entities. In the same way, synthetic chemistry uses chemical bonds to create an endless variety of molecules from a limited number of elements. Supramolecular chemistry uses non-covalent interactions to create various "supermolecules" and "supramolecular ensembles" from these molecules. [2, 8, 9]

Today supramolecular chemistry is a major, interdisciplinary branch of science dealing with the chemical, physical, biological, the technological aspects of synthesis and the study of complex chemical systems based on non-covalent interactions.[3]

1.2 Crystal Engineering

Crystal engineering can be viewed as the area of supramolecular chemistry devoted to the controlled design of crystalline materials, and the phrase "crystal engineering" was first used by Schmidt in 1971.[10, 11] More recently (2007) the phrase was defined by Desiraju as "the understanding of intermolecular interactions in the context of crystal packing and in the utilisation of such understanding in the design of new solids with the desired physico-chemical properties".[12] Crystal engineering is currently expanding at a brisk pace and creative schemes for supramolecular synthesis, correlations between molecular structures, crystal packing and novel physical properties are presented in the literature regularly.

Crystal engineering has significant overlap with supramolecular chemistry, X-ray crystallography, materials science, and solid-state chemistry and yet it is a distinct discipline in itself. The main focus of "crystal engineering" is the design of periodic structures with a desired supramolecular organization which makes it possible to achieve or modify a desired property in the newly synthesised material.[2] The design is based on the possibility of predicting structural features and properties of a material

based on the knowledge of the nature of the individual molecules or "building blocks" which form the solid phase.

The fundamental question concerning crystal engineering is "what building blocks should be chosen to make a crystal display the required properties (or structure)?" To date there is no universal answer.[2]

Any successful strategy for supramolecular synthesis requires a method to connect various molecules into predictable arrangements and therefore it is important to identify the intermolecular interactions that are selective enough to be reliable and strong enough to be transferable between different systems.[11] In this context, it is necessary to know how specific functional groups interact with one another when several possibilities exist.

The crystal structure is a result of a fine balance between a range of intermolecular forces and even a small change in molecular structure could lead to great and unpredictable changes in the molecular arrangement.[11] Given that intermolecular interactions direct molecular recognition, it is understood that every crystal structure is the eventual the result of a recognition process which leads to a thermodynamically favourable assembly of molecules. Therefore, each crystal structure contains important information about the way in which intermolecular interactions function to eventually afford an energetically balanced system.[11]

Crystal structures are a good source of information for understanding intermolecular interactions. An improved understanding of the intermolecular interactions becomes essential when designing or engineering "smart materials".

1.2.1 Intermolecular Interactions

Molecular solids are the most popular targets for crystal engineering.[11] Molecular solids are held together by a variety of intermolecular forces. These forces are classified as either medium-range or long-range interactions. Medium-range interactions are isotropic in nature, define molecular shape, supports overall crystal stability and provides a driving force towards close

packing. Medium-range interactions include π-π interactions while long-range interactions are electrostatic in nature, exert very specific controls and constraints on the crystal structure and are highly directional. Long-range interactions include halogen-halogen interactions as well as hydrogen bonds.[13]

1.2.2 The Hydrogen Bond

Within supramolecular chemistry, molecular recognition, and crystal engineering, it has been recognized that hydrogen bonding is an indispensable tool for designing molecular aggregates.[14] In particular, hydrogen bonds are responsible for the overall shape of many proteins, the recognition of substrates by numerous enzymes and even for the double helix structure of DNA. The hydrogen bond also plays a role in phenomena such as optical properties, thermal stability, solubility, colour, conductivity, crystal habit and mechanical strength.[6]

From a geometric point of view a hydrogen bond can be described in terms of r, d, D, θ and Φ where r is the distance between the donor atom (X) and the hydrogen atom, d (known as the hydrogen bond) is the distance between the hydrogen atom (H) and the acceptor atom (A), D is the distance between the donor atom and the acceptor atom, X-H···A is the hydrogen bond angle and is indicated by θ, and the H···A-Y angle is indicated by Φ. The torsion angle X-H···A-Y indicates the planarity of the system.[15]
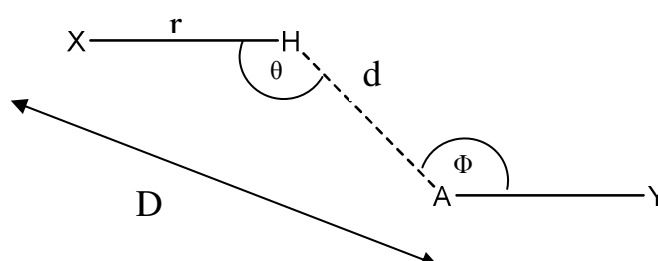
Figure 1. Geometric definition of a hydrogen bond X-H···A-Y (with X as the donor atom, H as the hydrogen atom, A as the acceptor and Y as the atom directly bonded to the acceptor atom A).

The hydrogen bond, primarily electrostatic in nature, has arguably been quoted most often as the architect in design strategies in crystal engineering.

Correlations between bond lengths and angles and geometric variations as a function of donor and acceptor strengths have been presented for a series of functional groups.[6] It was found that a single, strong hydrogen bond may be sufficient to determine solid-state structure and exert a marked influence on the solution and gas phases. Weaker hydrogen bonds play a role in structure stabilization and can be significant when large numbers of them act together.[3]

The energy of a hydrogen bond is extremely variable. In the case of neutral molecules, the energy of the hydrogen bond can vary from 10 - 65 kJ mol^{-1}. This implies that the hydrogen bond is stronger than the van der Waals interactions, but still weaker than conventional covalent bonds. However, when one constituent of the hydrogen bond is ionic, the range of the bond strengths rises to 40 - 190 kJ mol^{-1}. It has been shown that a strong hydrogen bond is energetically similar to a weak covalent bond.[6]

1.2.3 Halogen-Halogen Interactions

The term "halogen bonding" was coined by Dumas *et al.* in order to describe the attractive donor-acceptor interactions that involve halogen atoms functioning as Lewis acids.[16] The halogen-halogen interaction was first reported in 1863 by Guthrie. However, halogen bonding has only recently become an object of study as a well-defined, strong, specific and directional interaction for the assembly of complex supramolecular architectures.[17] Studies by Hassel *et al.* suggested that there is an analogy between the halogen-halogen interactions and hydrogen bonding.[18] His theoretical and experimental data showed that the two interactions have comparable strengths and that both are also highly directional. Similar to the bonding geometry in hydrogen bonding, halogens are directly linked to donor atoms with a bonding direction that roughly coincides with the axes of the lone pair orbitals in the non-complexed donor molecule. The halogen bonding interaction energy falls within the range of 10 - 200 kJ mol^{-1}.[19]

Furthermore, Desiraju argued that the halogen-halogen interaction is an attractive force that can be used for manipulating and organising the

supramolecular structure within a crystal.[13] Halogen bonding has further proven to be an effective and reliable tool for crystal engineering. Single-crystal X-ray structures of complexes of drugs containing halogen atoms and their specific proteinaceous receptors revealed that halogen bonding optimizes the receptorial fitting. New protocols, based on halogen bonding were developed to overcome the low affinity between perfluorocarbons and hydrocarbons to design new molecular conductors and to resolve racemic mixtures.[19]

These results have opened new opportunities in the design and manipulation of the molecular organization processes. The use of halogen containing "building blocks" extends to diverse fields such as organic chemistry, biopharmacology and material science.[19] Halogen atoms that are involved in halogen-bonding or halogen bond formation can be bound to nitrogen, carbon or other halogen atoms (Figure 2).
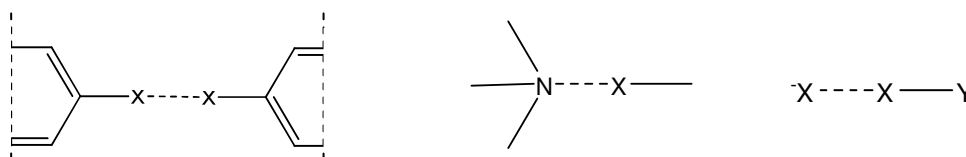
Figure 2. Typical halogen interactions with X = I, Br, Cl, F and Y = C, N.

In general, the tendency of different halogens to be involved in strong halogen bonding is opposite in sequence to their electronegativity, I > Br > Cl > F, and the more electron withdrawing the carbon framework of the halocarbon is, the stronger the halogen bonding. An order of acceptor strength was determined as $X - X > X - C(sp) > X - C(sp^2) > X - C(sp^3)$, with X being iodine, bromine, chlorine or fluorine.[19]

1.2.4 π-π Interactions

π-Stacking is one of the most important cohesive forces in the crystallization of small molecules, drug-receptor recognition, molecular recognition processes, host-guest binding in supramolecular assemblies, crystal engineering, the helical structure of DNA and protein folding.[20]

The π-electron density of an aromatic hydrocarbon is polarisable and this polarisability improves the stabilization of the dispersion interactions between various aromatic molecules. The stabilization of the dispersion interactions is further improved when more polarizable atoms or groups are involved in the π-delocalization.[21] Therefore, the introduction of electron-withdrawing or donating groups and heterocyclic aromatic rings favours the stacking of π-frameworks. The stability sequence of the various stacking interactions between π-systems is as follows: π-deficient – π-deficient > π-deficient – π-rich > π-rich – π-rich.[20]

In conjunction with the polarization of an aromatic hydrocarbon, there is also an electrostatic component of inter-molecular stabilization that provides directionality. In an aromatic hydrocarbon, small polarization of the C-H bonds occurs which generates a partial negative charge over the π-bonded core relative to the partially positive rim of hydrogen atoms on the edge of the molecule. This may or may not introduce a molecular dipole, but it certainly will introduce multipoles.[21]

The maximization of the electrostatic stabilization energy between occurring multipoles is the source of directionality in aromatic interactions and it leads to the two commonly observed geometric relationships between adjacent aromatic molecules.
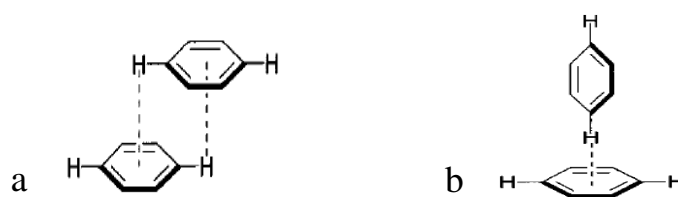
Figure 3. a) The OFF π-stacking and b) The EF π-stacking.

They are known as the offset-face-to-face (OFF) motif and the edge-to-face (EF) motif (Figure 3).[21] In the OFF geometry, the molecules are not exactly eclipsed but are naturally offset so that the oppositely charged regions of the molecules are closest to each other (Figure 3a). In the EF motif (also known as vertex-to-face or T-shaped) the relatively positive hydrogenic rim is

directed towards the central negative π-electron density (Figure 3b). The relative stabilization energy for benzene rings in either the OFF or EF arrangements is 9 kJ mol^{-1} and this is equal to approximately 40% of the energy of a hydrogen bond formed between two water molecules.[21]

Molecular shape is another factor that determines aromatic interactions.[21] The aromatic moiety of a molecule is generally flat and disc shaped and, while stacking of discs is clearly efficient, it generates substantial intermolecular space around the edge of the discs. It is known that the area of the disc relative to its thickness influences the modes of association of the aromatic compounds. For relatively small areas the EF motif can be more effectively arranged than the OFF motif and, as a consequence, the herringbone pattern of the EF motif is more commonly observed. As the area of the aromatic compound increases, the OFF motif becomes more apparent.[21]
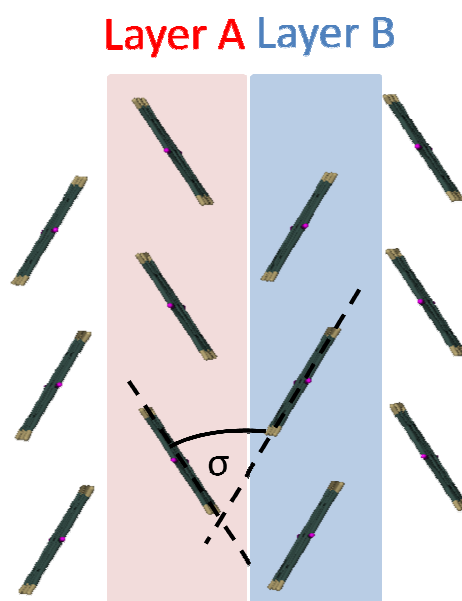
Figure 4. The herringbone angle.

When the mean plane drawn through a molecule in layer A intersects with the mean plane drawn through a molecule in layer B, the resulting angle, σ, is known as the herringbone angle (Figure 4). Two of the most commonly observed herringbone patterns are the gamma packing arrangement and the sandwich herringbone motif (Figure 5). Both of these herringbone patterns are due to the EF arrangement of the aromatic molecules.

1.2.5 Close Packing

Examination of solid state structures reveals a tendency of molecules to minimize void space by adopting close packed arrangements, which are energetically more favourable. There is an energy cost attached to the formation and preservation of empty space between molecules. As molecules progress towards dimers, trimers, higher oligomers and ultimately crystals they gain substantial stabilization energy.[3] Close packing is an essential driving force for the formation of crystals.

1.3 Soft and Smart Materials

The term "materials" generally represents durable solids composed of organic compounds such as polymers or inorganic compounds such as semiconductors and other coatings. The term "material" can be constructively applied to any chemical compound with interesting or useful physical properties.[3]

We can readily distinguish between hard and soft materials. Soft materials, often organic compounds, are held together by supramolecular interactions such as hydrogen bonds, van der Waals forces or other weak intermolecular bonds. A great deal of supramolecular chemistry, especially with respect to crystal engineering, involves the design and synthesis of soft materials.

Smart materials are materials that react in a desired way based on external stimuli. The material is therefore able to 'sense' an external event such as a

change in temperature and respond accordingly with a change in dimensions, for instance.[3] The ability of supramolecular chemists to use intermolecular interactions to design and construct soft materials may pave the way to the tailored design of smart materials.

1.4 Thermal Expansion

Thermal expansion is a very well known phenomenon: when objects are heated, they expand or contract. Thermally tailored materials play a prominent role in various applications such as electronic and biomedical applications and even in cookware. A few examples include the matching of the thermal expansion of printed circuit boards and heat sinks to that of silicon. Another example is the matching of the thermal expansion of dental fillings to that of teeth.[22]

On the simplest level, positive thermal expansion (PTE) can be explained by the asymmetric shape of an interatomic potential well. For a simple diatomic molecule, the gradual population of higher energy vibrational levels will lead to an increase in bond distance with increasing temperature (Figure 6).[23, 24]
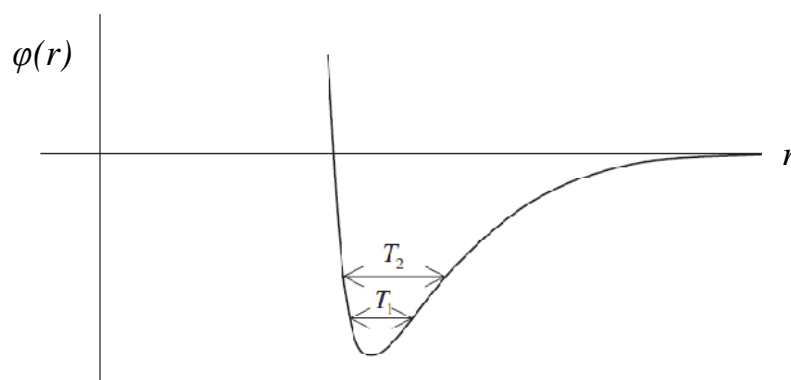
Figure 6. A typical anharmonic pair potential φ, as a function of interatomic distance r, showing the mean amplitudes of vibration at two different temperatures ($T_2 > T_1$), indicating positive thermal expansion.

A hard, steep potential results in relatively small PTE while a softer, shallow potential leads to substantial PTE. Examples of compounds which have shallow potentials are found in organic molecular materials where the molecules are held together by weak van der Waals forces. The potential of

covalent bonds are steeper than those of the weaker van der Waals forces and therefore PTE is caused by changes in the intermolecular distances rather than the small temperature dependence of the covalent bonds.[25]

A crystalline material can be broken down into its smallest repeating unit known as the unit cell (Figure 7a). Thermal expansion can be defined in relation to the unit cell: [26]

- Linear or uniaxial expansion
- Superficial or biaxial expansion
- Cubical or triaxial expansion

Linear thermal expansion occurs when the length of a single axis increases with an increase in temperature (Figure 7b). Biaxial thermal expansion entails the expansion of two of the three axes (Figure 7c). Cubical expansion (also referred to as volumetric expansion) occurs when the length of all three axes expand upon heating (Figure 7d).

a   b   c   d
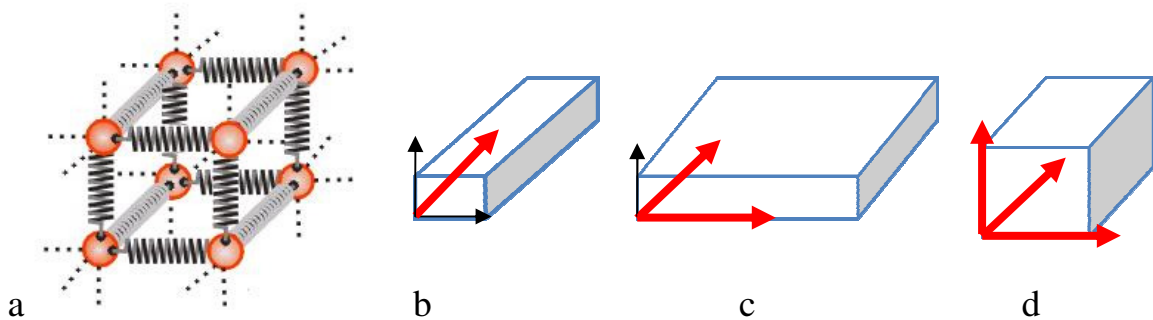
Figure 7. Thermal expansion in terms of axial expansion of a) a unit cell b) uniaxial expansion c) biaxial expansion and d) cubical thermal expansion along all three axes.

Increasing temperature usually causes an increase in volume for both solid and liquid materials. Linear thermal expansion, ΔL, is calculated using Equation 1 while the coefficient of linear thermal expansion, α, is calculated using Equation 2.

$$\Delta L = \alpha L_0 \Delta T \qquad (1)$$

Therefore,

$$\alpha = \frac{\Delta L}{L_0 \Delta T} \qquad (2)$$

ΔL represents the difference between the length of the material (or the length of an axis) after a change in temperature, ΔT is the difference between the final temperature and the initial temperature and L_0 is the length of the material or axis at some initial temperature T_0.[26] The coefficients of some well known materials that display PTE are reported in Table 2. It is worth noting that α is reported in K^{-1}. Generally, the dimensions of these materials vary by about 0.1% per 100 °C.[27]

Table 2. Coefficients of Linear Expansion.

Material	α (K^{-1})
Aluminum	24×10^{-6}
Brass	20×10^{-6}
Copper	17×10^{-6}
Glass	$4 - 9 \times 10^{-6}$
Steel	12×10^{-6}

Thermal expansion is commonly used as a synonym for PTE, but negative thermal expansion (NTE) can also occur, i.e. when a compound undergoes an increase in size when the temperature is decreased. The best known example of negative thermal expansion is ice. Both the normal hexagonal and cubic forms of ice have a density lower than that of water which leads to the observation of ice floating on water. It was found that solid hexagonal ice shows NTE, albeit only at very low temperatures.[22] To date there are very few examples of organic crystals that exhibit NTE and almost all of these exhibit linear NTE.[25, 28]

Unlike PTE, NTE cannot be explained by the anharmonic two-centre potential. Generally, NTE results from special geometrical arrangements of atoms/molecules which outweigh the thermal movement of those atoms/molecules. In other words, NTE occurs for geometrical reasons.[25] It follows that for a material to display NTE there must be structural factors that outweigh the tendency of bonds to expand with increasing temperature.

Several inorganic materials show either volumetric or uniaxial NTE. ZrW_2O_8 is the best-known example of a compound which has a large linear NTE over a wide temperature range. In β-ZrW_2O_8 (the low temperature phase) and α-ZrW_2O_8 (the high temperature phase) the linear expansion coefficients are -8.7×10^{-6} K^{-1} and -4.9×10^{-6} K^{-1}, respectively. It has been established that the rotation of the rigid WO_4 building blocks causes an overall contraction in the ZrW_2O_8 material with increasing temperature.[29, 30]

Examples of organic materials that display negative thermal expansion include polyethylene[31], pentacene[25], (S,S)-octa-3,5-diyn-2,7-diol[32] and the dipeptide TrpGly·H_2O[28]. Each of these four compounds exhibits different mechanisms for the observed NTE and have linear negative thermal expansion coefficients of -5.6×10^{-6} K^{-1}, -35.6×10^{-6} K^{-1}, -203.6×10^{-6} K^{-1} and -1.1×10^{-6} K^{-1} respectively.

Polyethylene contracts along the covalent chains as a consequence of increased vibrations perpendicular to the chains.[25] In the case of pentacene, the herringbone angle increases with temperature and this causes an anisotropic rearrangement of the molecules within the layers. The underlying mechanism for the observed NTE in (S,S)-octa-3,5-diyn-2,7-diol is reminiscent of a three-dimensional folding trellis. The resulting NTE is due to a change in the relative "tilting" angle between the stacked columns along the crystallographic a-axis and the diyne spines (Figure 8). This results in exceptionally large and reversible uniaxial PTE and biaxial NTE of the crystal.
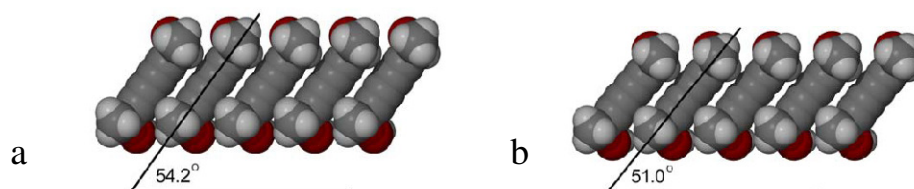
Figure 8. Changes in the relative "tilting" angle of (S,S)-octa-3,5-diyn-2,7-diol at a) 225 K and b) 330 K.[32]

The dipeptide crystal TrpGly·H_2O exhibits an ordering of the water molecules within the supramolecular peptide helices with decreasing temperatures.[25, 28]

It becomes apparent from the abovementioned examples that predicting the NTE of materials, especially those of the organic materials, suffers from the fundamental question: "what are ideal building blocks for developing this desired property?" Geometrically fascinating compounds are a good starting point for discovering and studying organic NTE compounds but serendipity or "trial and error" still remains the leading method for uncovering such phenomenon. It should be noted that when compounds undergo a change in their dimensions with a change in temperature, the topic of polymorphism may arise.

1.5 Polymorphism

Polymorphism is a unique feature of the solid-state and it is a well studied but not well understood phenomena in terms of its predictability. The first use of this term is generally credited to Mitscherlich, who recognized different crystal structures of the same compound in a number of arsenate and phosphate salts.[33] As with many terms in chemistry, a comprehensive definition of polymorphism is difficult to define.

This problem was examined by McCrone in 1965, whose working definition is as relevant today as when it was first proposed. McCrone defined a polymorph as "a solid crystalline phase of a given compound resulting from the possibility of at least two different arrangements of the molecule in the solid state".[33] Considering McCrone's definition there still remains much ambiguity, especially with regard to hydrates and solvates. In order to further clarify this definition we can add Bernstein's definition of polymorphism: "classification of a system as polymorphic would be if the crystal structures are different but lead to identical liquid and vapour states".[33]

In spite of the discussions surrounding the inclusion or exclusion of certain terms, there is general agreement about the meaning, consequences, and relevance of polymorphism.

1.6 Project Outline and Objectives

This study is an investigation into the phenomenon of NTE of organic materials. Most known compounds exhibit PTE. A few compounds, the majority of which are inorganic, exhibit NTE. However a literature survey has revealed that, to date, only seven organic compounds have been reported to show NTE behaviour.

In *section 1.4*, (S,S)-octa-3,5-diyn-2,7-diol was highlighted as a compound that exhibits NTE behaviour (Das *et al*).[32] Although this was a serendipitous discovery, we have become interested in identifying more organic compounds that exhibit similar behaviour.

The objectives of this study are:

- Deploying an in-house program (namely CSD_Thermal) to identify compounds in the Cambridge Structural Database that potentially exhibit NTE behaviour.
- Investigating compounds similar to 4,4'-diiodobiphenyl, 4-iodobenzoic acid and methyl paraben.
- Identifying the key structural features that are central to the mechanism of the NTE.

A list of potential compounds was selected systematically and three main classifications of compounds were identified based on their structural motifs (Scheme 1).

The first category of compounds consists of the di-substituted biphenyl molecules where both substituents are the same. The second category is the di-substituted benzene type. The third category is a variation of the di-substituted benzene type where one substituent is kept constant (iodine or

bromine) while the other is varied. The parabens make up a sub-category of category three wherein the iodine atom/substituent is also exchanged.

Scheme 1. Systematic approach developed for determining compounds that exhibit NTE.
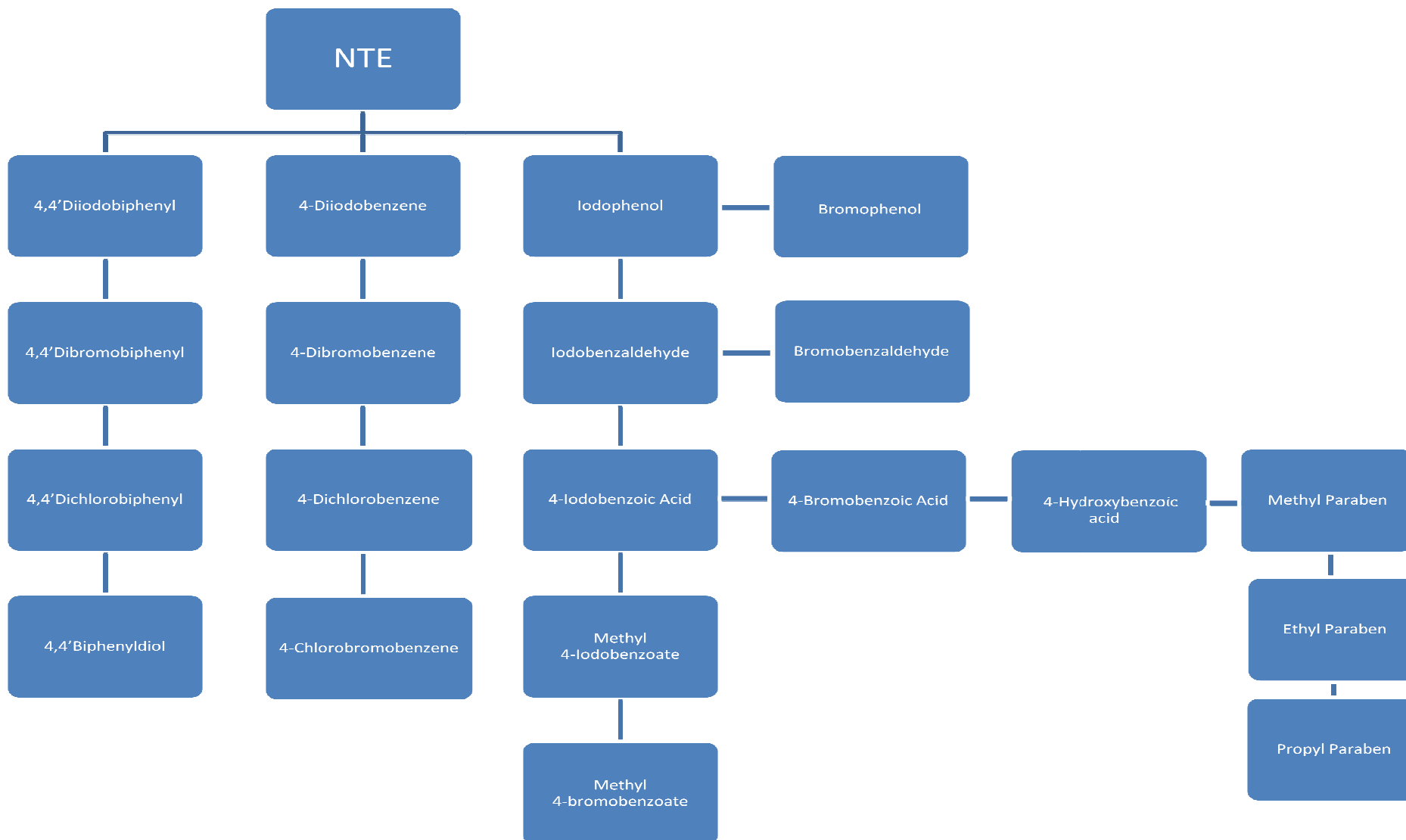
Chapter 2
Instrumentation and Analytical Techniques

A description of the analytical instruments and software packages that were used during the course of this study is given. Methods of sample preparation and crystal growth are discussed in the relevant chapters.

2.1 Single-Crystal X-ray Diffraction (SCD)

Single-crystal X-ray diffraction is a non-destructive analytical technique in which X-rays are employed to determine the atomic coordinates of molecules in the crystalline state. Analysis of diffraction data provides information on the bond lengths and angles, three-dimensional structure and the absolute configuration of molecules in the crystalline state.

Crystals for SCD experiments were selected based on their ability to extinguish plane-polarised light uniformly and on their size. In all cases, the crystals were glued onto a glass fibre using an epoxy resin and then placed onto the goniometer head of the single crystal X-ray diffractometer prior to data collection. Diffraction data were collected on a Bruker-Nonius SMART Apex diffractometer equipped with a Mo fine-focus sealed tube and a 0.5 mm MonoCap Collimator (monochromated Mo-Kα radiation, λ = 0.71073 Å). Data were captured with a CCD (Charge-Coupled Device) area-detector with the generator powered at 40 kV and 30 mA. Coupled to the diffractometer is an Oxford Cryosystems Cryostat (700 series Cryostream Plus) that produces a constant stream of nitrogen, which enables variable temperature data collection for all structures.

For the purposes of this study, a single-crystal of each compound was subjected to a full data collection both at 100 K and 298 K. A temperature ramp rate of 120 K h^{-1} was employed and the crystals were allowed to equilibrate to the given temperature before the data collection was started. APEX2 software was employed to implement the appropriate data collection strategy after a reliable unit cell had been determined. Standard ω-scans were used to obtain intensity data which were subsequently reduced and refined using SAINT software. A multi-scan absorption correction was performed with SADABS.[34] Structures were solved and refined using the SHELX-97 suite of programs and the X-seed graphical interface.[35-37] In general, non-hydrogen atoms were located by direct methods (SHELXS-97) and structures were expanded using difference electron density maps (SHELXL-97).

Structures were refined anisotropically against F^2 using full-matrix least squares calculations and hydrogen atoms of aromatic rings were placed using a riding model based on idealized coordinates and geometrical constraints.[38]

2.2 Computer Packages

2.2.1 The Cambridge Structural Database (CSD)

The Cambridge Structural Database is an integrated package that contains all the published single crystal data as well as powder structural data for organic molecules.[39] The CSD allows the user to search through the records as well as place restrictions and conditions on a search in order to filter and refine the data obtained from a database search.

2.2.2 CSD Thermal Search

CSD Thermal Search is a program developed to search the SCD for compounds that have been determined at least two temperatures. The user conducts a search of the CSD and exports the unit cell parameters and experimental conditions. The program reads the file, searches for entries of the same compound at different temperatures and compares the unit cell parameters. The program reports the CSD reference code, temperature at which the data collection took place, unit cell parameters and the thermal expansion coefficient which it calculates from the reported data.

2.2.4 Crystal Explorer

Crystal Explorer is a software package that employs calculated Hirshfeld surfaces of molecules within a crystal structure to determine the intermolecular interactions between selected molecules or for the entire crystal structure.[40,41] Hirshfeld surfaces are created by extending the weight function which relates an atom in a molecule to the molecule in a crystal.[42]

The isosurface generated from these functions surrounds the molecule and by partitioning the electron density of the molecular fragments it delineates the space occupied by a molecule in a crystal. Hirshfeld surfaces are different

from other molecular surfaces such as fused van der Waals (or CPK) and smoothed Connoly surfaces in the sense that Hirshfeld surfaces are determined by both the enclosed molecule and its closest neighbours. The only prerequisite for obtaining useful data on intermolecular interactions from Hirshfeld surfaces is that the crystal structures must be characterised to the extent that all the hydrogen atoms are located accurately.[42] The surfaces used in this study were calculated using the function d_{norm} which normalises the contact distance according to Equation 3:[43]

$$d_{norm} = \frac{d_i - r_i^{vdW}}{r_i^{vdW}} + \frac{d_e - r_e^{vdW}}{r_e^{vdW}} \qquad (3)$$

The distance d_i is the distance from the surface to the nearest atom interior to the surface while d_e is the distance from the surface to the nearest atom exterior to the surface. The sum of d_i and d_e would be the approximated contact distance (Figure 9).
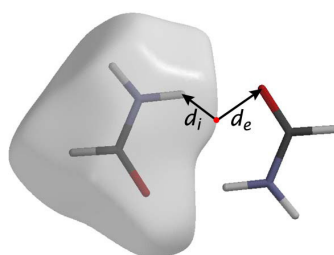
Figure 9. The d_i and d_e distances.

Hirshfeld surfaces are depicted with a sliding colour scheme which indicates their distances relative to the van der Waals radii. Contact distances shorter than the van de Waals radii are depicted as red, contact distances longer than the van de Waals radii are depicted as blue and contact distances that are approximately equal to the van de Waals radii are depicted as white (Figure 10a).
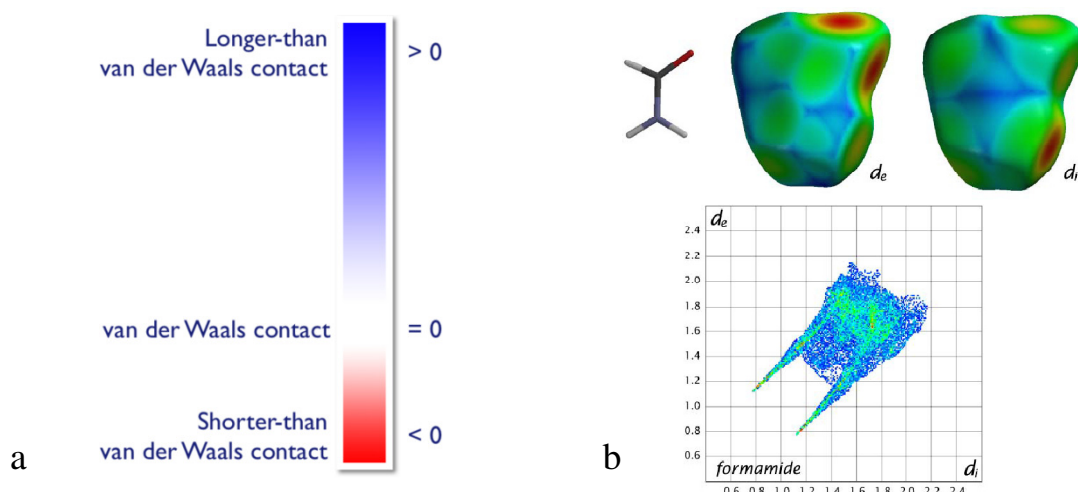
A better visual representation of the relationship between d_i and d_e can be seen when they are binned at intervals of 0.01 Å with the colouring of each of these bins as a function of the fraction of surface points in that bin. It is important to realise that each plot is highly sensitive to a molecule's immediate environment and introducing a sliding colour scale to indicate the concentration of points in a bin provides an easy and efficient way of comparing crystal structures.[42] These 2-D plots are also known as fingerprint plots and are unique to each crystal structure (Figure 10b). Specific interactions can be highlighted in the plot by selecting the relevant atom types, these are depicted in blue, while the remaining interactions are then depicted in grey.

2.2.5 POV-Ray

POV-Ray (Persistence of Vision Raytracer) was used to render structural images.[44] POV-Ray renders images using a technique called *ray-tracing*, which is a method used to produce high quality graphics.

2.2.6 SAINT+

SAINT+ was used to convert raw frame data to a set of integrated intensities with standard deviations, direction cosines, and XYZ centroids.[34] This is achieved by an integration method using 3-D profiling algorithms.

2.2.7 SADABS

SADABS (Siemens Area Detector Absorption Corrections) is an application within the APEX suite that is used to scale and correct data collected on a Bruker AXS area detector utilising .raw files generated by SAINT+.[34]

2.2.8 SHELX-97

SHELX-97 was used for crystal structure solution and refinement.[35] SHELX-97 is comprised of a set of six computer programs (SHELXS, SHELXL, CIFTAB, SHELXA, SHELXPRO and SHELXWAT) routinely used for the determination of crystal structures from single-crystal X-ray diffraction data. During this study SHELXS-97 was used for structure solution using direct methods and SHELXL-97 was used for structure refinement by employing full-matrix least squares calculations based on F^2.[36]

2.2.9 X-Seed

X-Seed[36, 37] was used as a graphical interface for the SHELX-97 software suite. X-Seed was also used as a graphical interface for POV-Ray.

2.3 Materials and the Characterisation of Negative Thermal Expansion

2.3.1 Estimated Standard Deviation

The compounds that are presented undergo slight structural changes (changes in orientation and intra- and intermolecular distances) with a change in temperature. It is therefore important for this study to discuss estimated standard deviations (e.s.d.s) for the purpose of distinguishing between uncertainty of the measurement and an actual structural change. The International Organization for Standards (ISO) has issued a document (ISO, 1993) with the purpose of establishing general rules for evaluating and expressing uncertainty in measurements.[45] The need for these general rules derives from the fact that measurements are now considered complete only when accompanied by a quantitative statement of uncertainty.[45]

Schwarzenbach *et al.* recommend expressing e.s.d.s with sufficient accuracy to minimize the effect of round-off errors in subsequent calculations and the International Union of Crystallography has adopted this recommendation. In order to minimize the round-off error, e.s.d.s should be quoted to two significant digits in the range 10 to 19 and to one significant digit in the range 2 to 9.[45] In general, e.s.d.s should be rounded up rather than to the nearest digit. For example, a bond length of 1.54249 Å with a e.s.d of 0.01532 should be reported as 1.542(16) Å. A bond of 2.16352 Å with a e.s.d of 0.00481should be reported as 2.164(5) Å.[45] It should be noted that it is not possible to calculate the e.s.d.s of centroid-to-centroid distances using standard crystallographic programs.

2.3.2 Identifying NTE

The study of the negative thermal expansion was undertaken by firstly using the program CSD_Thermal Search, described earlier. Potential candidates were then examined by determining their unit cell parameters at two different temperatures. As a 'rule of thumb", unit cell parameters that contract by more than three times their e.s.d.s at higher temperatures were regarded as showing NTE.

Table 3 presents an example of a compound whose unit cell parameters were determined at two different temperatures. The compound appears to undergo negative thermal expansion along the *b*-axis. However this is not the case since the high-temperature unit cell parameters are within three times the estimated standard deviation (e.s.d) of the low-temperature measurements.

Table 3. Unit cell example.

	Low temperature			High temperature
Axis	**Length (Å)**	**e.s.d**	**Length ± 3 × e.s.d**	**Length (Å)**
a	12.345	0.003	12.354, 12.336	12.447
b	*11.542*	*0.016*	*11.590, 11.494*	*11.499*
c	10.556	0.002	10.562, 10.550	10.675

Subsequently, if the compound showed the desired negative thermal expansion, a full dataset was collected at both temperatures. Those compounds that showed negative thermal expansion are reported here and their respective thermal coefficients were calculated according to the method introduced earlier.[26]

Chapter 3
Results

In this chapter we report on the compounds 4,4'-diiodobiphenyl, 4-iodobenzoic acid and 4-methyl paraben all of which undergo negative thermal expansion. Single crystal X-ray diffraction was employed to characterise each of the systems. It is noteworthy that the mechanism of negative thermal expansion is different in each case. We therefore define relevant parameters for each example of negative thermal expansion as we encounter them.

3.1 Compounds of the Study

Twenty compounds were investigated, all of which have similar structural characteristics. These compounds, along with their measured unit cell parameters, are reported in Table 4.

Table 4. Unit cell parameters of the studied compounds.

Compound	Space group	100 K			298 K		
		a	b	c	a	b	c
4-Dichlorobenzene	$P2_1/a$	14.811(2)	5.781(3)	3.992(3)	14.992(2)	5.893(3)	4.034(2)
4-Dibromobenzene	$P2_1/a$	4.108(3)	5.836(5)	15.477(2)	4.120(3)	5.981(5)	15.487(3)
4-Diiodobenzene	$Pbca$	7.168(6)	6.098(5)	16.854(2)	7.374(3)	6.116(4)	17.070(2)
4,4'-Biphenyldiol	$P2_1/c$	10.555(4)	5.327(2)	7.856(3)	10.561(2)	5.362(2)	8.032(2)
4,4'-Dichlorobiphenyl	$P2_1/a$	7.615(8)	5.761(3)	9.913(9)	7.653(2)	5.811(2)	9.958(3)
4,4'-Dibromobiphenyl	$P2_1/n$	9.712(8)	14.114(2)	15.558(2)	9.767(2)	14.147(2)	15.676(2)
4,4'-Diiodobiphenyl*	$Pccn$	7.375(2)	25.681(7)	5.939(2)	7.532(3)	25.571(8)	6.040(2)
Bromophenol	$I41/a$	15.745(4)	15.745(4)	10.119(3)	15.891(3)	15.891(3)	10.211(2)
Iodophenol	$I41/a$	15.761(2)	15.761(2)	10.391(2)	15.961(3)	15.961(3)	10.501(2)
Bromobenzaldehyde	$P2_1$	6.532(2)	12.768(3)	7.001(2)	6.633(3)	12.882(3)	7.122(3)
Iodobenzaldehyde	$P2_1$	6.913(6)	13.152(2)	7.811(3)	7.103(4)	13.205(3)	7.993(3)
4-Bromobenzoic	$P2_1/a$	3.752(5)	5.911(3)	28.561(4)	3.871(2)	6.012(4)	29.611(2)
4-Iodobenzoic*	$P2_1/n$	4.056(6)	5.941(8)	30.263(3)	4.161(2)	6.034(2)	30.111(8)
4-Hydroxybenzoic acid	$P21/a$	18.508(7)	5.228(2)	6.342(3)	18.5201(4)	5.302(2)	6.411(4)
Methyl 4-bromobenzoate	$Pbca$	13.849(2)	5.892(2)	19.613(2)	13.951(2)	5.956(2)	19.711(2)
Methyl 4-Iodobenzoate	$Pbca$	14.378(2)	5.944(2)	20.361(4)	14.469(2)	5.995(2)	20.445(4)
Methyl Paraben*	Cc	12.912(2)	17.334(2)	10.814(9)	13.597(2)	16.958(3)	11.033(2)
Ethyl Paraben	$P2_1/c$	11.550(2)	13.191(2)	11.669(2)	11.570(2)	13.212(2)	11.762(2)
Propyl Paraben	$P2_1/n$	11.738(6)	13.778(7)	11.811(6)	11.801(4)	13.832(2)	12.072(3)
Butyl Paraben	$P2_1/n$	20.175(2)	24.501(2)	14.390(2)	20.280(4)	8.317(2)	14.811(3)

*Exhibits NTE

The program CSD Thermal Search identified several compounds from the CSD which appeared to exhibit NTE. However, once preliminary unit cell determinations were carried on these compounds, none of them showed NTE. The reason for this is that the data were collected for different crystals in different laboratories by different research groups, and this is not taken into account by the program. Only when the data are collected under the same conditions, is it possible to reliably determine if a compound exhibits NTE behaviour.

3.2 4,4'-Diiodobiphenyl

3.2.1 Overview of 4,4'-Diiodobiphenyl

Crystals were grown by dissolving 15 mg of 4,4'-diiodobiphenyl in approximately 5 mL of solvent, which was allowed to evaporate over the course of a few days. Several different solvents were used, including acetone, acetonitrile, carbon tetrachloride, dichloromethane, dimethylformamide and tetrahydrofuran. A prismatic crystal grown from tetrahydrofuran was used for data collection. The unit cell parameters determined at both 100 and 298 K are reported in Table 5.

The Laue symmetry is *mmm*, indicating the orthorhombic crystal system. Investigation of the reciprocal lattice layers confirmed the reflection conditions *hkl: none; 0kl: l = 2n; h0l: l = 2n; hk0: h + k = 2n.* The program XPREP was used to confirm the space group as *Pccn.*

Table 5. Unit cell parameters of 4,4'-diiodobiphenyl at 100 and 298 K.

Temperature	100 K	298 K
Crystal system	Orthorhombic	Orthorhombic
Space group	*Pccn*	*Pccn*
a (Å)	7.375(2)	7.532(3)
b (Å)	25.681(7)	25.571(9)
c (Å)	5.939(2)	6.040(2)
Volume ($Å^3$)	1124.7(2)	1163.2(2)
Z	4	4
Density (g cm^{-3})	2.398	2.318
Mu (mm^{-1})	5.549	5.549
F(000)	744	744
R(int)	0.0226	0.0239
R1	0.0188	0.0233
wR2	0.0859	0.0592
GooF (S)	1.07	1.06
$\Delta\rho_{max}$ (e $Å^{-3}$)	-0.95, 0.85	-0.37, 0.72

4,4'-Diiodobiphenyl is a centrosymmetric molecule with the centre of inversion located along the C4-C4b bond (Figure 11).[46] Therefore, the molecule

is planar. Bond lengths determined at 100 and 298 K are reported in Table 6. The atomic numbering scheme is provided in Figure 11.

Table 6. Bond lengths of 4,4'-diiodobiphenyl.

Bonds	Bond length (Å)	
	100 K	298 K
C1-I	2.098(4)	2.094(5)
C1-C2	1.395(2)	1.382(4)
C2-C3	1.378(3)	1.377(4)
C3-C4	1.408(3)	1.402(3)
C4-C4b	1.486(3)	1.483(4)
C4-C5	1.410(2)	1.401(4)
C5-C6	1.389(3)	1.378(4)
C6-C1	1.398(3)	1.382(3)
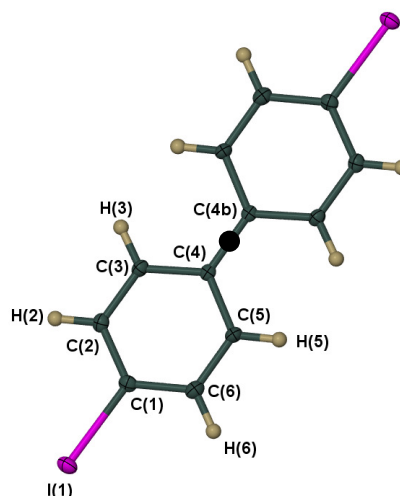
Figure 11. The molecular structure of 4,4'-diiodobiphenyl (determined at 100 K) showing the thermal ellipsoids at the 50 % probability level.

The shortening of the bond lengths with increasing temperature indicates that the aromatic carbons exhibit more sp^2 character at elevated temperatures (Table 6).[47] Carbon-carbon bonds with sp^2 character are known to be shorter than those with sp^3 character (an average length of 1.33 Å for sp^2 and 1.54 Å for sp^3).[47] In the sections below it will be shown that the molecules undergo changes in their orientation (changes in various tilting angles) with increasing temperatures. These orientational changes place more electron density around the phenyl rings which therefore increases the sp^2 character of the phenyl carbons. Thus, bond lengths involving C1, C2 and C6 are on average shorter.

3.2.2 Packing of 4,4'-Diiodobiphenyl

The asymmetric unit consists of one half of a 4,4'-diiodobiphenyl molecule. The unit cell contains four symmetry related molecules. The molecules are arranged in layers, which form a zigzag pattern parallel to the *b*-axis while the iodophenyl moieties abut at *b*/4 and 3*b*/4 (Figure 12).
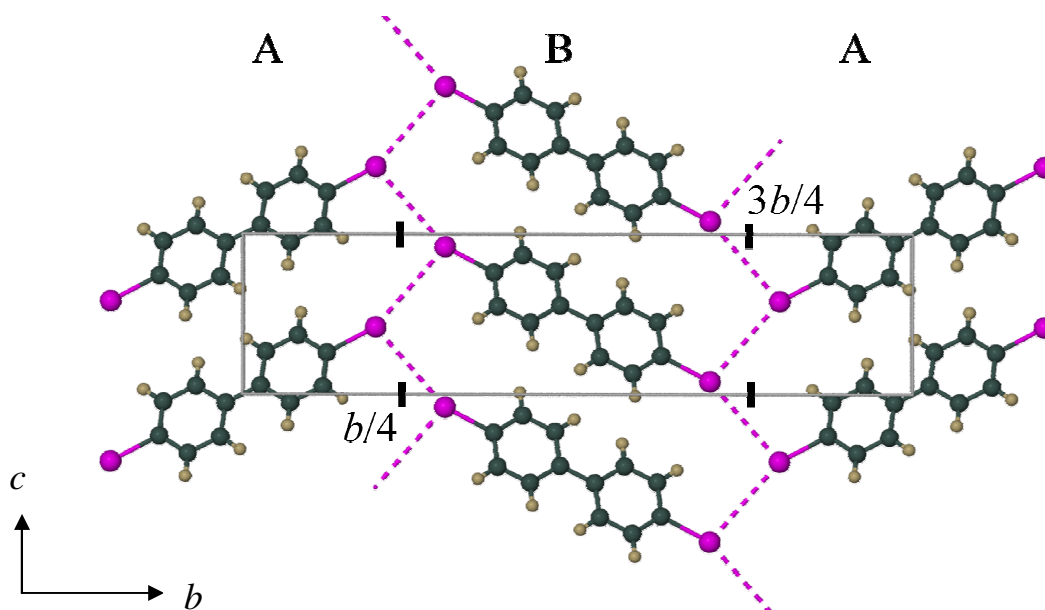
Figure 12. Packing diagram viewed along [100]

Halogen-halogen interactions span the crystal, forming infinite chains which are parallel to *c* and located at *b*/4 and 3*b*/4. Furthermore, the molecules are arranged in layers which comprise a repeating array ⋯ABAB⋯ as shown in Figure 12.

3.2.3 Negative Thermal Expansion of 4,4'-Diiodobiphenyl

It is clear from the data listed in Table 5 that 4,4'-diiodobiphenyl undergoes negative thermal expansion along the *b*-axis. The change in the length of the *b*-axis is 0.110 Å (>> 3 × e.s.d) when warming from 100 to 298 K. The linear thermal expansion coefficient (α) is -21.7 × 10^{-6} K^{-1} over this temperature range.

Three identifiable steps occur simultaneously within the crystal when it undergoes NTE.

- The molecules undergo an in-plane tilting relative to a reference plane (definition follows).
- The molecules undergo an out-of-plane tilting relative to the same reference plane.
- The molecules undergo a slight rotation

The application of these steps to a single molecule simplifies the visualisation of the mechanism of NTE (Figure 13).

31
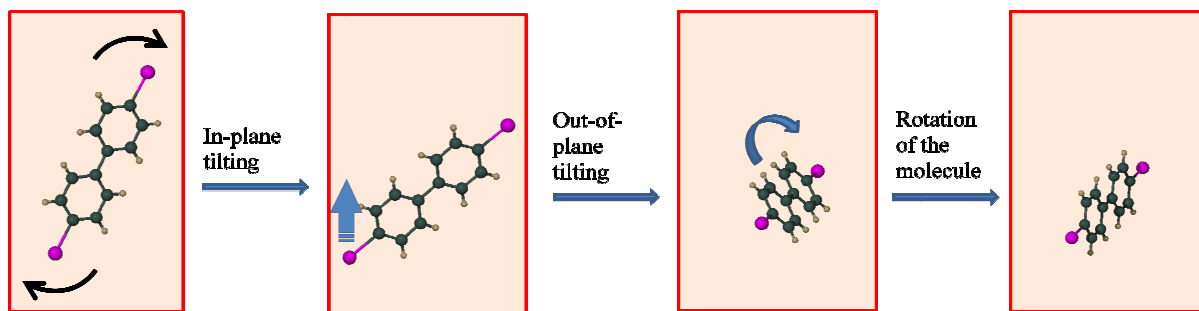
Figure 13. An exaggerated representation of what happens to a molecule with an increase in temperature.

3.2.3.1 The Mechanism of Negative Thermal Expansion in 4,4'-Diiodobiphenyl

3.2.3.1.1 STEP 1: In-Plane Tilting

In order to facilitate an understanding of the mechanism by which 4,4'-diiodobiphenyl undergoes NTE, we define a mean plane through each molecule as shown in Figure 14.

a   b
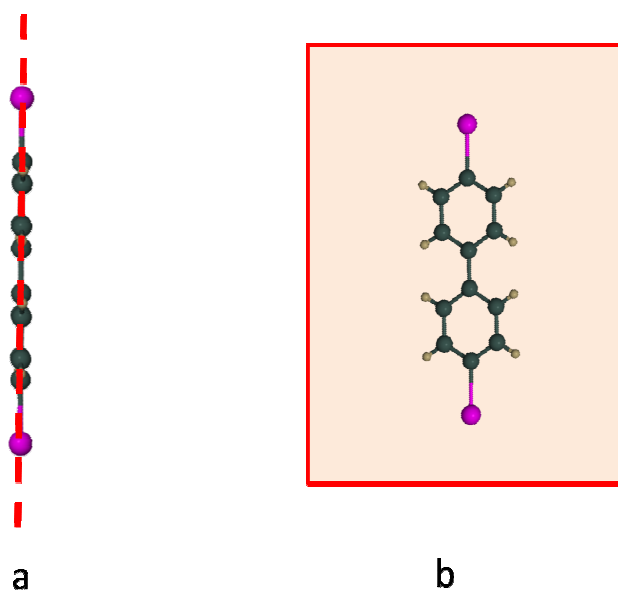
Figure 14. a) An illustration along the mean plane passing through 4,4'-diiodobiphenyl. b) A perpendicular view of the mean plane.
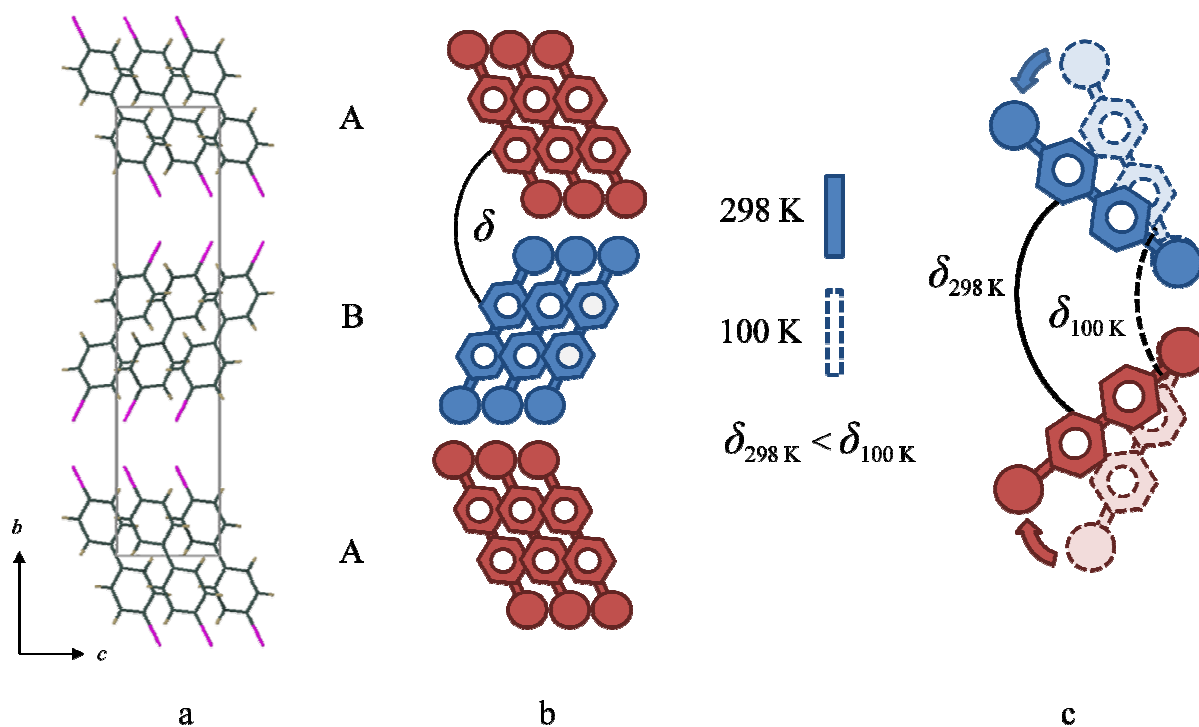
Figure 15. a) View along [100] showing the layers. b) A schematic representation of the layers. c) A exaggerated schematic representation of the tilting of the molecules belonging to layers A and B.

The molecules located in layers A and B tilt in the plane towards each other (Figure 15a). The degree of tilting can be measured by determining the change in the angle (δ) between layers A and B (Figure 15b). The δ angle decreases from 127.8 (3)° at 100 K to 126.4 (2)° at 298 K (Figure 15c).

As the *b*-axis contracts the molecules adjust their orientations relative to one another to maintain a level of shape complementarity. This aids the efficient packing of the molecules, which maximises their interaction energies.[32] Furthermore, increased tilting of the molecules (with an increase in temperature) simultaneously causes an expansion along the *c*-axis (Figure 16).
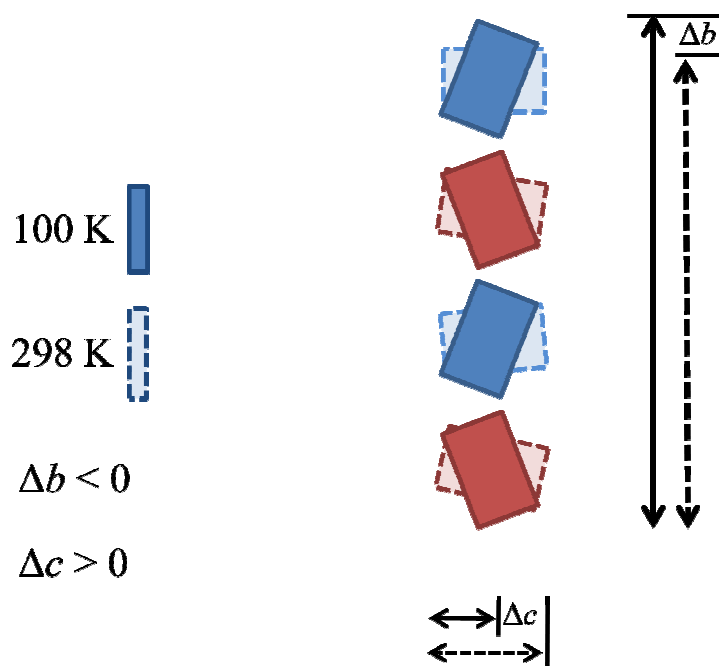
Figure 16. A schematic representation illustrating the tilting of the layers and the resulting shortening of the *b*-axis.

3.2.3.1.2 STEP 2: Out-of-Plane Tilting

In addition to the molecules tilting in the mean plane, they also tilt out of the mean plane as illustrated in Figure 17.
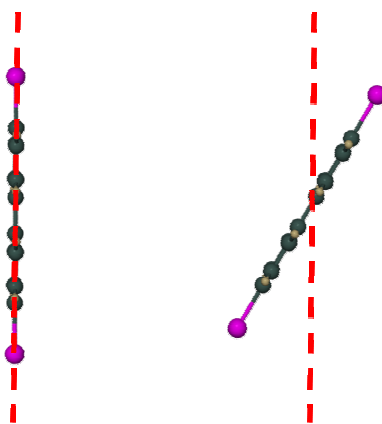
Figure 17. Out-of-plane tilting relative to the mean reference plane.

The degree of tilting experienced by successive layers along *a* is measured as the change in the angle ε, as shown in Figure 18.
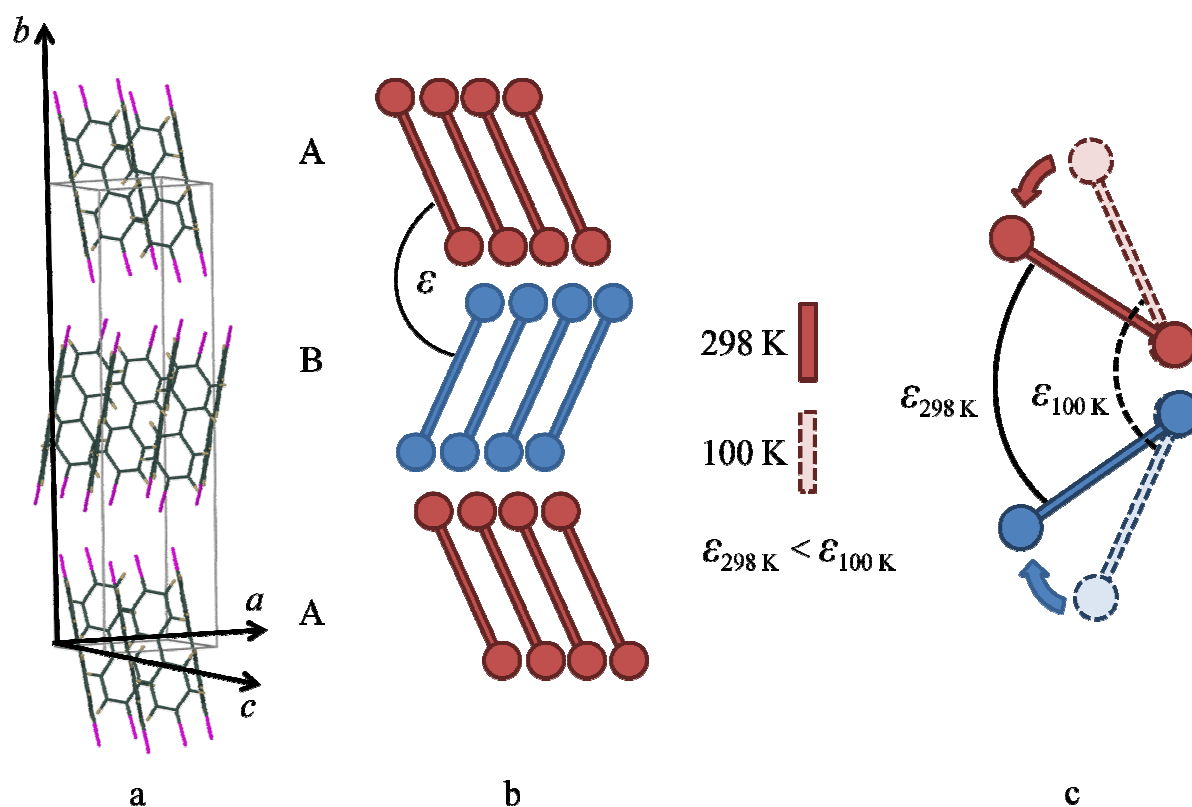
Figure 18. a) The arrangement of the molecules. b) A schematic representation with some molecules omitted for clarity. c) An exaggerated illustration of the change of the angle ε.

The angle ε decreases from 159.4(8)° at 100 K to 158.8(7)° at 298K (Figure 18c). In a manner similar to that of in-plane tilting, the out-of-plane tilting causes the b-axis to contract. In this case the unit cell expands along the a direction.
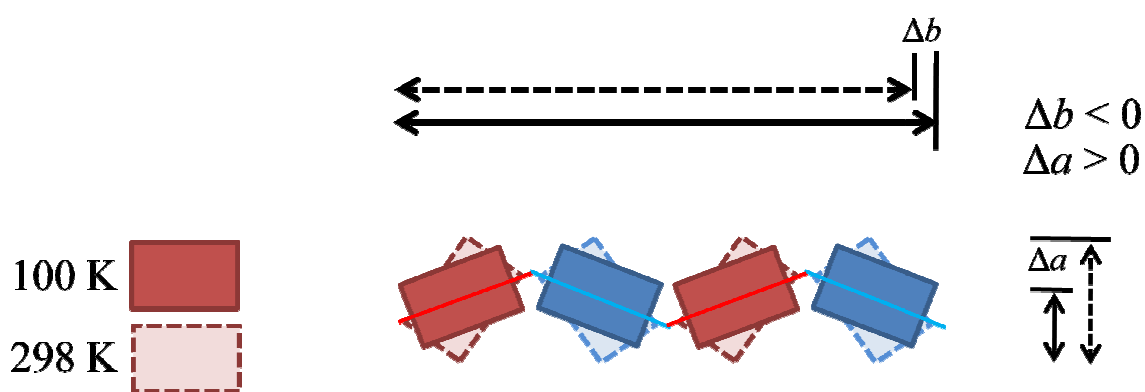
Figure 19. A schematic representation of the out-of-plane tilting of the layers and the related expansion of the a-axis.

3.2.3.1.3 STEP 3: Rotation of the Molecule

A single layer viewed along [012] illustrates the herringbone packing arrangement with its related herringbone angle, σ (Figure 20a). It is apparent

from the figure that there are two distinct orientations of the molecules, represented by C and D. The molecules belonging to the structure collected at 100 K are rotated relative to those collected at 298 K. The molecules in C rotate clockwise while those in D rotate anti-clockwise (Figure 20b). The rotation of the molecules is as a result of the close packing effect mentioned previously.
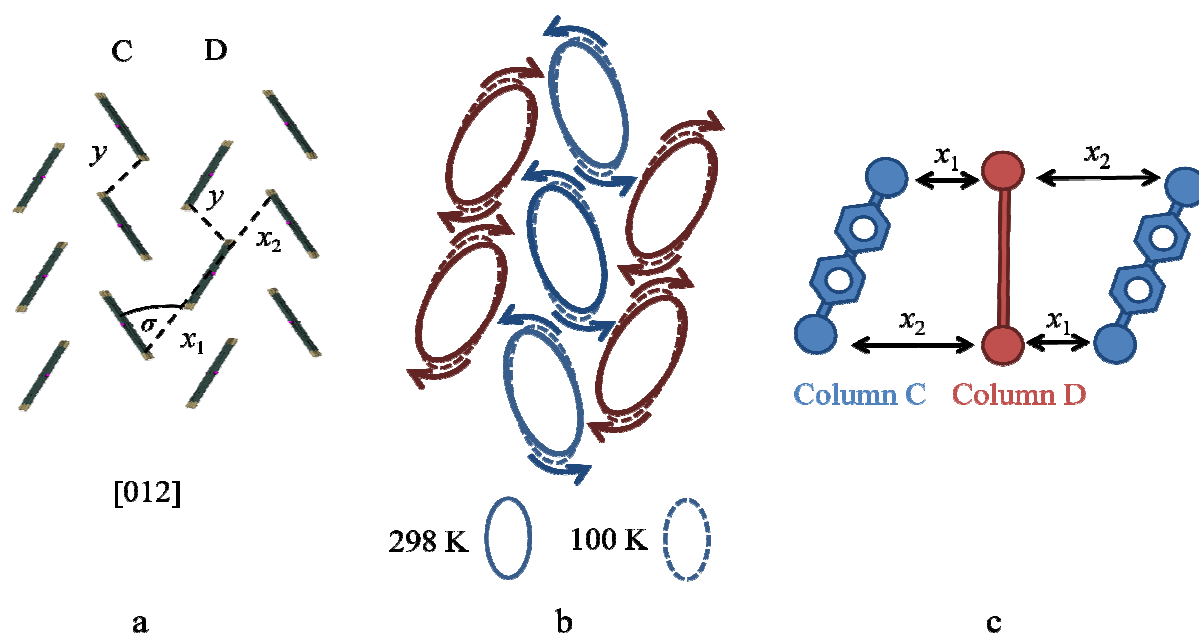
Figure 20. a) Stick representation showing the herringbone angle. b) Rotation of the molecules within a layer. c) A schematic illustration the distances between layers.

As the molecules in C and D are rotated, an increase in the herringbone angle occurs (Table 7). The inter- and intra-layer distances represented by x and y also change during rotation (Figure 20a). Furthermore, the distances between C and D are not equal (Figure 20a). This implies that the molecules are not parallel to each other but rather are inclined (Figure 20c). The distances are reported in Table 7.

Table 7. Change of the herringbone angle and the distance between molecules with temperature.

Temperature	σ (°)	x_1 (Å)	x_2 (Å)	y (Å)
100 K	56.5(6)	3.795(3)	4.038(4)	4.303(4)
298 K	57.8(8)	3.875(4)	4.121(6)	4.446(4)
$\Delta\sigma$, Δx, Δy	1.3	0.080	0.084	0.142

The rotation of the molecules leads indirectly to an increase in the length of the *a*-axis and a decrease in the length of the *c*-axis, even though the alignment of the molecules does not coincide with any of the crystallographic axes (Figure 21).
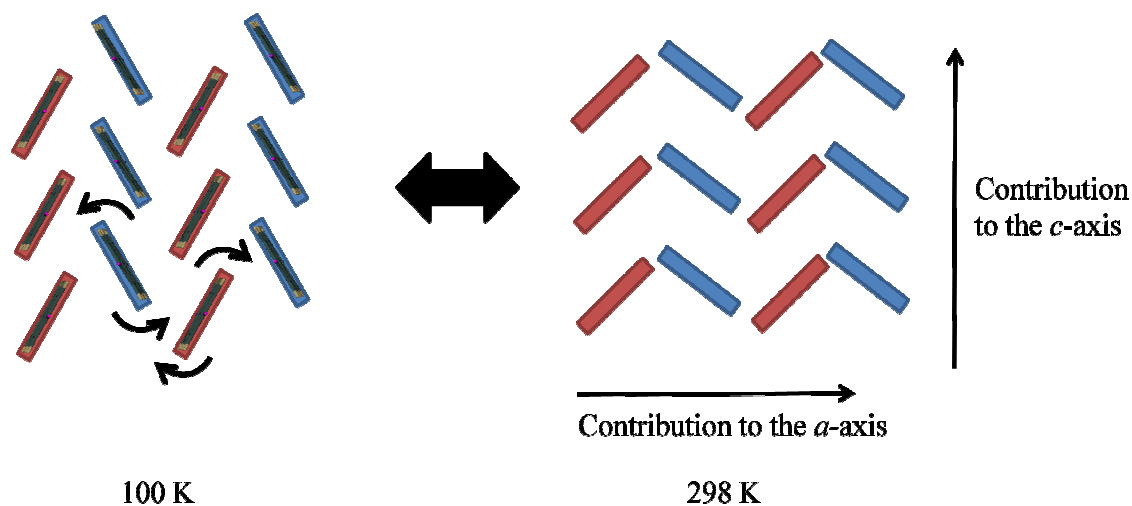
Figure 21. The effect of the rotation of the molecules.

3.2.4 Intermolecular Interactions

Hirshfeld surfaces and fingerprint plots were generated in order to examine the changes in the intermolecular interactions and in the packing arrangements after undergoing NTE. In order to obtain useful data for this study, the fingerprint plots were decomposed to reveal the contribution of each interaction towards the total surface area in the respective structures (Figure 22).

4,4'-Diiodobiphenyl

	Iodine-iodine	Iodine-carbon	Iodine-hydrogen	Carbon-hydrogen	Hydrogen-hydrogen
298 K	16.0	1.1	25.2	39.9	17.8
100 K	16.2	1.0	24.7	40.9	17.2

■ Iodine-iodine interactions ■ Iodine-carbon interactions
■ Iodine-hydrogen interactions ■ Carbon-hydrogen interactions
■ Hydrogen-hydrogen interactions
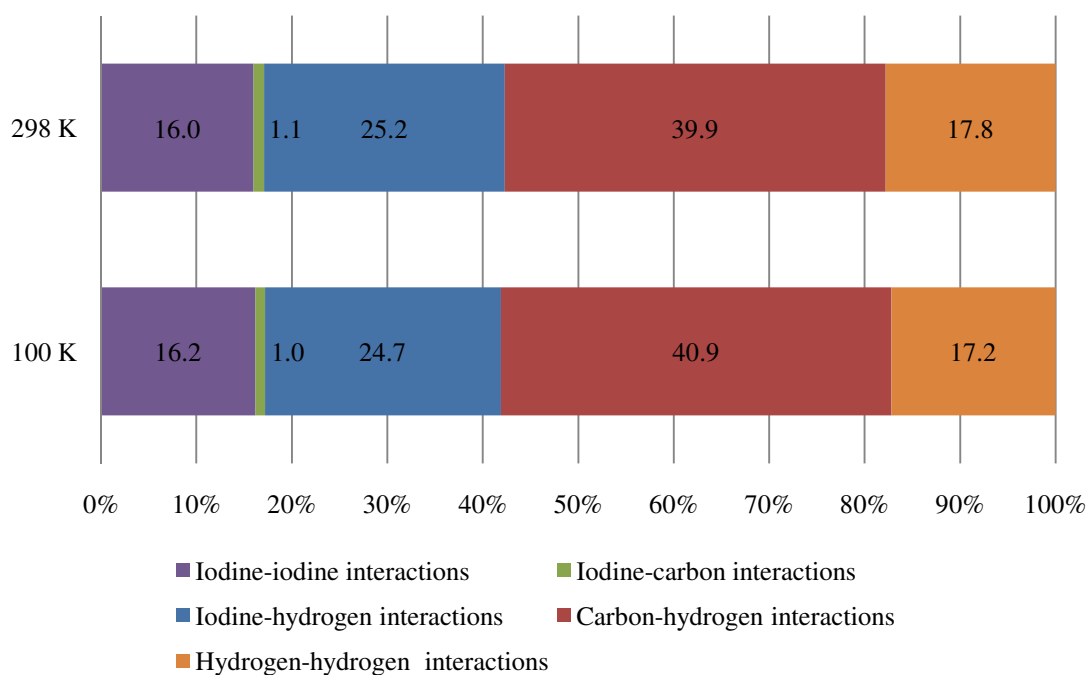
Figure 22. The contribution of each interaction towards the total surface area of 4,4'-diiodobiphenyl at 100 and 298 K.

Fingerprint plots are sensitive to changes in the environment of the molecule and any differences which may arise as a result of these changes are reflected therein (Figure 23). Each of the changes induced by temperature is discussed with regard to identifying the interactions that contribute to the observed negative thermal expansion.

a   b
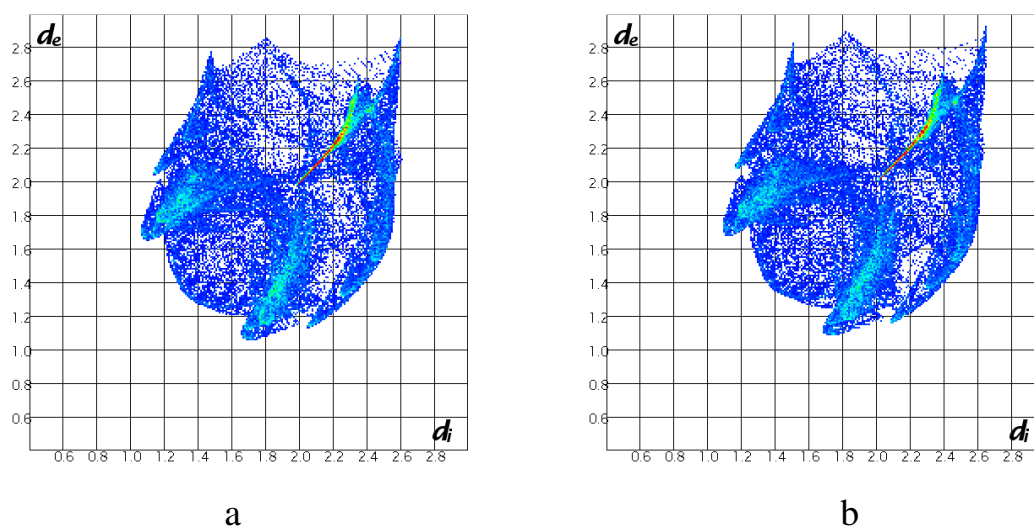
Figure 23. Fingerprint plots of all the interactions at a) 100 K and at b) 298 K.

3.2.4.1 Iodine-Iodine Interactions

Larger halogens such as iodine bonded to carbon are known to have anisotropic charge distributions and the shorter radius is always along the halogen-carbon bond vector.[48] Nyburg *et al*. called this "polar flattening" and found that the van der Waals radii for perfect head-on contacts and side-on contacts are 3.52 Å and 4.26 Å, respectively.[48] Close packing of atoms with head-on contacts generally gives rise to less repulsion due to "polar flattening", while side-on connections are more favourable for polarisation-induced attractive interactions.[49] Because polarisation increases with atomic size, polarisation-induced attraction forces are more prominent in the larger halogens such as iodine.

The "sideways" iodine-iodine connections can also be explained in terms of the anisotropic potential. The negative electrostatic potential distributions for iodine can be represented as shown in Figure 24a,[50] and they have been suggested as an explanation for the observed zigzag motif.[51] Figure 24b is a schematic representation of the negative electrostatic potential distributions around iodine that provide the basis for the observed zigzag motif.

a   b
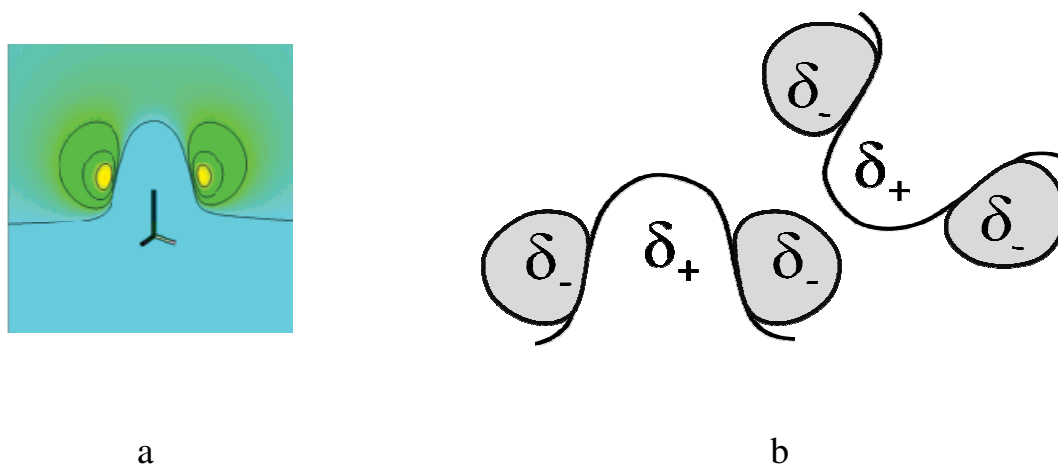
Figure 24. a) Negative electrostatic potential distributions for CH₃I. b) Schematic representation of the electrostatic potential distributions for CH₃I illustrating the nature of iodine-iodine interactions.[50]

According to the Hirshfeld surfaces, each iodine atom makes two intra-layer contacts (Figure 25a) and three inter-layer iodine-iodine contacts (Figure 25b).

<div align="center">a   b</div>
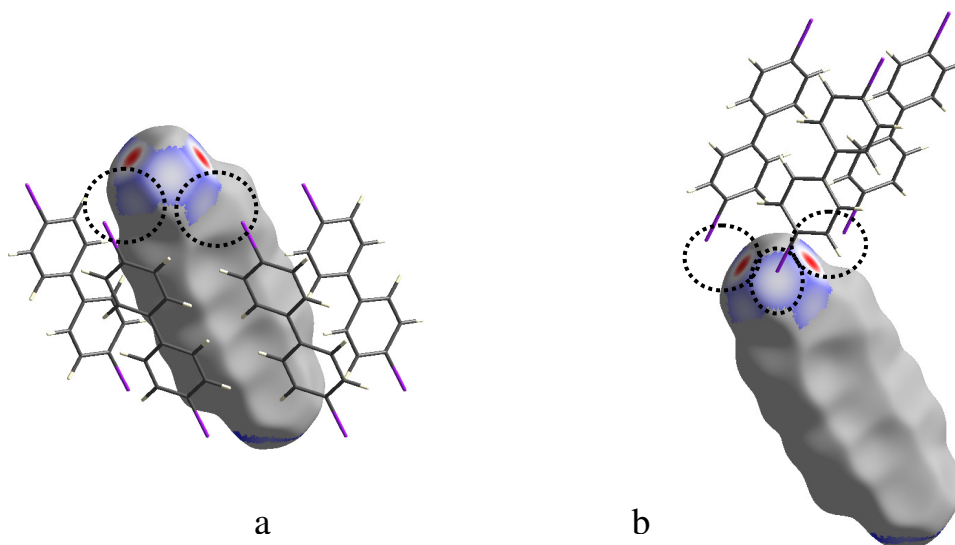
Figure 25. a) The iodine-iodine interactions within a layer. b) The iodine-iodine interactions between layers.

<div align="center">a   b</div>
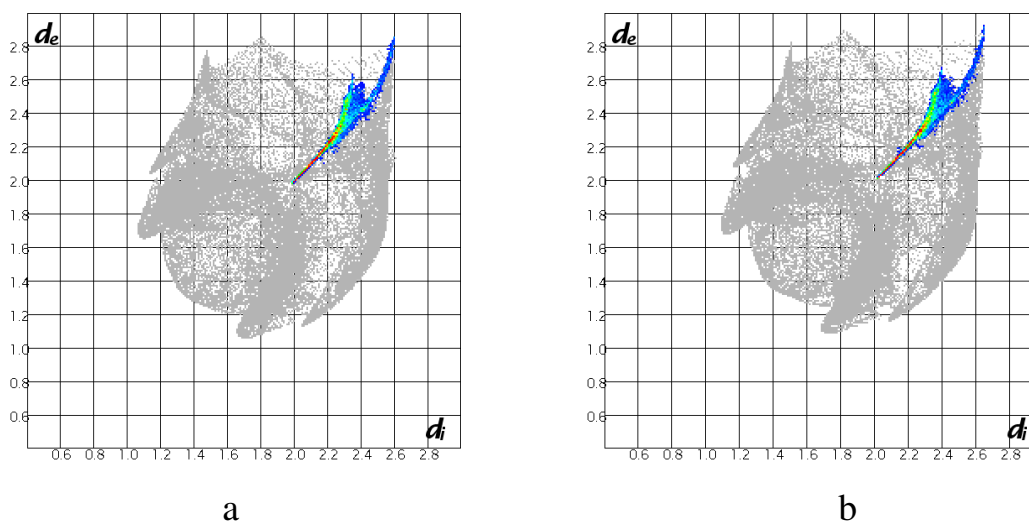
Figure 26. The iodine-iodine interactions at a) 100 K b) 298 K.

The observed contributions of the iodine-iodine interactions towards the total Hirshfeld surface area in the structure decreases marginally from 16.2% at 100 K to 16.0% at 298 K (Figure 26). In addition, examination of the iodine-iodine interactions reveals that both the distances and the angles between the interacting molecules change with temperature (Figure 27). The distance between iodine atoms increases with an increase in temperature.

The two inter-layer iodine-iodine contacts ($I_a \cdots I_b$ and $I_a \cdots I_c$) can be considered to be halogen bond interactions since their interaction distances are shorter than the sum of the van der Waals radii (4.30 Å).[52] The inter-layer distances increase from 3.995(2) Å to 4.057(2) Å (indicated by the red area on the Hirshfeld surface, Figure 25) while the intra-layer iodine-iodine distances increase from 5.021(2) Å to 5.124(2) Å with increasing temperature (indicated by the blue area on the Hirshfeld surface).
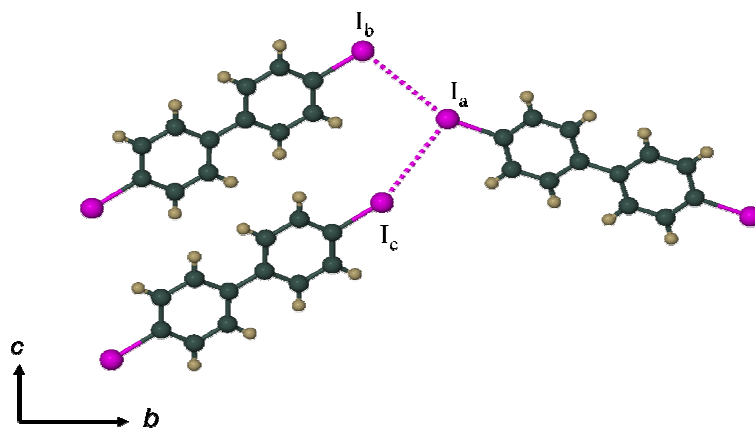
Figure 27. Iodine-iodine interactions between adjacent layers, as viewed along [100].

The C-$I_a \cdots I_b$ angle increases from 158.8(7)° to 159.4(8)° while the C-$I_a \cdots I_c$ angle decreases from 105.1(7)° to 104.3(9)° (Figure 27). These changes reflect the changes in the δ angle (Figure 28).
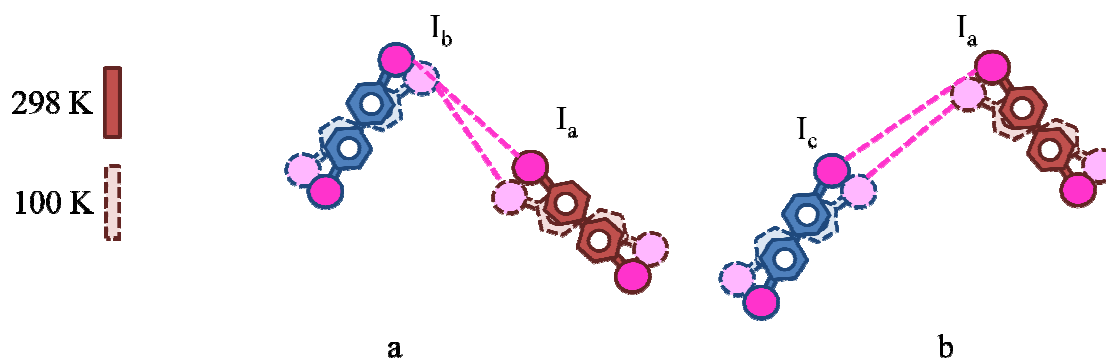
Figure 28. Schematic representation of the change in the angles between interacting iodine atoms. a) The change in angle C-$I_a \cdots I_b$. b) The change in angle C-$I_a \cdots I_c$.

3.2.4.2 Carbon-Iodine Interaction
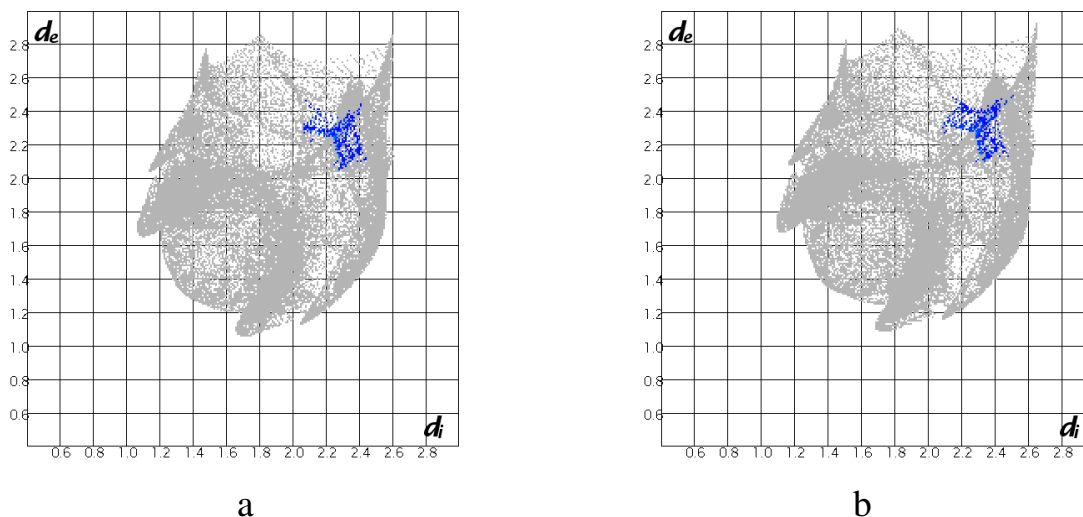
Figure 29. Fingerprint plots of the carbon-iodine interactions a) 100 K b) 298 K.

The contribution of the carbon-iodine interactions towards the total surface area in the structure increases slightly from 1.0% at 100 K to 1.1% at 298 K (Figure 29).

The increase in the carbon-iodine interactions results from the decrease in δ. As δ decreases the ortho-carbons are moved closer to the iodine atoms in the neighbouring molecules. In other words, as the molecules tilt together they slide past one another. This allows the iodine atoms in one molecule to move closer to the phenyl ring of a neighbouring molecule (Figure 30).
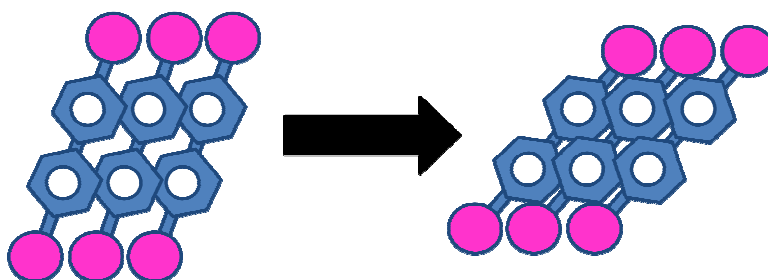
Figure 30. Effect of the decrease in tilt angle δ on the iodine-carbon interactions.

3.3 4-Iodobenzoic Acid

3.3.1 Overview of 4-Iodobenzoic Acid

Crystals were grown by dissolving 10 mg of 4-iodobenzoic acid in approximately 5 mL of solvent, which was allowed to evaporate over the course of several days. Several different solvents were used, including acetone, dichloromethane, dimethylformamide, ethanol and methanol. A plate-shaped crystal grown from acetone was used for data collection. The unit cell parameters determined at both 100 and 298 K are reported in Table 8.

Table 8. Unit cell parameters of 4-iodobenzoic acid at 100 and 298 K respectively.

Temperature	100 K	298 K
Crystal system	Monoclinic	Monoclinic
Space group	$P2_1/n$	$P2_1/n$
a (Å)	4.056 (6)	4.161(2)
b (Å)	5.941(8)	6.034(2)
c (Å)	30.263(3)	30.111(8)
β	91.08 (2)	90.52 (3)
Volume (Å^3)	729.3(3)	755.8(2)
Z	4	4
Density (g cm^{-3})	2.259	2.179
Mu (mm^{-1})	4.32	4.32
F(000)	464	464
R(int)	0.0279	0.0306
R1	0.0342	0.0512
wR2	0.1061	0.1403
GooF (s)	0.865	0.987
Δρ$_{max}$ (e Å^{-3})	-1.55, 1.39	-0.93, 1.35

The Laue symmetry is $2/m$ indicating the monoclinic crystal system. Investigation of the reciprocal lattice layers confirmed the reflection conditions $h0l: h+l = 2n; 0k0: k = 2n$. The program XPREP was used to confirm the space group as $P2_1/n$. Bond lengths determined at 100 and 298 K are reported in Table 9. The atomic numbering scheme is provided in Figure 31.

Table 9. Bond lengths of 4-iodobenzoic acid.

Bond	Bond length (Å)	
	100 K	298 K
C1-I	2.094(2)	2.099(4)
C1-C2	1.380(2)	1.372(3)
C2-C3	1.383(3)	1.374(2)
C3-C4	1.398(3)	1.378(3)
C4-C7	1.487(3)	1.485(3)
C7-O1	1.302(2)	1.287(3)
C7-O2	1.231(2)	1.237(2)
C4-C5	1.397(2)	1.385(3)
C5-C6	1.401(2)	1.381(2)
C6-C1	1.394(2)	1.385(3)
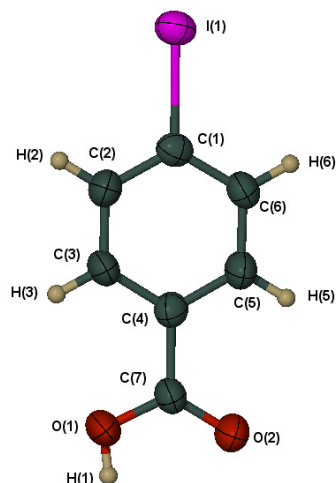
Figure 31. The molecular structure of 4-iodobenzoic (determined at 100 K) showing the thermal ellipsoids at the 50% probability level.

The shortening of the bond lengths with an increase in temperature is attributed to changes in the orientation of the molecules. The temperature-dependant orientational changes of the molecules increase the electron density around the aromatic ring and consequently increases the sp^2 character of the carbon atoms.

Studies regarding the position of the hydrogen atom between the dimeric carboxylic acid units have been reported in the literature. The reader is referred to the literature as this is not within the scope of the current investigation.[53] Moreover, it was reported that structures containing any number of molecules where each one possesses only a single carboxylic acid group have a high probability of cyclic dimer formation (c.a. 95%). This is also the case for 4-iodobenzoic acid.[54]

3.3.2 Packing of 4-Iodobenzoic Acid

The asymmetric unit consists of a single 4-iodobenzoic acid molecule. The unit cell contains four symmetry-related molecules, and these are arranged in layers. 4-Iodobenzoic acid forms planar centrosymmetric dimers which are arranged in a zigzag pattern (Figure 32).[55] The layers are arranged such that the iodophenyl moieties abut at *c*/4 and 3*c*/4. Halogen-halogen interactions span the crystal, forming infinite chains parallel to *b*. Additionally, the

molecules are arranged in layers that consist of a repeating ···ABAB··· array (Figure 32).
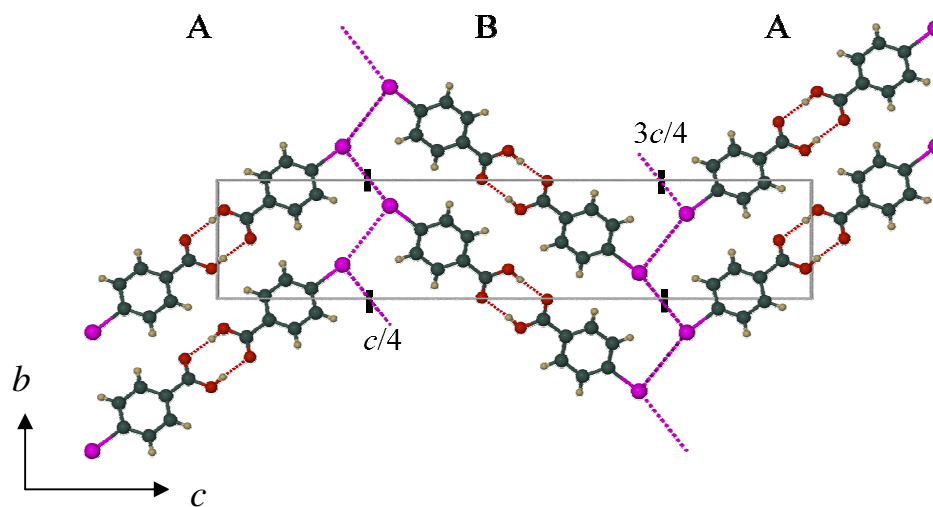
Figure 32. Packing diagram viewed along the [100].

The hydrogen bonding of the dimer is illustrated in Figure 33, and the hydrogen bond parameters are reported in Table 10.
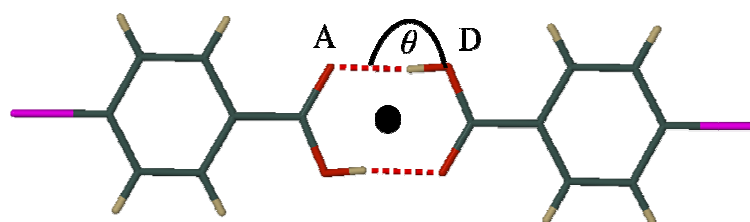
Figure 33. Hydrogen bonding in 4-iodobenzoic acid.

Table 10. Hydrogen bond data.

	Temperature (K)	
Hydrogen bond angles (°)	**100**	**298**
θ	114.3(3)	116.0(4)
Oxygen-oxygen distance (Å)		
A - D	2.609(5)	2.624(7)

3.3.3 Negative Thermal Expansion of 4-Iodobenzoic Acid

The data listed in Table 8 shows that 4-iodobenzoic acid undergoes negative thermal expansion along the *c*-axis. The change in the length of the *c*-axis is 0.150 Å (>> 3 × e.s.d) going from 100 to 298 K. The linear thermal expansion coefficient, α, is $-31.1 \times 10^{-6} \, K^{-1}$.

Two identifiable steps occur simultaneously within the crystal when the temperature is changed.

- The molecules undergo in-plane tilting relative to a reference plane.
- The molecules also undergo out-of-plane tilting relative to the same reference plane.

By applying these steps to a single molecule it is easier to visualise the effects that they have on the crystal (Figure 34).
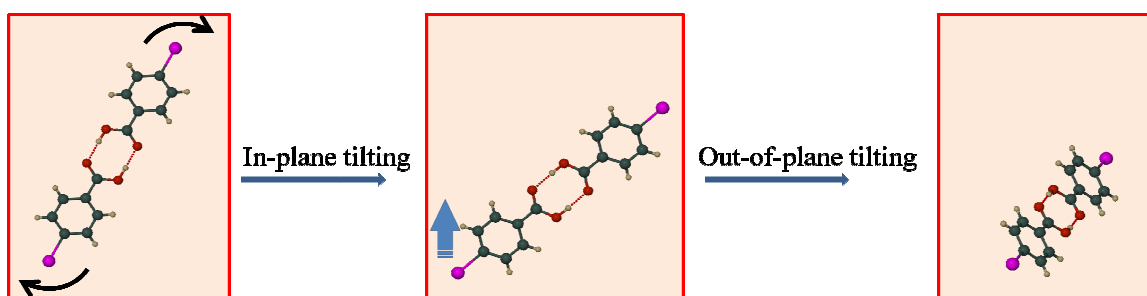
Figure 34. An exaggerated representation of what happens to a molecule with an increase in temperature.

3.3.3.1 The Mechanism of Negative Thermal Expansion in 4-Iodobenzoic acid

3.3.3.1.1 STEP 1: In-Plane Tilting

We define a mean plane which passes through each molecule (Figure 35). The maximum deviation of any atoms from the calculated plane was 0.0031 Å. In order to understand the reasons behind the shrinkage of the *c*-axis with increasing temperature, we can examine the relative positions of the molecules at both 100 and 298 K.

a   b
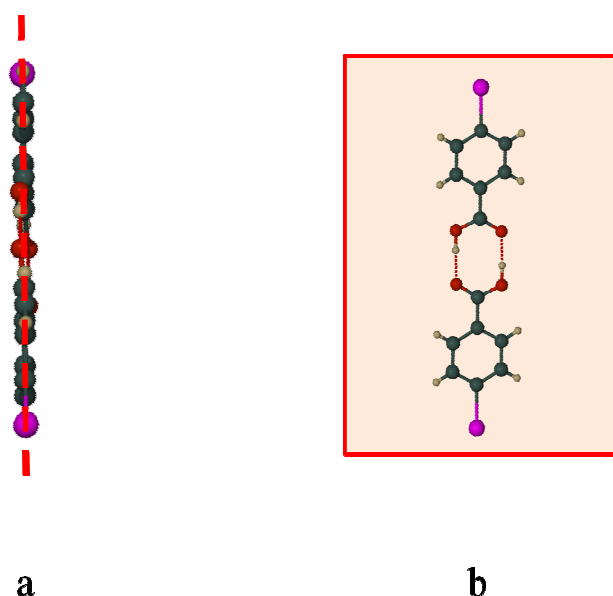
Figure 35. a) An illustration of the mean plane passing through 4-iodobenzoic acid. b) A perpendicular view of the mean plane.

The molecules located in layers A and B (shown in Figure 36a) tilt towards each other. The degree of tilting can be determined by measuring the change in the angle (δ) between layers A and B (Figure 36b).

a   b   c
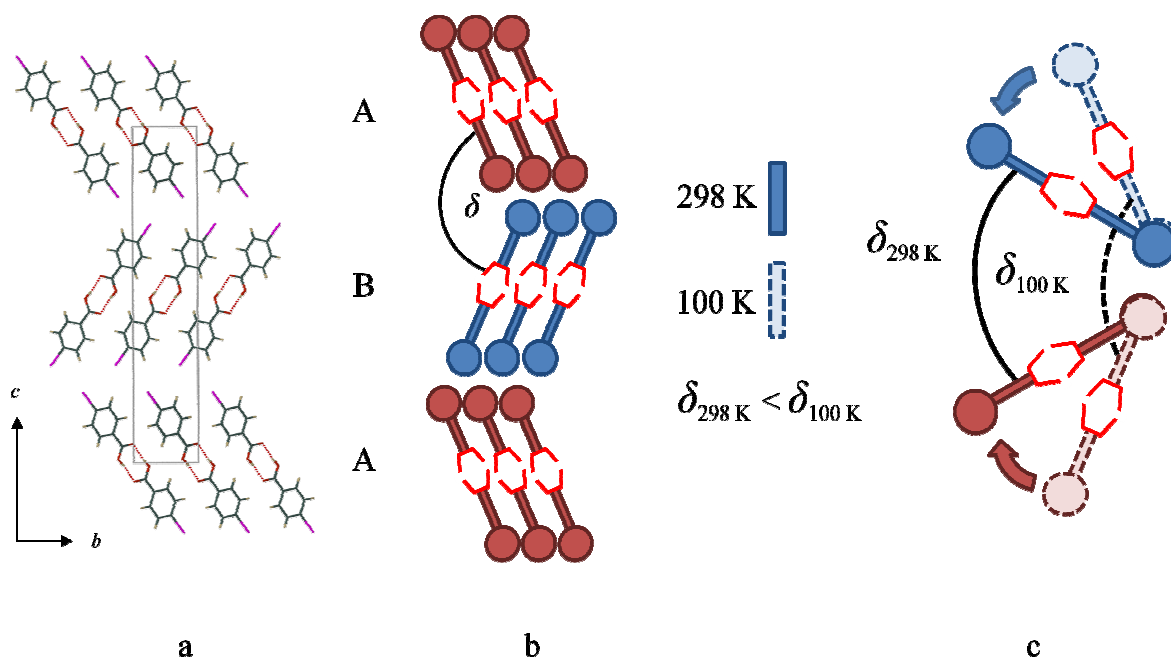
Figure 36. a) View along the *a*-axis showing the layers. b) A schematic representation of the molecules. c) An exaggerated schematic representation of the in-plane tilting angles, $\delta_{100\ K}$ and $\delta_{298\ K}$.

The angle δ decreases from 107.2(2)° at 100 K to 106.7(3)° at 298 K. Therefore, as the molecules adjust their orientations relative to one another, the *c*-axis contracts, maintaining packing complementarity and thus

maximizing interaction energies.[32] This change in orientation relates to a change in the tilt angle of the molecules, which results in contraction of the *c*-axis (Figure 37).
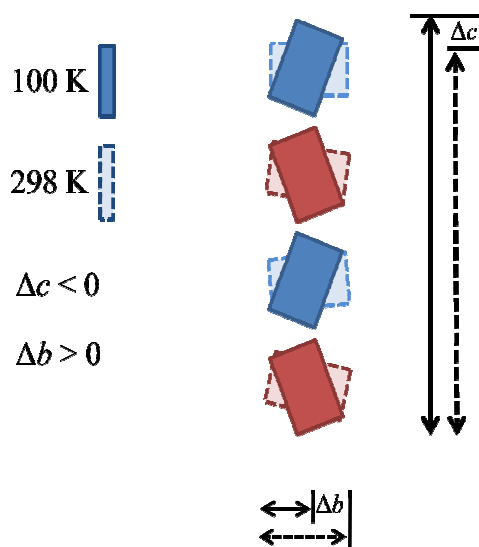
Figure 37. A schematic representation illustrating tilting of the layers with concomitant contraction and expansion of the axes.

When a single layer is viewed along the direction [672], it is evident that molecules within the layer are parallel to one another (Figure 38). It follows that there are no herringbone angles present in the packing arrangement. The centroid-to-centroid distance *x* increases from 4.057 Å to 4.161 Å with increasing temperature while the centroid-to-centroid distances *y* increase from 7.194 Å to 7.329 Å.
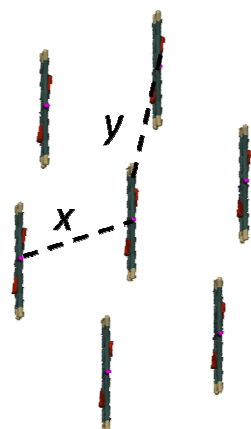
Figure 38. Stick representation of a layer viewed along to one of the assigned reference planes.

Even though the intermolecular distances increase at higher temperatures, the molecules remain parallel to one another.

3.3.3.2 STEP 2: Out-Of-Plane Tilting

As the temperature increases the molecules tilt out of the mean reference plane (described earlier) (Figure 39).
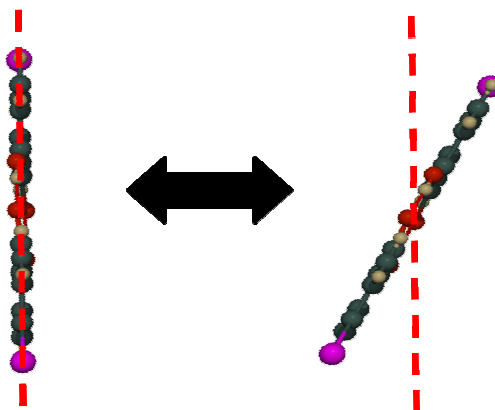
Figure 39. Out-of-plane tilting relative to the mean plane through the molecule.

Adjacent layers are angled relative to each other (Figure 40), giving rise to a second tilt angle.
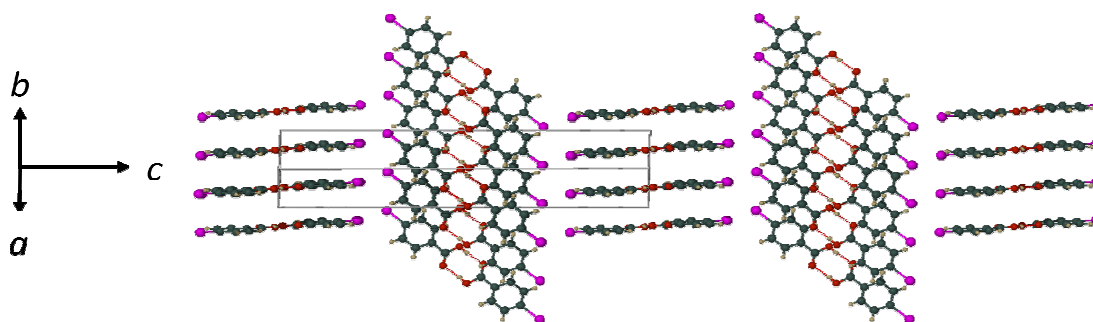
Figure 40. The different orientations of the layers viewed along [110].

The degree of tilting made by successive layers along a is measured by the change in the angle ε, shown in Figure 41.
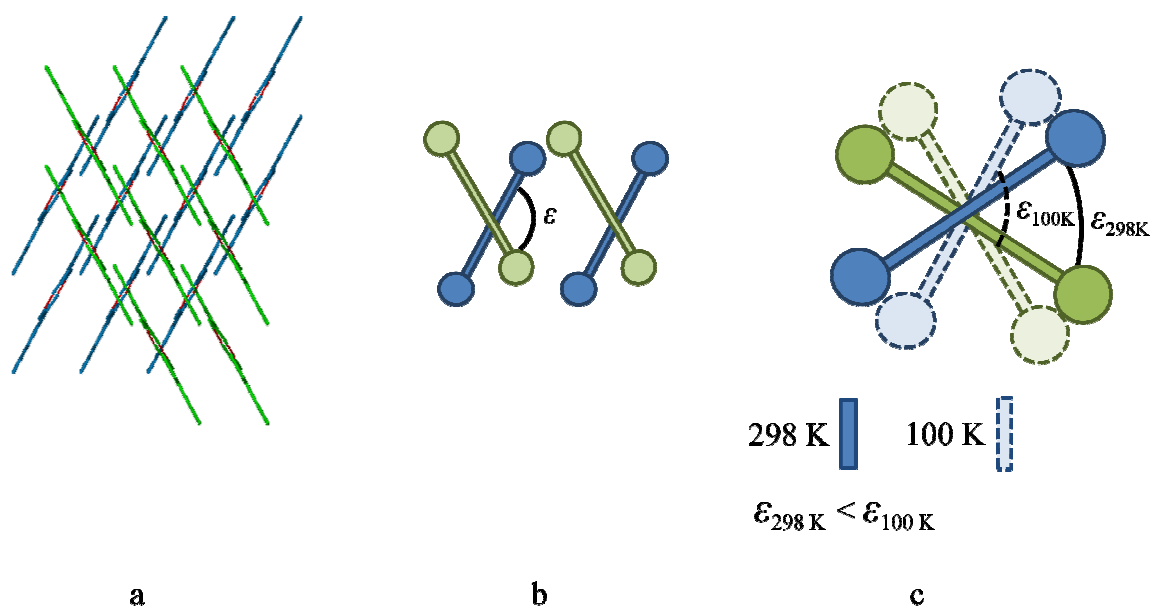
Figure 41. a) View along the *c*-axis. b) A schematic representation. c) A schematic representation of the out-of-plane tilting angles, ε_{100K} and ε_{298K}.

The degree of tilting can be measured by determining the change in the tilt angle ε (Figure 41b). The angle increases from 56.9(2)° at 100 K to 58.2(2)° at 298 K (Figure 41c). The contraction along the *c*-axis is accompanied by an expansion of *a* (Figure 42).
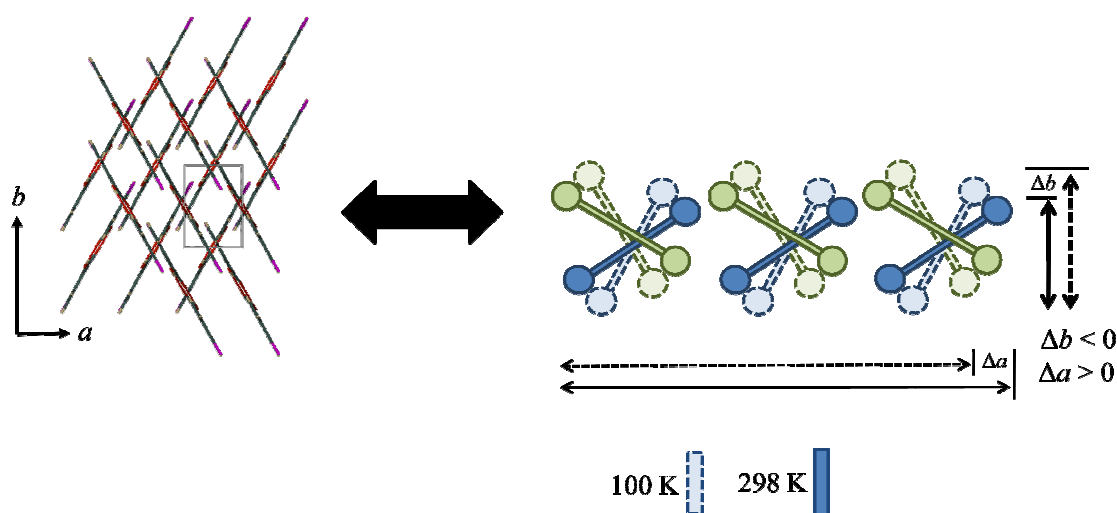
Figure 42. A schematic representation illustrating the expansion and contraction of the molecules along *a* and *b*.

A comparison of the lengths of the *a*- and *b*-axes at 100 and 298 K shows that they expand by 0.105 Å and 0.093 Å, respectively. The reason for the *a*-axis expanding more than the *b*-axis is owing to better alignment of the molecules along the *a*-axis than along the *b*-axis (Figure 42).

3.3.4 Intermolecular interactions

In order to obtain useful data for this study, the fingerprint plots were decomposed to reveal the contribution of each interaction towards the total Hirshfeld surface area in their respective structures (Figure 43).
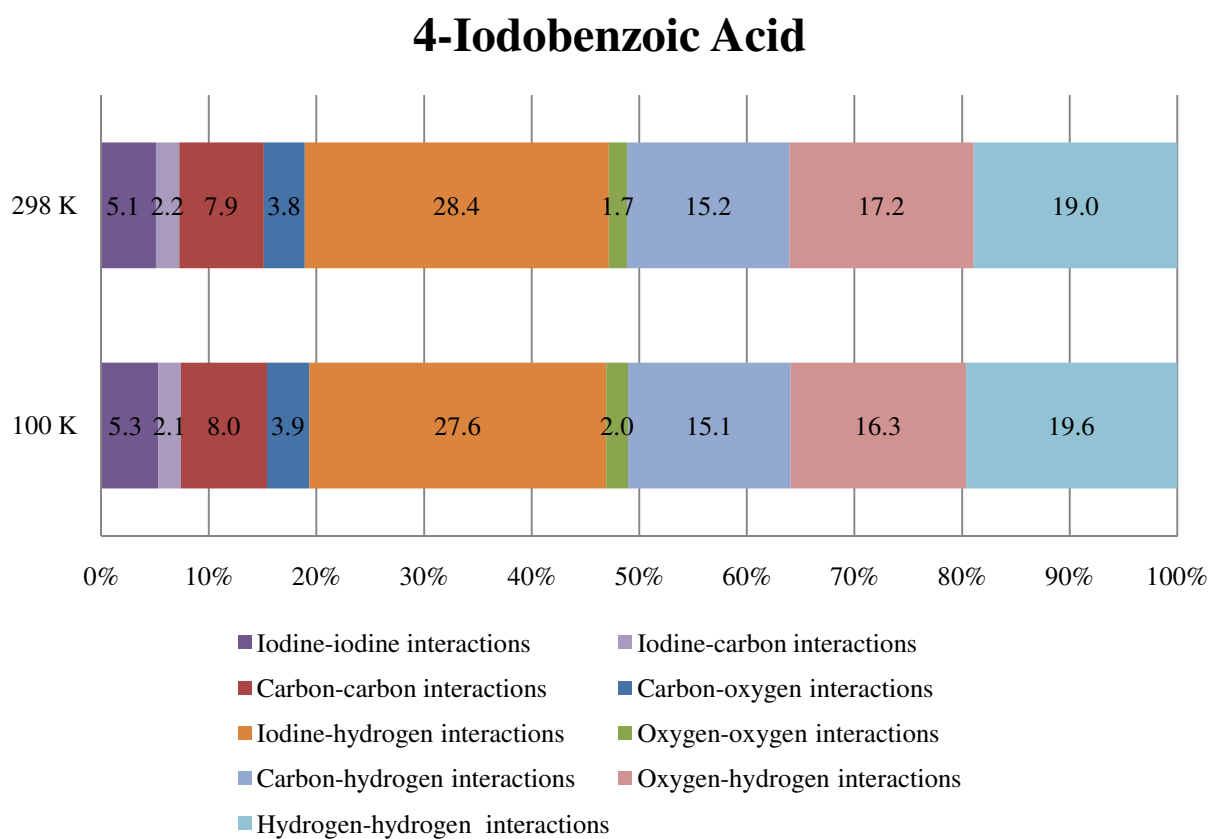
4-Iodobenzoic Acid

Figure 43. The contribution of each interaction towards the total Hirshfeld surface area for 4-iodobenzoic acid.

Fingerprint plots are sensitive to changes in the environment of the molecule and any differences that may arise as a result of these changes are reflected therein (Figure 44).
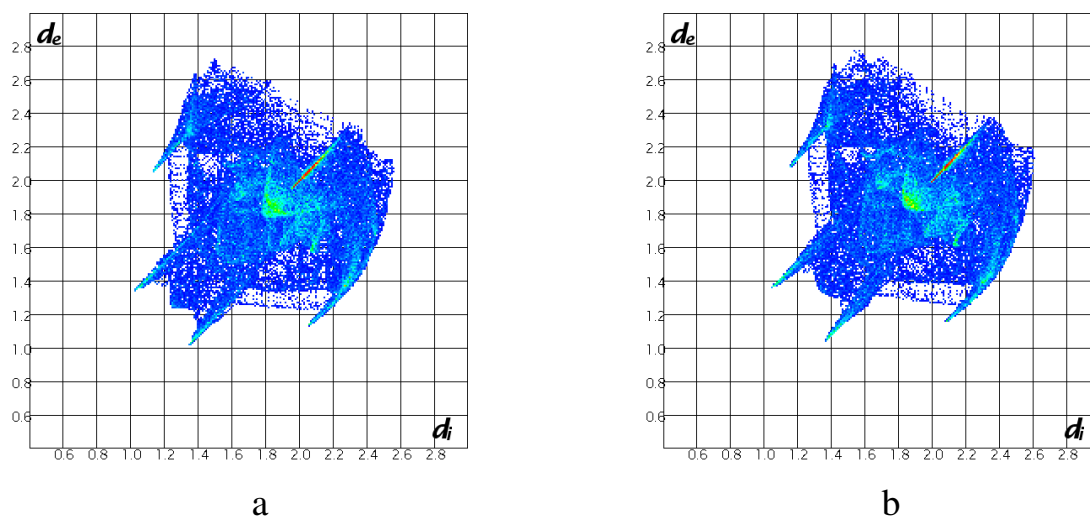
3.3.4.1 Iodine-Iodine Interactions

There are two inter-layer iodine-iodine interactions and two intra-layer iodine-iodine interactions (Figure 45).
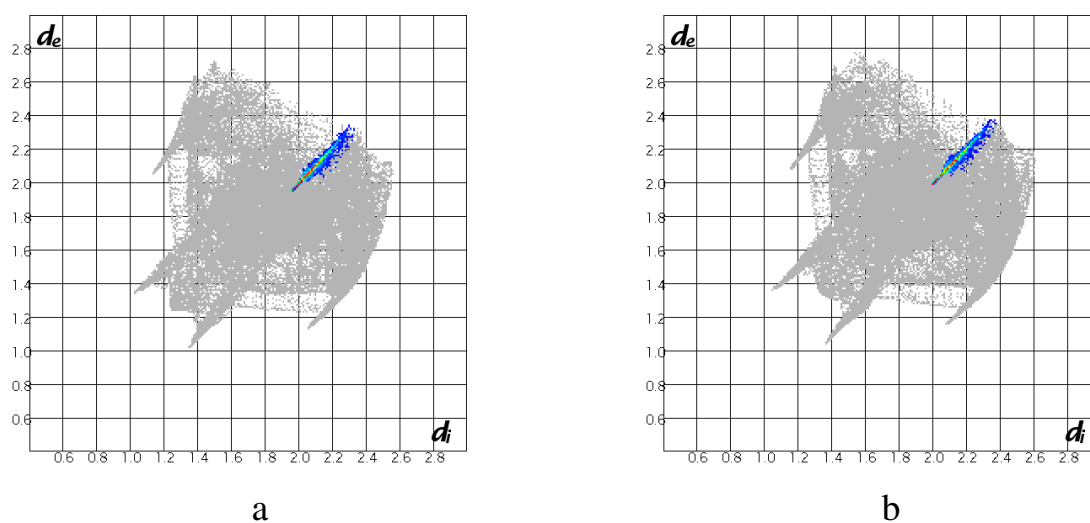
Figure 45. Fingerprint plots of iodine-iodine interactions at a) 100 K and b) 298 K.

The contribution of the iodine-iodine interactions towards the total Hirshfeld surface area in the structure decreases from 5.3% at 100 K to 5.1% at 298 K. Additionally, inspection of the iodine-iodine interactions reveals that both the distance and the angle between the interacting iodine atoms change with temperature (Figure 46a).
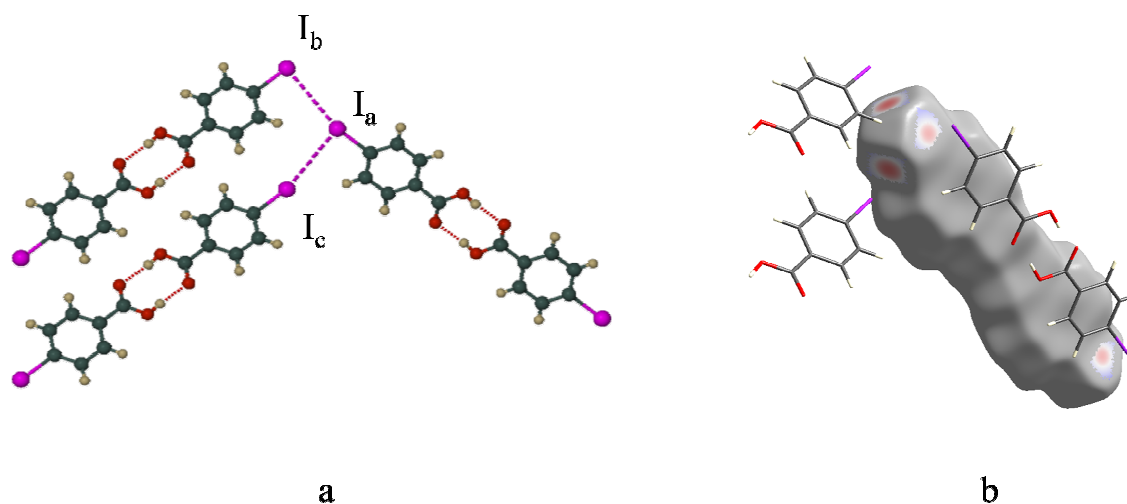
Figure 46. a) The iodine-iodine interactions between adjacent layers viewed along [100]. b) The iodine-iodine interactions within and between the various layers.

The two inter-layer iodine-iodine contacts ($I_a \cdots I_b$ and $I_a \cdots I_c$) are considered to be halogen bond interactions since they are shorter than the sum of the van der Waals radii (4.30 Å).[52] The four iodine-iodine interactions are indicated as red spots on the Hirshfeld surface (Figure 46b). The distance (*d*) between the iodine atoms of facing molecules increases from 4.057(6) Å to 4.161(2) Å.
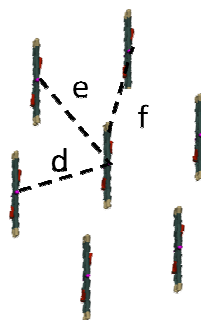
Figure 47. The intra-layer distances.

The remaining intra-layer iodine-iodine distances *e* and *f* increase from 5.942(8) Å to 6.034(2) Å and from 7.329(2) Å to 7.915(7) Å, respectively (Figure 47). These distances are longer than the sum of the van der Waals radii. The $C-I_a \cdots I_{b,c}$ angles also change with temperature. The $C-I_a \cdots I_b$ angle increases while the $C-I_a \cdots I_c$ angle decreases (Figure 46a). The changes in the $C-I_a \cdots I_{b,c}$ angles are attributed to the changes in the δ angle (Figure 48).
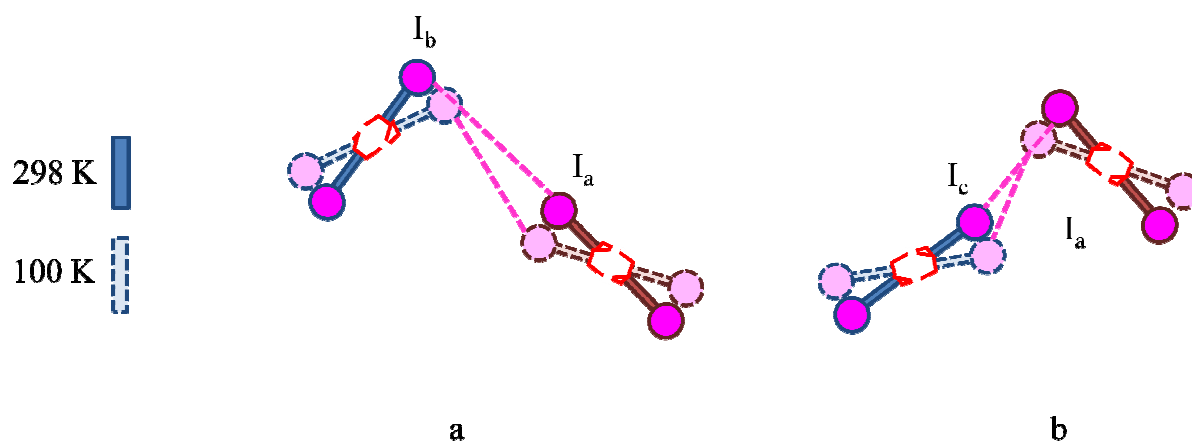
Figure 48. Schematic representation of the change in the angles between iodine molecules. a) The change in angle $C-I_a\cdots I_b$. b) The change in angle $C-I_a\cdots I_c$.

3.3.4.2 Carbon-Iodine Interactions
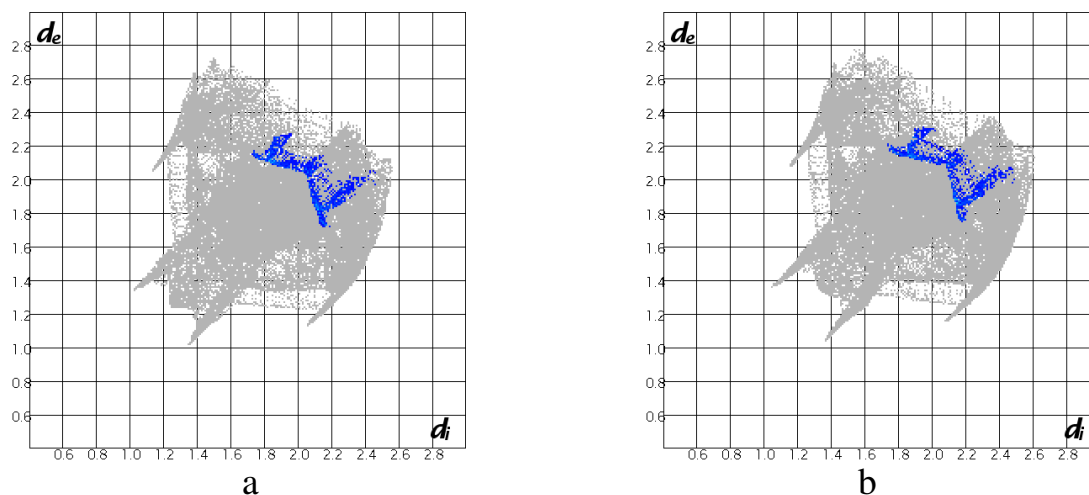
Figure 49. Fingerprint plots of the carbon-iodine interactions at a) 100 K and b) 298 K.

The contribution of the carbon-iodine interactions towards the total Hirshfeld surface area in this structure increases slightly from 2.1% at 100 K to 2.2% at 298 K (Figure 49).

The carbon-iodine bond length increases from 2.094(2) Å at 100 K to 2.099(4) Å at 298 K. However, the lengthening of carbon-iodine interactions results from the decrease in the δ angle. As the angle δ decreases the iodine atoms are moved closer to the ipso-carbons (red stars) in the neighbouring molecules (Figure 50a).
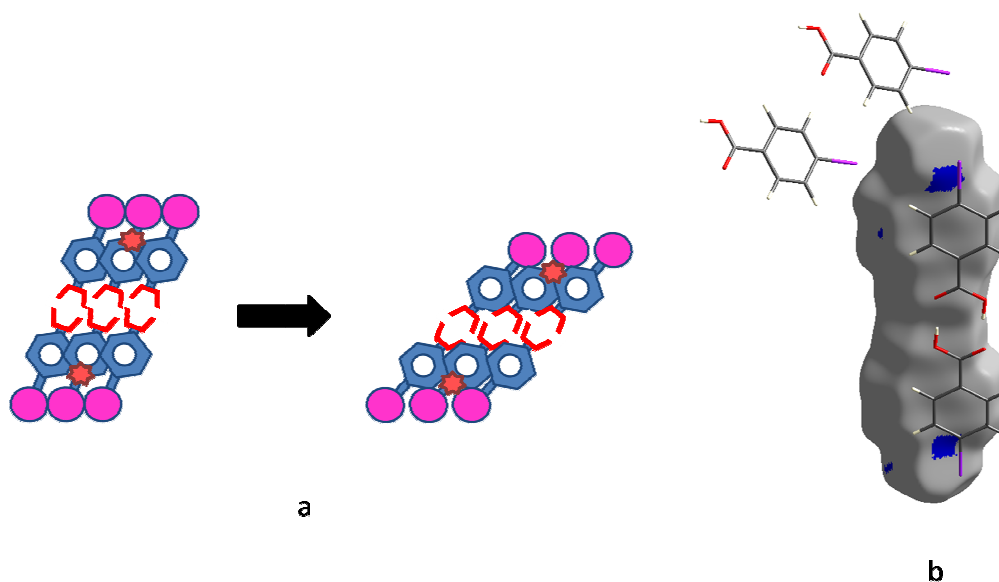
Figure 50. a) A schematic showing the effect of δ on the iodine-carbon interactions. b) Hirshfeld surface of the carbon-iodine interactions.

The Hirshfeld surface shows that the iodine atoms from adjacent layers do not take part in the carbon-iodine interactions. The adjacent layers are too far apart. Only the iodine atoms from neighbouring molecules are close enough to interact with the carbon atoms as shown in Figure 50b.

3.4 Methyl Paraben

3.4.1 Overview of Methyl Paraben

Clear crystals were grown by dissolving 20 mg of methyl paraben in 10 mL of solvent, which was allowed to evaporate over the course of a few days. Several different solvents were used namely: acetone, ethanol, methanol, tetrahydrofuran and xylene. A crystal grown from tetrahydrofuran was used for data collection. The unit cell parameters are reported in Table 11.

The Laue symmetry is 2/*m* indicating the monoclinic crystal system. Investigation of the reciprocal lattice layers confirmed the reflection conditions *hkl: h + k = 2n; h0l: l = 2n.* The program XPREP was used to confirm the space group as *Cc*.

Table 11. Unit cell parameters of Methyl paraben at 100 and 298 K respectively.

Temperature	100 K	298 K
Crystal system	Monoclinic	Monoclinic
Space group	*Cc*	*Cc*
a (Å)	12.912(13)	13.597(2)
b (Å)	17.334(19)	16.958(3)
c (Å)	10.814(9)	11.033(2)
β	118.89(2)	120.124(2)
Volume ($Å^3$)	2119.1(3)	2200.2(2)
Z	12	12
Density (g cm^{-3})	1.431	1.378
Mu (mm^{-1})	0.106	0.106
F(000)	960	960
R(int)	0.0309	0.0358
R	0.0463	0.0642
wR2	0.958	0.1468
GooF	0.957	0.983
$\Delta\rho_{max}$ (e $Å^{-3}$)	-0.20, 0.21	-0.45, 0.32

Bond lengths at 100 and 298 K are reported in Table 12. The atomic numbering scheme is provided in Figure 51.

Table 12. Bond lengths of Methyl paraben.

	Bond Length (Å)					
	Molecule 1		Molecule 2		Molecule 3	
Bond	100 K	298 K	100 K	298 K	100 K	298 K
O1-C1	1.366(2)	1.369(2)	1.360(3)	1.357(2)	1.364(2)	1.356(4)
C1-C2	1.382(4)	1.368(2)	1.391(3)	1.382(3)	1.389(3)	1.382(2)
C2-C3	1.391(2)	1.391(2)	1.380(3)	1.377(2)	1.390(3)	1.377(2)
C3-C4	1.393(2)	1.392(2)	1.396(2)	1.389(2)	1.388(2)	1.389(2)
C4-C7	1.473(3)	1.474(2)	1.482(2)	1.471(3)	1.492(3)	1.471(2)
C4-C5	1.405(3)	1.386(2)	1.407(4)	1.406(2)	1.404(4)	1.401(2)
C5-C6	1.386(2)	1.387(2)	1.392(3)	1.382(2)	1.388(2)	1.382(2)
C6-C1	1.399(2)	1.396(2)	1.403(2)	1.397(3)	1.400(3)	1.397(2)
C7- O2	1.219(2)	1.220(2)	1.214(2)	1.214(2)	1.214(2)	1.214(3)
C7- O3	1.333(2)	1.333(3)	1.338(3)	1.328(2)	1.346(3)	1.328(3)
O3-C8	1.447(3)	1.447(3)	1.453(3)	1.446(2)	1.457(3)	1.446(2)
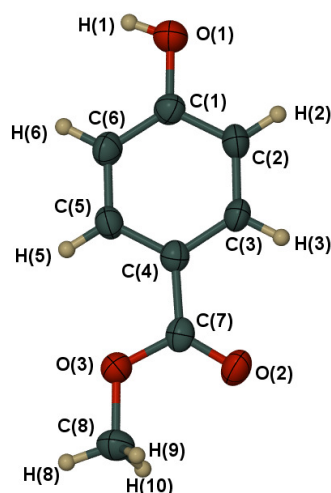
Figure 51. Thermal ellipsoid plot of methyl paraben (determined at 100 K) showing the thermal ellipsoids at the 50% probability level.

3.4.2 Packing of Methyl Paraben

The asymmetric unit consists of three crystallographically independent methyl paraben molecules (Figure 52a). The unit cell therefore contains twelve symmetry related molecules arranged in layers running parallel to the *b*-axis (Figure 52b).
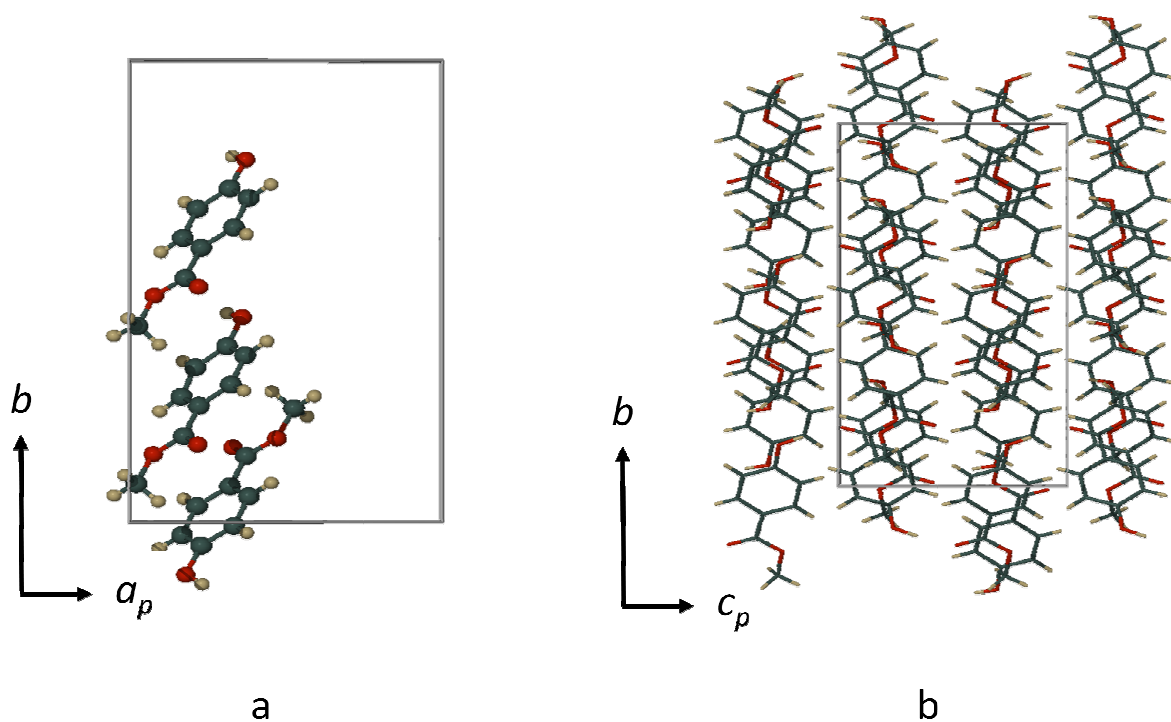
The layers are held together by hydrogen bonding between the hydroxyl group of one molecule and the ester group of another as shown in Figure 53. The hydrogen bonds form infinite chains, which span the crystal.
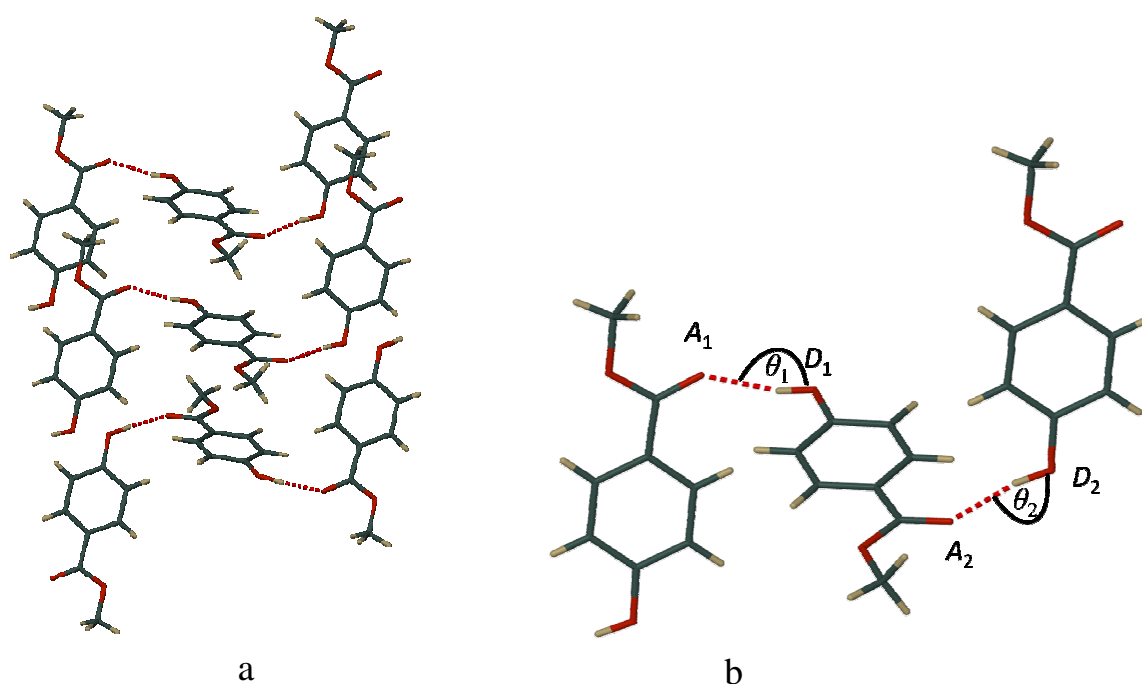
The hydrogen bond distances and angles are recorded in Table 13; they increase with increasing temperature.

Table 13. Hydrogen bond data at 100 and 298 K.

	Molecule 1		Molecule 2		Molecule 3	
Hydrogen bond angles (°)	**100 K**	**298 K**	**100 K**	**298 K**	**100 K**	**298 K**
θ_1	113.4(2)	146.0(4)	116.1(2)	146.5(4)	112.8(2)	145.0(4)
θ_2	113.4(2)	146.0(4)	112.8(2)	145.0(4)	116.1(2)	146.5(4)
Oxygen-oxygen distances (Å)						
A_1 - D_1	2.776(4)	2.785(6)	2.733(4)	2.776(7)	2.732(4)	2.771(7)
A_2 - D_2	2.776(4)	2.785(6)	2.732(4)	2.771(7)	2.733(4)	2.776(7)

3.4.3 Negative Thermal Expansion of Methyl paraben

The data listed in Table 11 indicate that methyl paraben undergoes negative thermal expansion along the *b*-axis. The change in the length of the *b*-axis is 0.378 Å (>> 3 × e.s.d) going from 100 K to 298 K, with α = -109.6 × 10^{-6} K^{-1}.

Three identifiable steps occur simultaneously as the crystal undergoes NTE:

- The molecules experience out-of-plane tilting relative to a reference plane
- The ester moieties of each of the methyl paraben molecules undergo a change in the torsion angle (τ_1) with a change in temperature.
- The methoxy moieties of each of the methyl paraben molecules undergo a change in the torsion angle (τ_2) with a change in temperature.

By applying these steps to a single molecule it is easier to visualise the effects that they have on the packing (Figure 54).
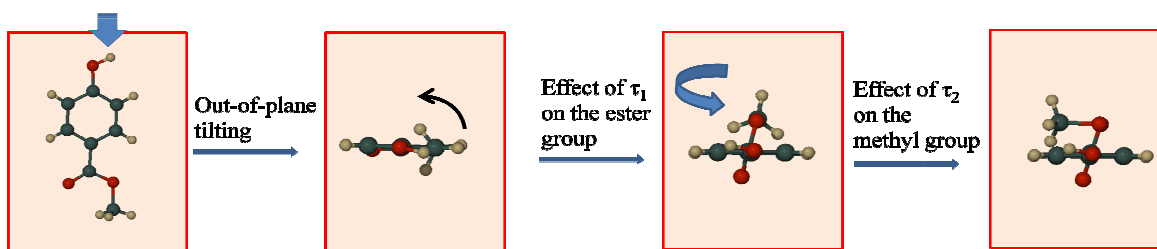
Figure 54. An exaggerated representation of what happens to a molecule with an increase in temperature.

3.4.3.1 The Mechanism of Negative Thermal Expansion in Methyl Paraben

3.4.3.1.1 STEP 1: Out-of-Plane Tilting

We define a mean plane passing through each molecule, as shown in Figure 55. The maximum deviation of any atom from the calculated plane was 0.0051 Å.
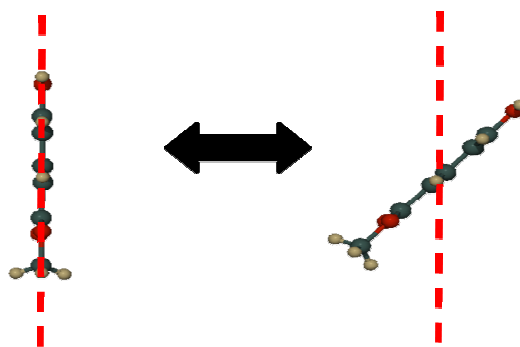
Figure 55. Out-of-plane tilting of methyl paraben.

Figure 56a shows the angular arrangement between the layers. The molecules tilt out of the plane when subjected to a temperature increase (Figure 56b and c).
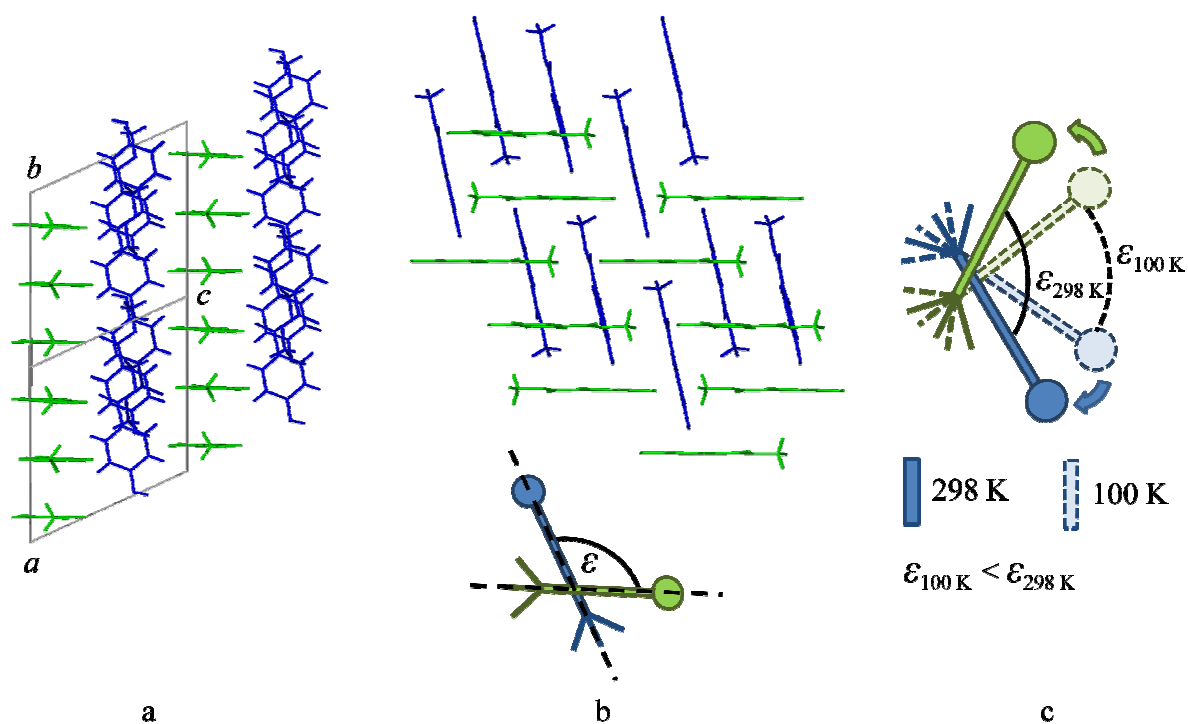
Figure 56. a) The different orientations of the layers. b) The angular relationship between the layers and a schematic representation (exaggerated) of the angle ε. c) A schematic representation of the out-of-plane tilting angles, ε_{100K} and ε_{298K}.

The degree of tilting is measured by the change in the angle ε (Figure 56b). The angle increases from 70.8(2)° at 100 K to 74.5(2)° at 298 K (Figure 56c). As ε increases, the b-axis contracts and the a-axis increases as shown in Figure 57.
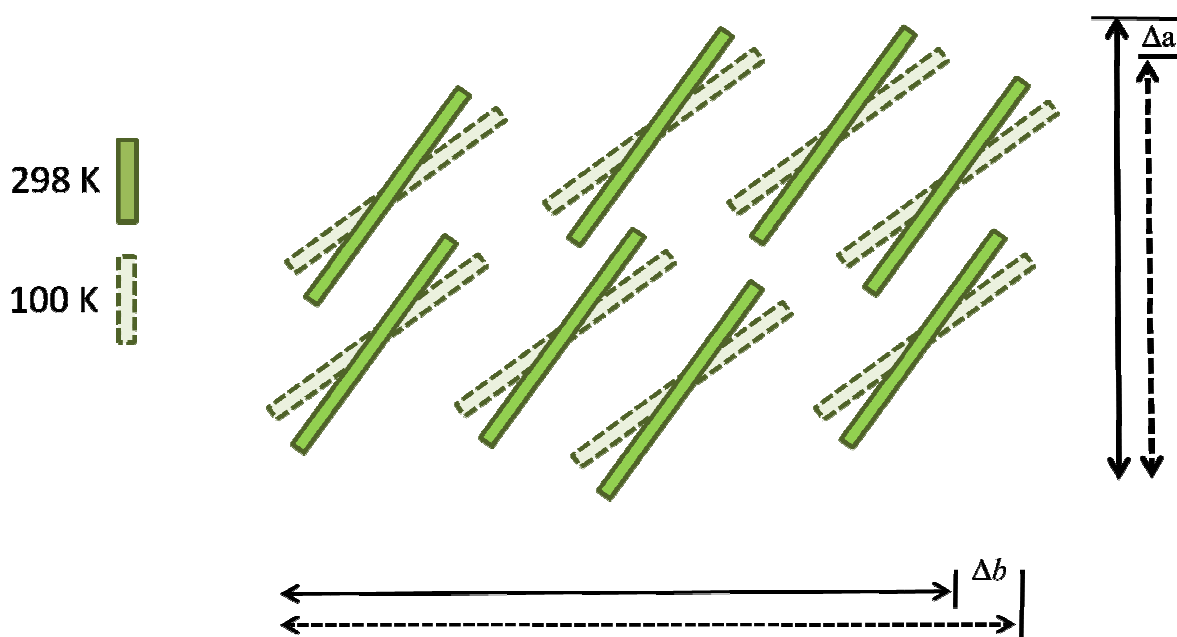
Figure 57. A exaggerated schematic representation of a single layer, illustrating the out-of-plane tilting of the molecules.

The change in ε also explains the larger positive thermal expansion along the *a*-axis relative to the *c*-axis (a change of 0.685 Å for the *a*-axis and 0.219 Å for the *c*-axis). When ε changes the *a*- and *b*-axes are affected (Figure 56a). However, the *c*-axis is not affected as much by the change in ε as the *a*-axis.

3.4.3.1.2 STEP 2: The Torsion Angle τ_1

Within each of the three unique molecules the ester moiety undergoes a change in the torsion angle τ_1.[56] The torsion angle is illustrated in Figure 58 and the magnitudes are recorded in Table 14.

τ_1: C1 - C2 - C3 - O4
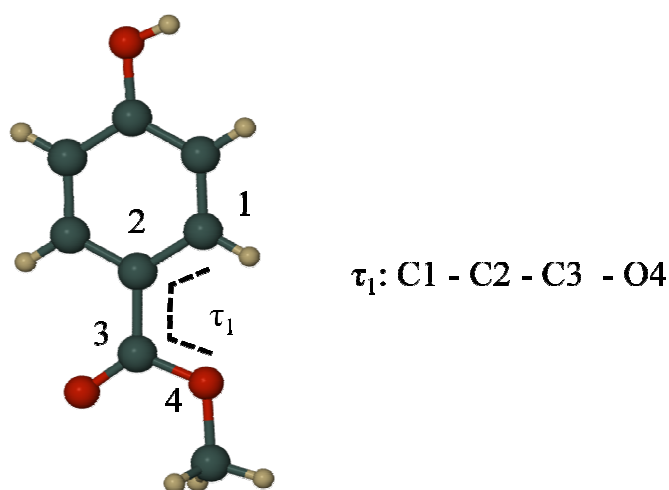
Figure 58. The torsion angle τ_1.

Table 14. Torsion angle τ_1 at 100 and 298 K.

	Temperature (K)	τ_1 (°)	$\Delta\tau_1$ (°)
Molecule 1	100	-4.21(2)	-0.29
	298	-4.50(3)	
Molecule 2	100	-1.31(2)	-1.97
	298	-3.28(3)	
Molecule 3	100	-3.21(2)	-0.05
	298	-3.26(2)	

Rotation of the torsion angle τ_1 moves the ester group out of the mean plane passing through the aromatic ring (Figure 59). Figure 59 shows an exaggerated representation of the torsion angle τ_1.
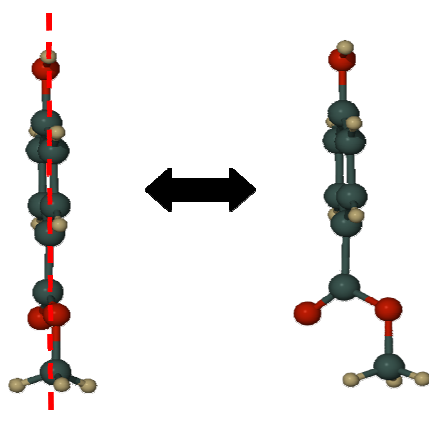
Figure 59. View along the mean reference plane, showing the torsion angle τ_1.
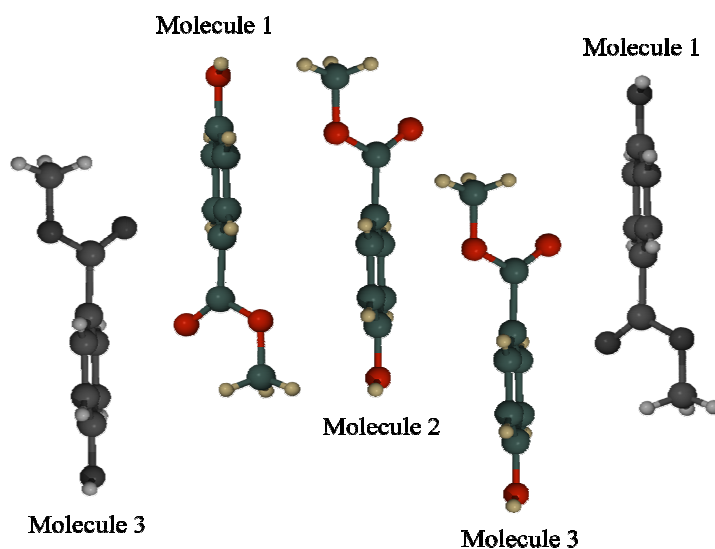
Figure 60. An exaggerated view of the effect of torsion angle τ_1 where the grey molecules are from adjacent instances of the asymmetric unit.

The influence of τ_1 on the structure is shown in Figure 60. The change in τ_1 causes an increase in the distances between molecules 1 and 2 and between molecules 2 and 3. The torsion angle also causes a decrease in the distances between molecules 1 and 3 of adjacent instances of the asymmetric unit and therefore allows for better interaction.

3.4.3.1.3 STEP 3: The Torsion Angle τ_2

Within each of the three unique molecules the methoxy moiety also undergoes a change in the torsion angle τ_2.[56] The torsion angle is illustrated in Figure 61 and the magnitudes are recorded in Table 15.

τ_2: O1 - C2 - O3 -C4
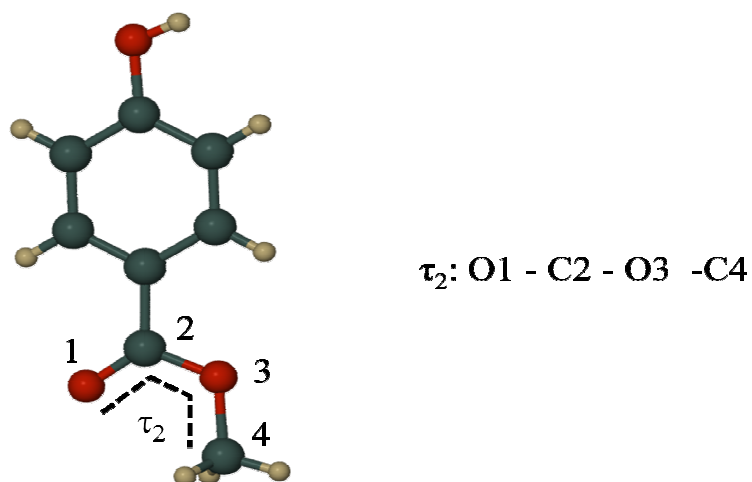
Figure 61. The torsion angle τ_2.

Table 15. Torsion angle τ_2 at 100 and 298 K.

	Temperature (K)	τ_2 (°)	$\Delta\tau_2$ (°)
Molecule 1	100	0.41(3)	-0.54
	298	-0.13(2)	
Molecule 2	100	-1.93(3)	4.02
	298	2.09(3)	
Molecule 3	100	2.08(2)	-4.54
	298	-2.46(3)	

Rotation of the torsion angle τ_2 moves the methoxy group out of the mean plane passing through the ester group (Figure 62). Figure 62 shows an exaggerated representation of the torsion angle τ_2.
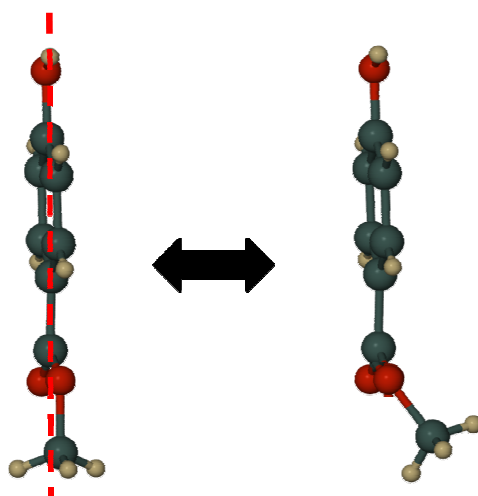
Figure 62. View along the mean reference plane showing the effect (exaggerated) of the torsion angle τ_2.

The change in τ_2 and its influence on the structure is shown in Figure 63. The change in τ_2 causes an increase in the distances between molecules 1 and 2 as well as between molecules 2 and 3. However, chnage in τ_2 also causes a decrease in the distances between molecules 1 and 3.
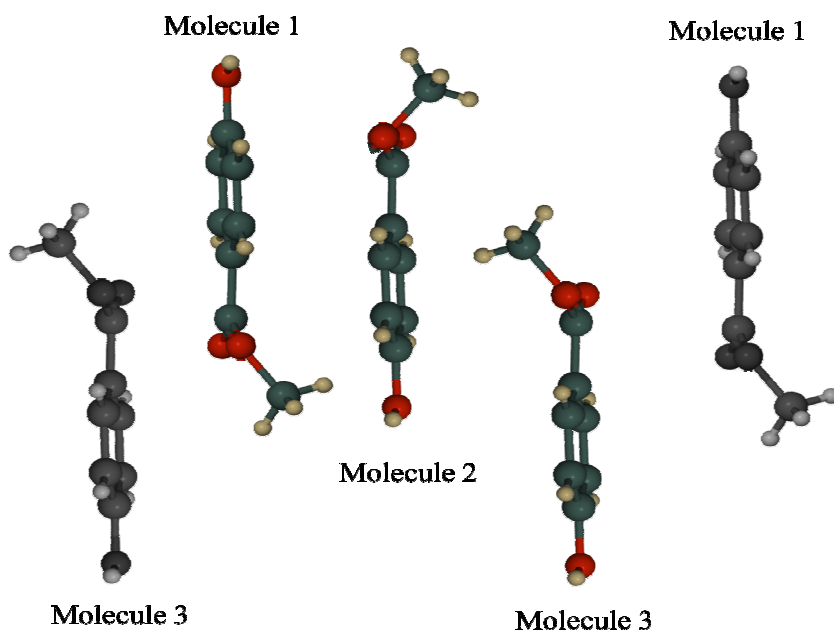
Figure 63. An exaggerated view of the effect of torsion angle τ_2 where the grey molecules are from adjacent instances of the asymmetric unit.

3.4.4 Intermolecular interactions

Hirshfeld surfaces and fingerprint plots were generated in order to examine the changes in the intermolecular interactions and in the packing arrangements after undergoing NTE. In order to obtain useful data from the fingerprint plots, they are decomposed to reveal the contribution of each interaction towards the total Hirshfeld surface area in the respective structures (Figures 64 and 65).

Methyl Paraben at 100 K

	Carbon-hydrogen	Carbon-carbon	Hydrogen-oxygen	Oxygen-oxygen	Hydrogen-hydrogen	Carbon-oxygen
Molecule 1	20.8	2.3	28.3	1.1	41.3	6.2
Molecule 2	21	2.4	29.3	0.8	40	6.4
Molecule 3	22.6	0.7	28.0	1.4	41.3	6.1
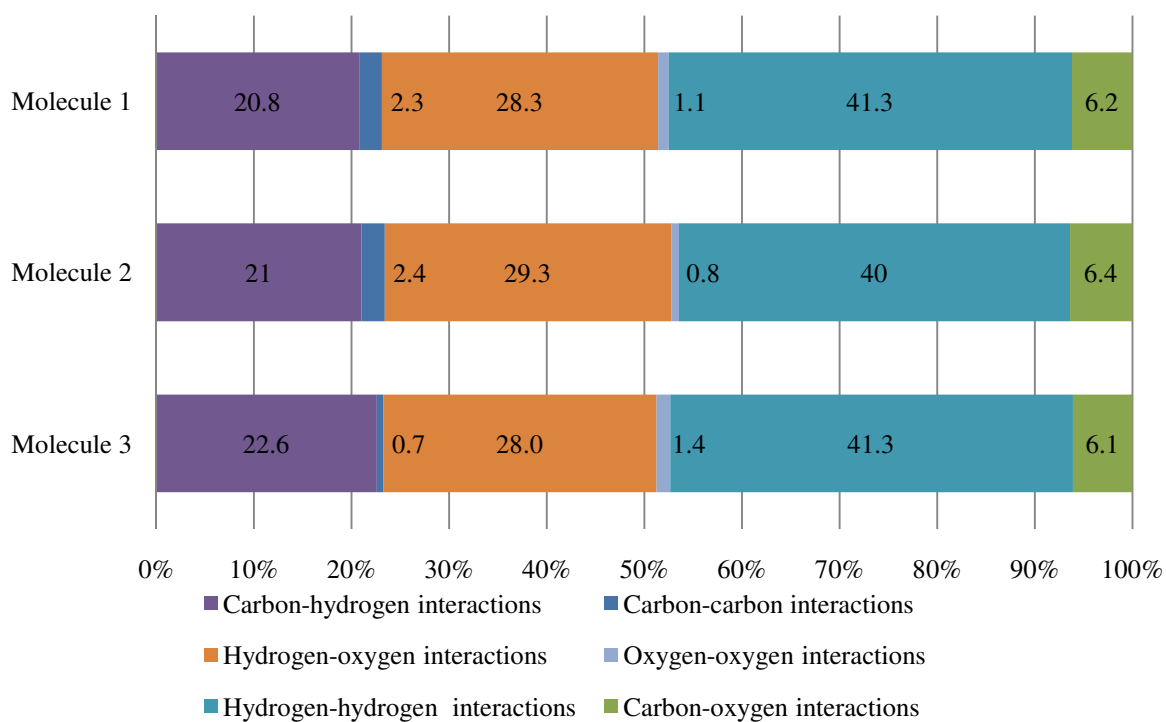
Figure 64. The contribution of all the interactions at 100 K towards the total surface area of methyl paraben molecules.

Methyl Paraben at 298 K

	Carbon-hydrogen	Carbon-carbon	Hydrogen-oxygen	Oxygen-oxygen	Hydrogen-hydrogen	Carbon-oxygen
Molecule 1	19.6	2.2	28.1	0.9	42.7	6.5
Molecule 2	19.1	2.8	29.5	0.4	41.6	6.5
Molecule 3	21.1	0.8	27.6	1	42.9	6.6
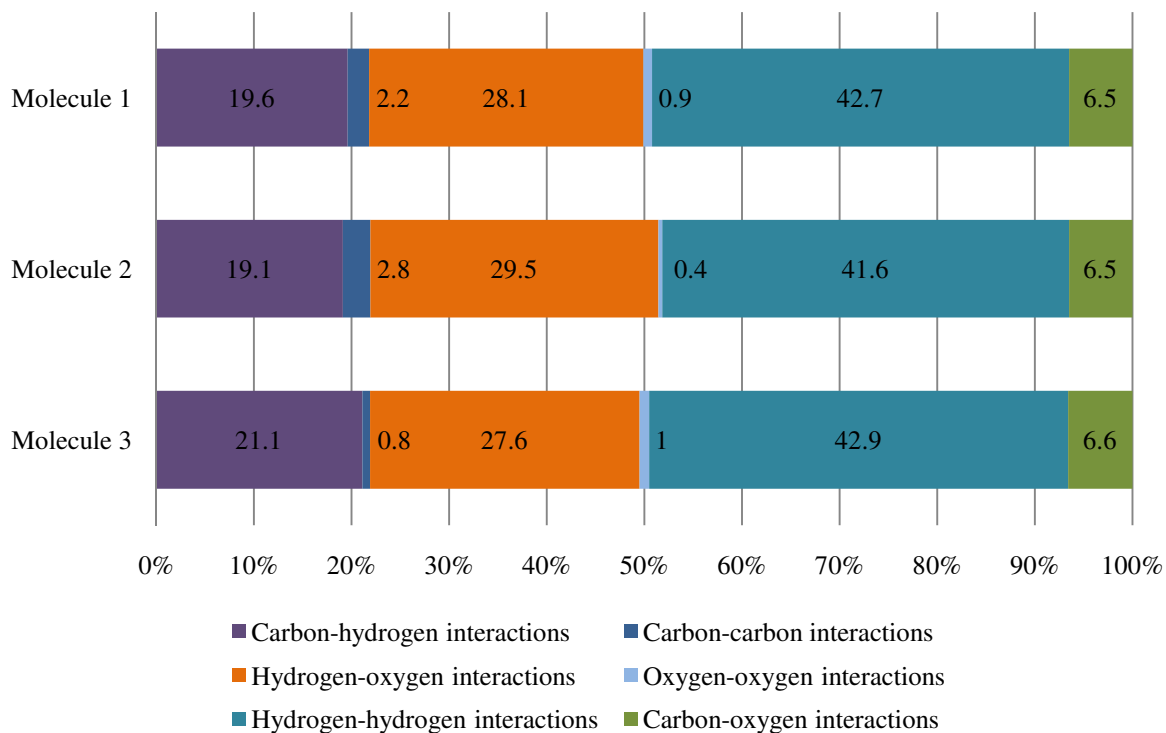
Figure 65. The contribution of all the interactions at 298 K towards the total surface area of methyl paraben molecules.

Fingerprint plots of each of the three molecules in the asymmetric unit are provided in Figure 66. It is evident that each of the three molecules is in a unique environment.

100 K

| Molecule 1 | Molecule 2 | Molecule 3 |

298 K

| Molecule 1 | Molecule 2 | Molecule 3 |
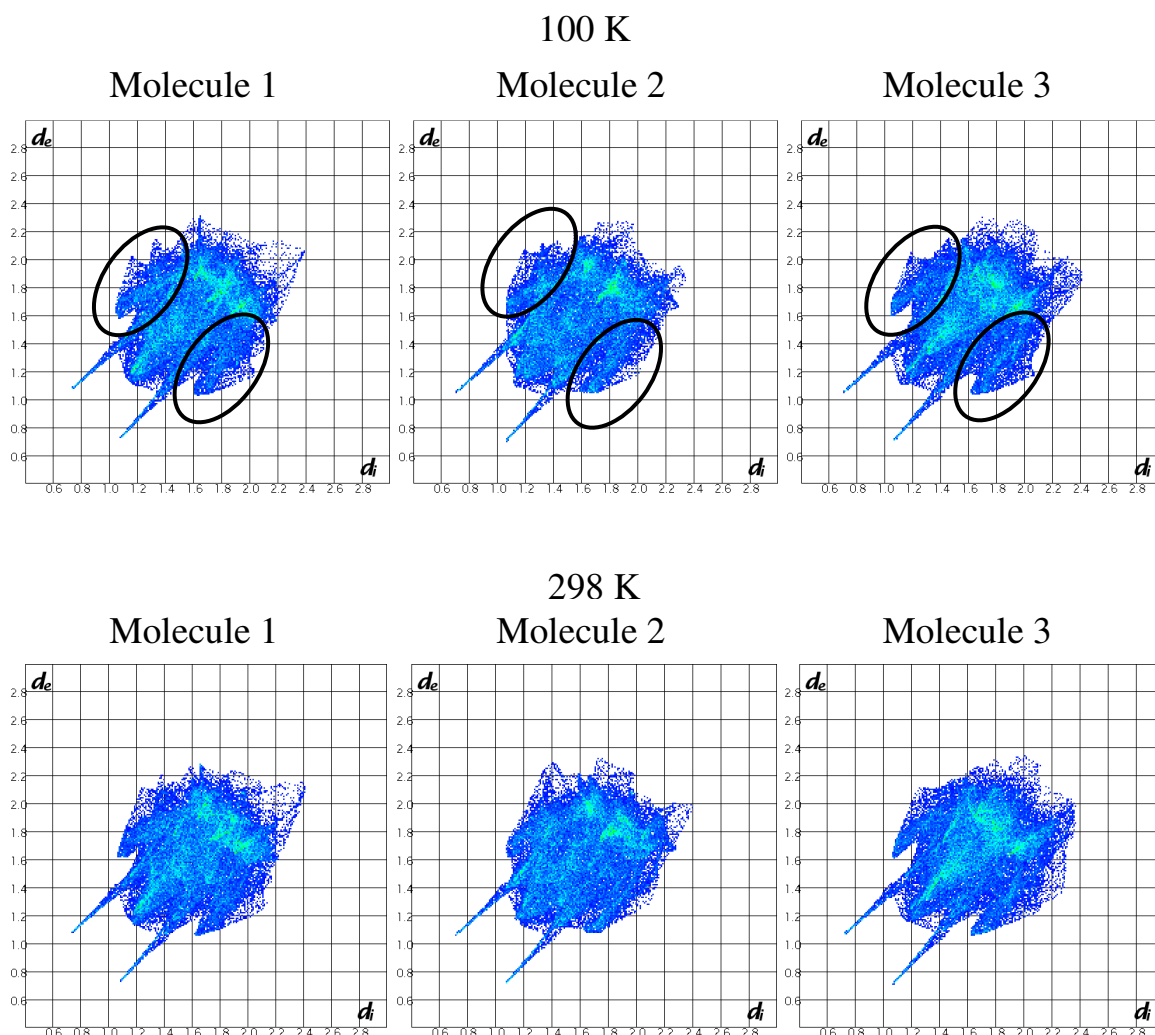
Figure 66. Fingerprint plots of the three molecules in the asymmetric unit at 100 K and at 298 K.

The largest differences between the fingerprint plots for the three molecules are indicated in Figure 66. The 'wings' seen in the plots for molecules 1 and 3 are a signature of CH···π interactions that are present for molecules 1 and 3 but not for molecule 2. This is due to the change in the torsion angles, which indicate that the ester groups of molecules 1 and 3 turn towards molecule 2. Molecules 1 and 3 therefore increase their distances to molecule 2 such that there are no CH···π interactions present. The torsion angles also indicate a favourable orientation between molecules 1 and 3. This is evidenced by the increase in CH···π interactions (Figure 66).

3.4.4.1 Carbon-Oxygen interactions

Figure 67 shows the contributions of the carbon-oxygen interactions towards the total Hirshfeld surface area in the structures of molecules 1, 2 and 3. The carbon-oxygen interactions of molecules 1, 2 and 3 increase with an increase in temperature.

Carbon-Oxygen Interactions

298 K	6.5 / 6.5 / 6.6	
100 k	6.2 / 6.4 / 6.1	

■ Molecule 1   ■ Molecule 2   ■ Molecule 3
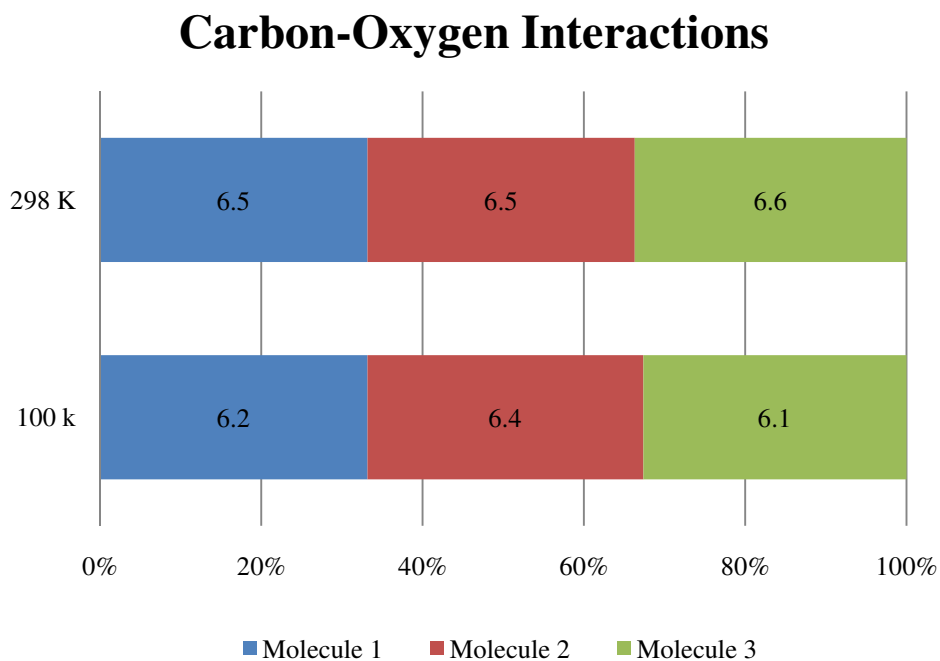
Figure 67. The contribution of the carbon-oxygen interactions to the Hirshfeld surface at 100 and 298 K.

The fingerprint plots of the carbon-oxygen interactions at 100 and 298 K are shown in Figure 68.

100 K

Molecule 1　　　　Molecule 2　　　　Molecule 3

298 K

Molecule 1　　　　Molecule 2　　　　Molecule 3
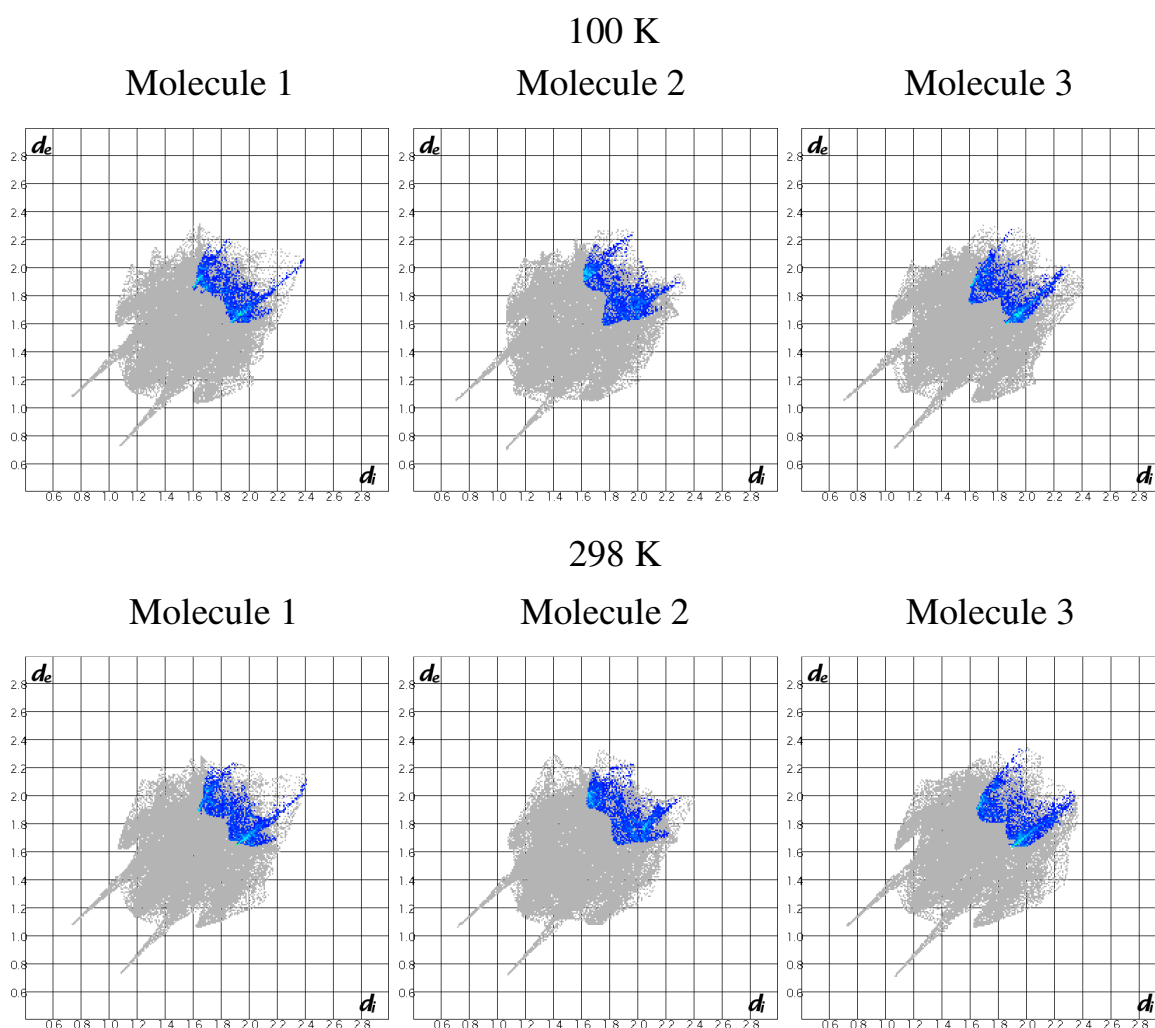
Figure 68. Fingerprint plots of the carbon-oxygen interactions of molecule 1, 2 and 3 at 100 K and at 298 K.

The increase in the contributions of the carbon-oxygen interactions towards the total surface area in the structures of the molecules can be seen in Figure 68. The carbon-oxygen interactions have a mean contact distance of 3.225 Å and range from 3.069 Å to 3.379 Å. The Hirshfeld surfaces of the carbon-oxygen interactions in molecules 1, 2 and 3 are shown in Figure 69.

3.4.4.2 Carbon-Carbon Interactions

Figure 70 shows the contributions of the carbon-carbon interactions towards the total Hirshfeld surface area for molecules 2 and 3.
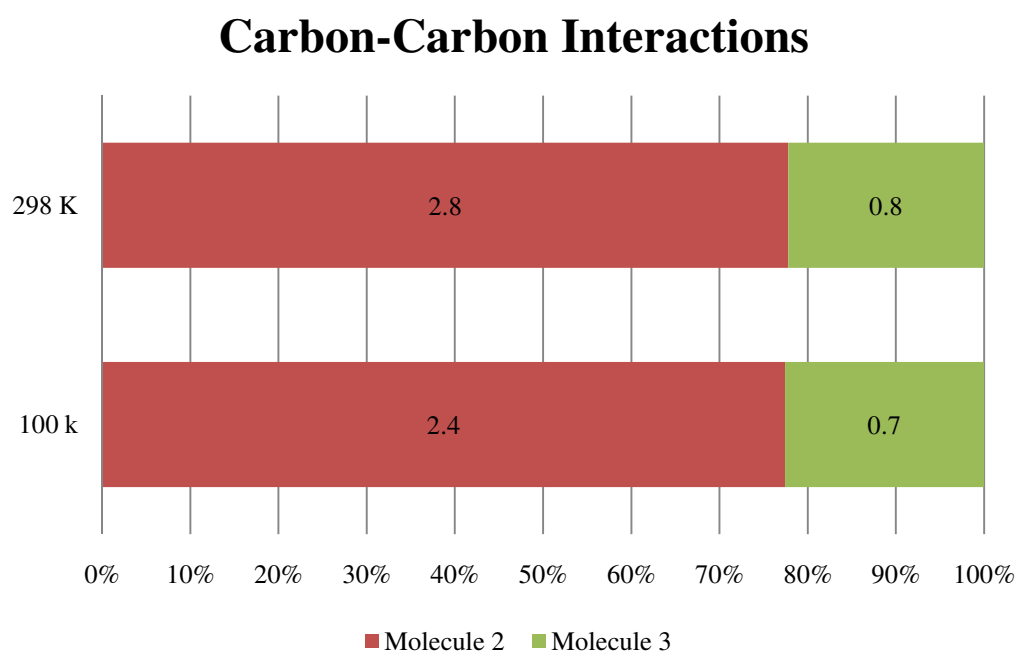
The fingerprint plots of the carbon-carbon interactions at 100 and 298 K are shown in Figure 71.

Molecule 2

Molecule 3

a

c

298 K

Molecule 2

Molecule 3

b

d

Figure 71. Fingerprint plots of the carbon-carbon interactions of molecules 2 and 3. Molecule 2 at a) 100 K and b) 298 K. c) Molecule 3 at 100 K and d) 298 K.

The mean carbon-carbon interaction distance is 3.412 Å and ranges from 3.401 Å to 3.566 Å. The Hirshfeld surfaces of the carbon-carbon interactions in molecules 2 and 3 are shown in Figure 72.

a   b   c
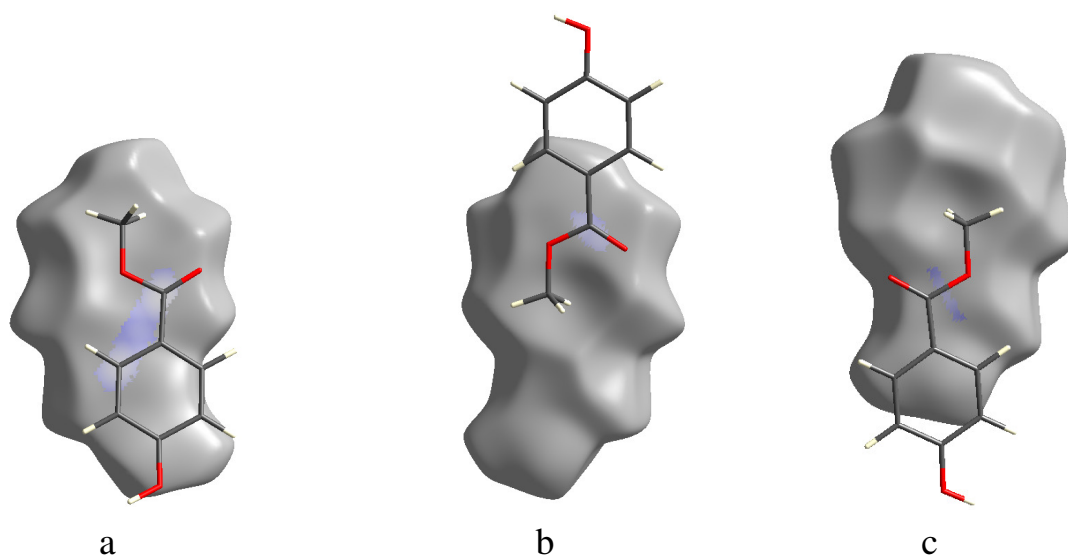
Figure 72. a) Carbon-carbon interactions between molecules 1 and 2. b) Carbon-carbon interactions between molecules 2 and 3. c) Carbon-carbon interactions between molecule 3 and a symmetry related instance of itself.

Chapter 4
Discussion and Conclusion

This chapter summarises the findings reported in *Chapter 3*. General conclusions are drawn about the mechanisms of the observed negative thermal expansion.

The main objectives of this study were to identify new compounds that undergo NTE, and to analyse some of the key aspects of the underlying mechanisms; both of these aims have been achieved.

Twenty compounds (Scheme 1 and Table 16) were investigated, all of which have similar structural characteristics. In addition, several compounds were identified from a literature survey and used for comparisons (Table 16).

Table 16. Compounds that were studied.

4,4'-disubstituted benzene	4,4'-disubstituted biphenyl	4-Halo-benzoic acid	Paraben
4,4'-Chlorobromobiphenyl	4,4'-Chlorobromobiphenyl	4-Cholorbenzoic acid	*Methyl paraben**
4,4'-Dichlorobiphenyl	4,4'-Bromoflourobiphenyl	4-Bromobenzoic acid	Ethyl paraben
4,4'-Dibromobiphenyl	4,4'-Dichlorobiphenyl	*4-Iodobenzoic acid**	Propyl paraben
4,4'-Diiodobiphenyl	4,4'-Dibromobiphenyl	4-Hydroxybenzoic acid	Butyl paraben
	4,4'-Diiodobiphenyl*		4-Bromobenzoate
			4-Iodobenzoate
			Methyl 4-iodobenzoate

* *Present study*

The first compound to show NTE was 4,4'-diiodobiphenyl and the compounds shown in Table 16 were obtained by systematically changing the substituent groups. 4-Iodobenzoic acid and methyl paraben were obtained from the CSD and a literature survey, respectively. These two were chosen because 4-iodobenzoic acid is somewhat analogous to 4,4'-diiodobiphenyl, while methyl paraben is analogous to 4-iodobenzoic acid.

4.1 Packing Arrangements

4.1.1 Molecular Geometry

4,4'-Diiodobiphenyl, 4-iodobenzoic acid and methyl paraben share certain similarities in their molecular geometries. For instance, 4,4'-diiodobiphenyl is a planar centro-symmetric molecule while 4-iodobenzoic acid forms a planar and centrosymmetric hydrogen bonded dimer. However, methyl paraben is planar but noncentrosymmetric. For the 4,4'-disubstituted biphenyls the non-planar molecules (i.e. molecules with a non-zero torsion angle between the

phenyl rings) do not exhibit NTE while, in the case of the benzoic acid analogs, only 4-iodobenzoic acid undergoes NTE. Of the four paraben molecules, only methyl paraben undergoes NTE.

Similarities between 4,4'-diiodobiphenyl, 4-iodobenzoic acid and methyl paraben are reflected in their packing arrangements as well. The compounds 4,4'-diiodobiphenyl and 4-iodobenzoic acid are arranged in two-dimensional layers with interpenetrating iodophenyl moieties. In both cases the interpenetration occurs at ¼ and ¾ along the longest axis (*b* or *c*) of the respective unit cells while they also exhibit the zigzag motif along those same directions.

The zigzag motif is a consequence of the negative electrostatic potential distributions and atomic size (described earlier) of the iodine atoms. The negative electrostatic potential distribution for CH_3X (where X = F, Cl, Br, I) serves as a sound basis from which to extend the concepts of negative electrostatic potential and atomic size to larger halogenated compounds such as 4,4'-diiodobiphenyl and 4-iodobenzoic acid.[50] Negative electrostatic potential distributions indicate that it is less favourable for the iodine interactions to occur in a linear head-to-head arrangement than it is for either fluorine or chlorine (Figure 73).
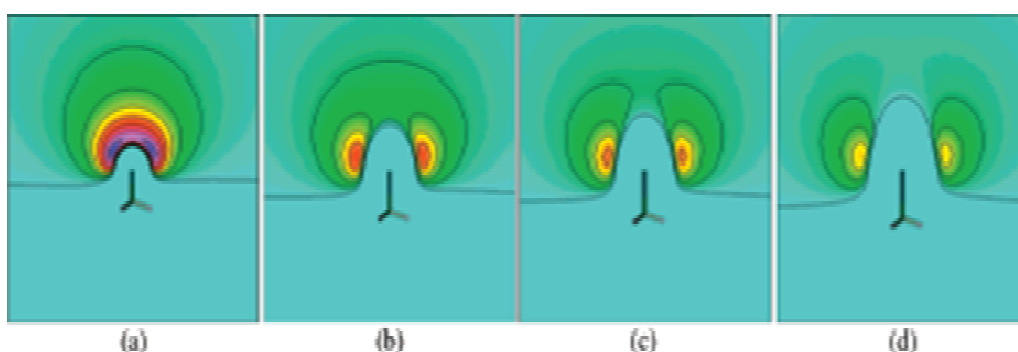
Figure 73. Negative electrostatic potential for CH_3X where X is a) F b) Cl c) Br d) I.[50]

The larger the halogen, the greater is its polarizability. An increased polarizability leads to greater tendency for the C-halogen⋯halogen angles to deviate from the ideal head-on geometry, as is observed for iodine.[49] As

previously mentioned size, shape and geometry of the molecular building blocks are more significant than reactivity in the formation of supramolecular entities.

The layers of 4-iodobenzoic acid and methyl paraben have similar arrangements. When the structures of 4-iodobenzoic acid and methyl paraben are both viewed along their *ab* diagonal, one can clearly see that they are analogous to each other in terms of the relative orientations of the alternate layers (Figure 74).
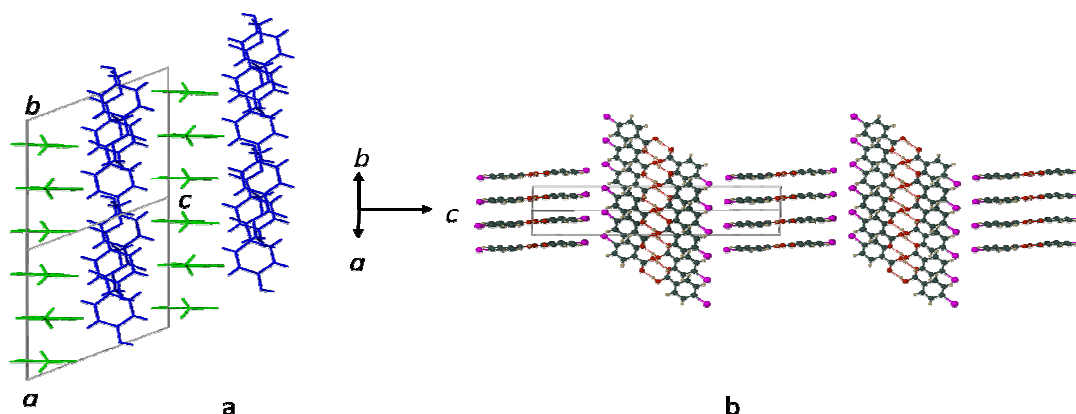
Figure 74. Packing of a) methyl paraben and b) 4-iodobenzoic acid.

4.1.1.1 4,4'-Disubstituted Biphenyl Analogs of 4,4'-Diiodobiphenyl

Fluorine atoms are much smaller than iodine atoms (fluorine is 15% the size of iodine) and are therefore able to interact in a more linear fashion (Figure 75).
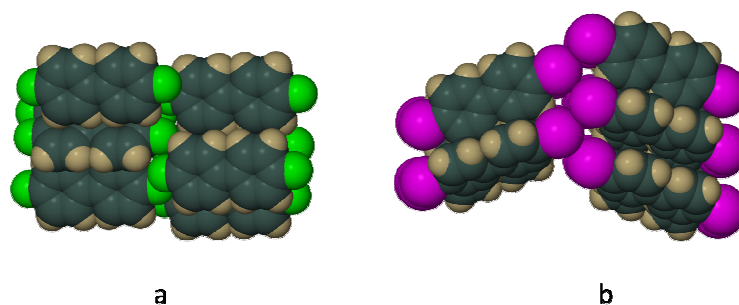
Figure 75. Packing of a) 4,4'-difluorobiphenyl and b) 4,4'-diiodobiphenyl.

An example of the head-to-head packing arrangement observed for 4,4'-disubstituted biphenyl is shown in Figure 76. It is clear that the layers do not pack in the zigzag motif.
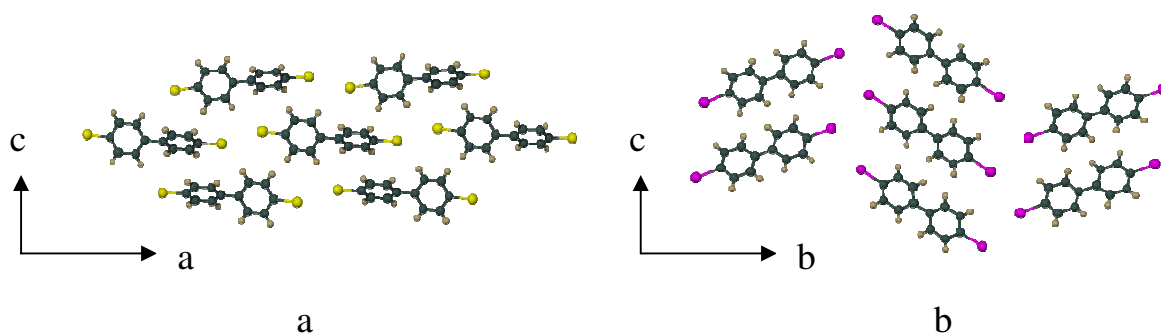
The 4,4'-difluoro- and 4,4'-dihydroxybiphenyl molecules are the only close analogs of 4,4'-diiodobiphenyl that are planar. However, unlike diiodobiphenyl, the layers of the difluoro and dihydroxy substituted biphenyls are parallel (Figure 77).
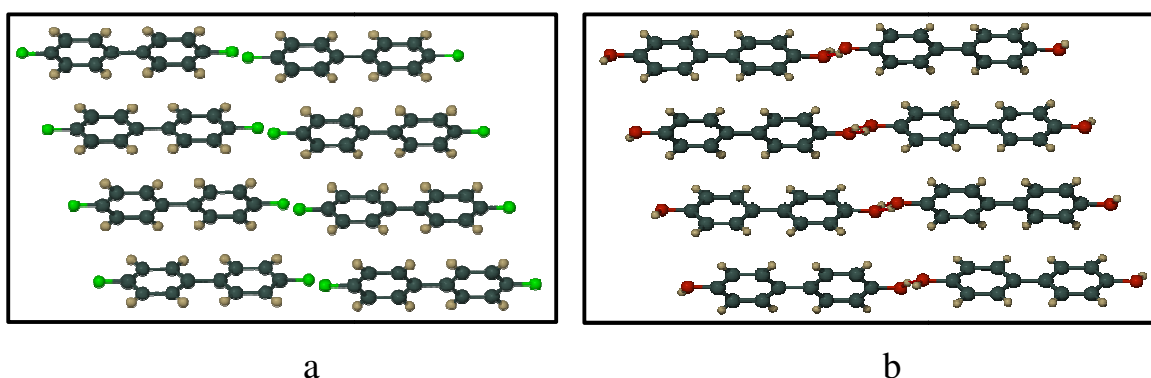
Figure 77. a) Packing of 4,4'-difluorobiphenyl. b) Packing of 4,4'-dihydroxybiphenyl.

Another common structural feature shared by the three di-substituted biphenyls is the presence of a herringbone packing arrangement of which the herringbone angle is a consequence (Figure 77). (The herringbone angle of 4,4'-diiodobiphenyl is discussed in *Chapter 3*). Herringbone packing has been reported as a key feature of the mechanism of NTE in pentacene.[25]
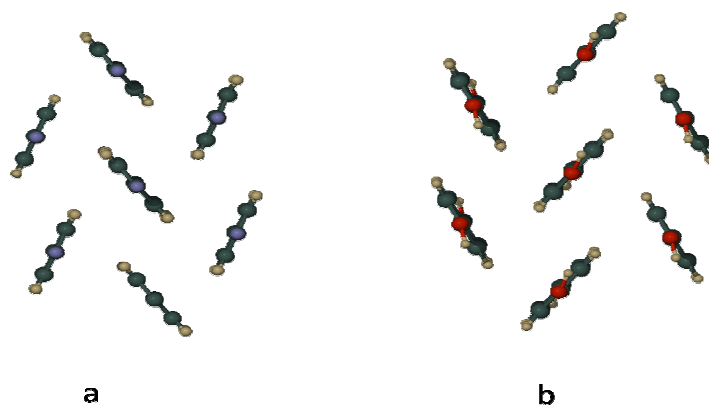
Figure 78. Herringbone packing arrangements of a) 4,4'-diflourobiphenyl and b) 4,4'-dihydroxybiphenyl.

Both 4,4'-difluoro- and 4,4'-dihydroxybiphenyl have the herringbone packing arrangement, but neither undergoes negative thermal expansion. Thus, the presence of the herringbone packing arrangement, and consequently the herringbone angle, is not essential for compounds to undergo NTE.

4.1.1.2 4-Halobenzoic Acid Analogs of 4-Iodobenzoic Acid

The 4-chloro and 4-bromobenzoic acid analogs of 4-iodobenzoic acid were also investigated but neither showed evidence of NTE. The primary differences between 4-chloro-, 4-bromo- and 4-iodobenzoic acid can be discerned from the packing arrangements of the molecules. The packing arrangement of 4-chloro- and 4-bromobenzoic acid show that the molecules are arranged parallel to one another in a head-to-head manner (Figure 79a and 79b). 4-Iodobenzoic acid packs in a zigzag arrangement, which it shares with 4, 4`-diiodobiphenyl (Figure 79c). All three 4-halobenzoic acid dimers are planar. Thus, planarity is not essential for compounds to undergo NTE.

a

b

c
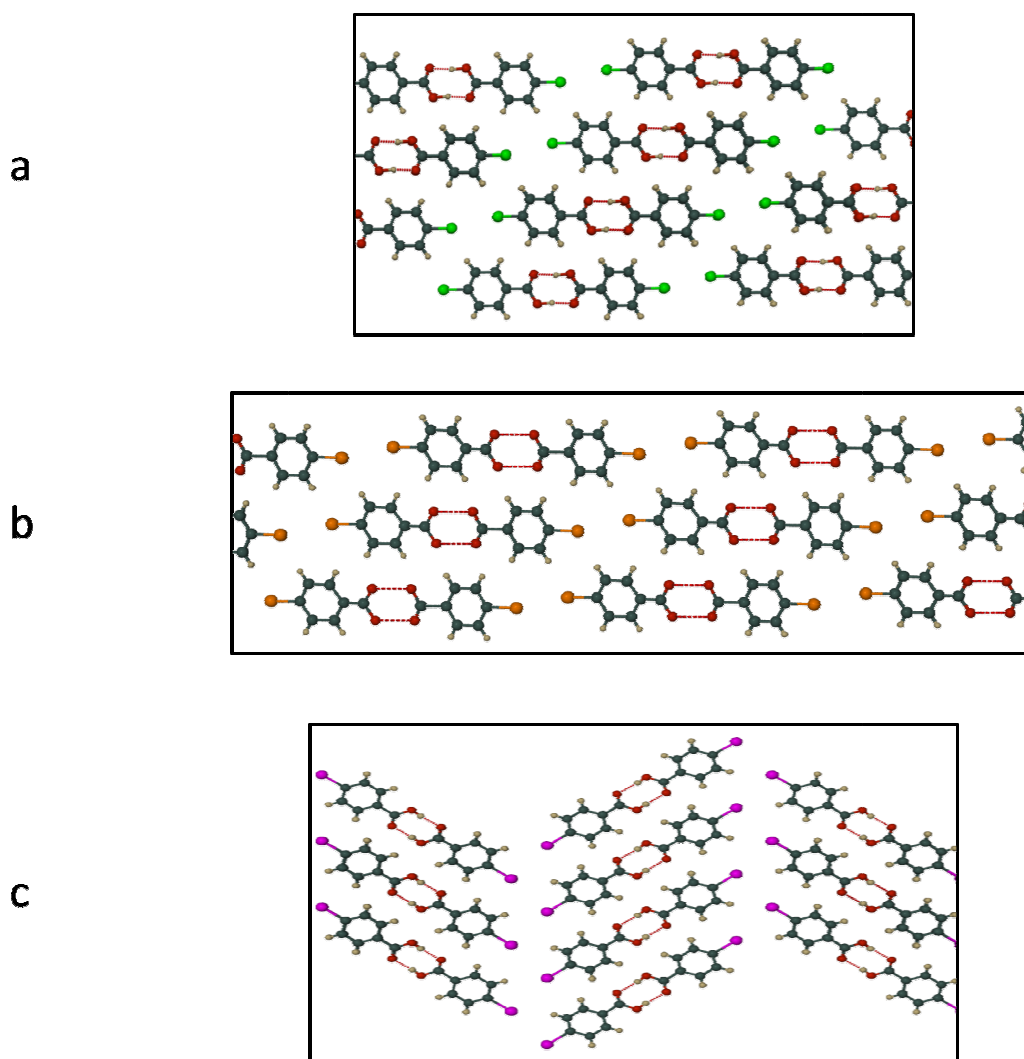
Figure 79. Packing diagrams of a) 4-chlorobenzoic acid, b) 4-bromobenzoic acid and c) 4-iodobenzoic acid.

None of the 4-halobenzoic acids exhibit the herringbone packing arrangement within the layers (Figure 80).

Figure 80. Packing of the molecules of the respective 4-halobenzoic acids (x = Cl, Br, I) as viewed along the halogen-halogen vector.

4.1.1.3 Paraben Analogs

Of the parabens, methyl paraben is the only one to show an angular arrangement between the layers. Ethyl and propyl paraben experience positive

thermal expansion, while butyl paraben appears to undergo a phase transition based on unit cell determinations (see Table 4). It seems that when the ester chain becomes longer than a methyl group the NTE behaviour is lost. It is therefore rationalized that the size and flexibility of the ester group outweighs the effect of the change of the torsion angles. This becomes apparent when comparing the torsion angles of the methyl and ethyl parabens to each other (Table 17).

Firstly, the changes in the torsion angle τ_1 of methyl and ethyl paraben are comparable. However, the change in the torsion angle τ_2 of ethyl paraben is much smaller than that of methyl paraben. This implies that the movement of the ethoxy group is much smaller than that of the methoxy group. It was also observed that the ethyl group in ethyl paraben undergoes an observable change in position as reflected by the change in the torsion angle τ_3 (Table 17).

Table 17. Torsion angles of methyl and ethyl paraben.

	Methyl Paraben		Ethyl Paraben		
	$\Delta\tau_1$ (°)	$\Delta\tau_2$ (°)	$\Delta\tau_1$ (°)	$\Delta\tau_2$ (°)	$\Delta\tau_3$ (°)
Molecule 1	-0.29	-0.54	0.48	0.05	7.38
Molecule 2	-1.97	4.02	0.90	0.28	7.13
Molecule 3	-0.05	-4.54			

τ_1: C1 – C2 – C3 – O5
τ_2: O4 – C3 – O5 – C6
τ_3: C3 – O5 – C6 – C7
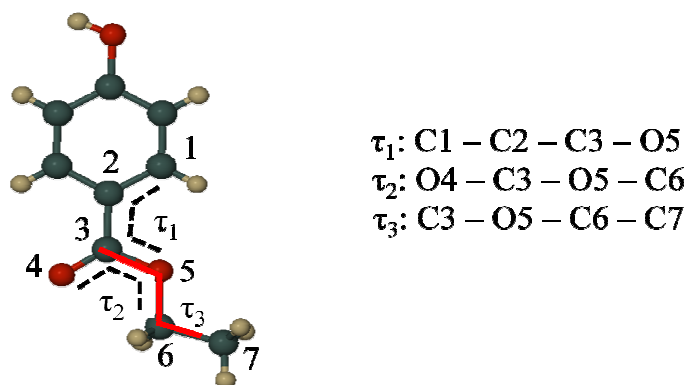
Figure 81. Torsion angles τ_1, τ_2 and τ_3 of ethyl paraben.

The torsion angle τ_3 is indicated by the red line in Figure 81 and involves atoms C3, O5, C6 and C7, which belong to the ethyl ester moiety. Ethyl

paraben does not have the angular arrangement between adjacent layers as observed with methyl paraben.

4.2 Interactions

Two of the three NTE compounds presented (4,4'-diiodobiphenyl and 4-iodobenzoic acid) experience an increase in the carbon-iodine interactions. It was also observed that the carbon-carbon and carbon-oxygen interactions of methyl paraben increase with increasing temperature. The increases in the interactions indicate that the molecules are moving closer to one another. The tendency of different halogens to be involved in strong halogen bonding is opposite in sequence to their electronegativity: I > Br > Cl > F.

The overall effect of the intermolecular interactions is that the cumulative strengths of the intermolecular interactions are sufficient to resist thermal stress as temperature increases. The resistance to thermal stress allows NTE to occur under relatively gentle conditions.

4.3 Mechanisms of NTE

The compounds presented here undergo three distinct processes during NTE. The first is an in-plane tilting of the molecules as seen by both 4,4'-diiodobiphenyl and 4-iodobenzoic acid. The second is out-of-plane tilting observed in all three compounds and the third is a rotation. This rotation is found with both 4,4'-diiodobiphenyl and methyl paraben as a rotation of the molecules or the substituents, respectively.

A comparison of the mechanism of NTE of the compounds reported here and those reported in the literature, reveals some common features. The principal processes that induce NTE in previously reported compounds can be divided into two categories:

1) Changes in tilt angle (in-plane or out-of-plane tilting)
2) Changes in the herringbone angle

A third mechanism for NTE was observed in a hydrated di-peptide. However, this phenomenon is as a result of the ordering of guest water molecules. This is not considered in here as the NTE is primarily related to the guest molecules and not the host structure.

4,4'-Diiodobiphenyl and 4-iodobenzoic acid are unique in the sense that they can be placed in both of the abovementioned categories whereas most compounds can only be placed in one. For example, (S,S)-octa-3,5-diyn-2,7-diol undergoes a change in tilt angle but there are no herringbone angles. Pentacene, on the other hand, undergoes a change in the herringbone angle but exhibits no tilting. Methyl paraben undergoes a change in a tilting angle (category 1) but it is the only compound to undergo changes in torsion angles.

Since 4,4'-diiodobiphenyl, 4-iodobenzoic acid and methyl paraben have similarities in their crystal structures, it is not surprising that there are similarities in the mechanisms. However, despite having certain common features in their mechanisms, each compound has a unique mechanism for NTE.

4.4 Concluding Remarks

Crystalline organic materials that exhibit NTE are unique in the sense that the mechanisms for NTE are fundamentally different from those found in other materials. Crystalline organic materials are generally held together by weak van der Waals and hydrogen-bonding interactions. These interactions expand easily with increasing temperature.[32] To counteract the expansion it is proposed that a change in a structural feature should outweigh the normal tendency for crystalline organic materials to expand upon heating. The work reported here has revealed several compounds that are capable of achieving this. Even though a number of mechanisms have been proposed to explain NTE, this behaviour is still not well understood. The compounds that were studied undergo only small changes (changes in orientation and intra- and

intermolecular distances) but it is the cumulative effect of these changes that bring about NTE. The cumulative strength of the interactions is able to redirect thermal stress into a structural response during heating rather than resulting in a melt.

Finding organic compounds that exhibit NTE still remains a challenge. The widely used CSD reports the majority of compounds at single temperatures and researchers rarely carry out variable temperature studies on compounds (for instance, determining unit cells at both low temperature and room temperature). For example, for 4,4'-diiodobiphenyl the structure of only a single temperature was reported in the CSD and it would thus not have been identified as a possible candidate. When differences arise that seem to be the result of NTE, questions surrounding the experimental conditions remain. Were the data collected on the same instrument? Were the data collected using the same crystal? Furthermore, it is often the tendency to dismiss NTE as experimental error, anisotropy or even poor crystal quality. It is evident that a standard procedure will be helpful when data are reported (e.g. in the CSD). Also, standard reporting procedures may assist in the determination of properties, such as NTE in this case.

This study has added three compounds to the list of organic compounds that experience NTE (a contribution of ≈ 40 %). We have described each crystal structure in terms of the nature of the molecular structure, the packing arrangement and the type of intermolecular interactions. We have identified certain common features present in molecules that undergo NTE:

- Planar aromatic molecules make up a large contingent (40%) of molecules currently known to exhibit NTE in the solid state.
- The type of halogen substituent has an influence on the packing of the molecules in the solid state
- Molecules that have hinge- or scissor-type motion in addition to their usual transverse vibrations may facilitate NTE.

It has been reported that conformational changes require small amounts of energy for their implementation.[57] Therefore, thermal stress in the compound is alleviated by a structural response rather than by melting. The structural response is energetically 'cheaper' than interrupting the halogen interactions or the cumulative stabilizing effects of the van der Waals interactions. The structural responses to thermal stress are what we observe as NTE.

In their publication on methyl paraben, Vujovic *et al.* suggested that methyl paraben forms conformational polymorphs in response to the thermal conditions.[56] In a follow-up publication, Threlfall *et al.* argued that these changes are not conformational polymorphs but rather affects of anisotropy.[58] They stated that the shortening of the *b*-axis is the result of anisotropicity of the lattice and presented sulfathiazole as a counter example. An study of sulfathiazole revealed that it has four polymorphs of which only one exhibits NTE.[59] This led to an investigation of the relationship between polymorphism and NTE.

The aim of the investigation into polymorphism and NTE was to determine if NTE could be an indicator for polymorphism and whether one can determine the 'tipping' point between NTE and polymorphism. The same approach used in searching for NTE compounds from the CSD was employed to search for polymorphs. Various compounds were found that exhibit similar characteristics (size, geometry, etc.) to the compounds reported here. Unfortunately, no distinctive conclusion could be drawn from the preliminary results recovered from the CSD. Further investigation into the topic is ongoing.

This study has highlighted the need for an improved understanding of the influence of the packing arrangements on the physical properties of the material. The present state of crystal engineering is such that it remains difficult or impossible to predict structures.[60,61] The ability to reliably influence the function of a material by manipulating its structure is the next challenge in materials design. These research goals are still in their early

stages and it is therefore still necessary to retrospectively explain any peculiar behaviour discovered in new materials by studying underlying processes at the molecular level.[32] This concept is key in crystal engineering and it would be useful to be able to devise design strategies that lead to new functional devices. Many properties of materials are used in technological applications and most of these properties depend on the anisotropy of the materials. Therefore, thermal expansion provides a means of influencing anisotropy and the properties that then depend on anisotropy.[32]

The results from this study have shed some light on the requirements for NTE by determining some of the geometrical as well as structural requirements for NTE of organic compounds. However, the most noteworthy contribution made in this study is the identification of three more organic compounds that undergo negative thermal expansion.

References

1. J.-M. Lehn, *Pure Appl. Chem.*, 1978, **50**, 871-892.
2. D. V. Soldatov, I. S. Terekhova, *J. Struct. Chem.*, 2005, **46**, S1-S8.
3. J. W. Steed, J. L. Atwood, *Supramolecular Chemistry*, Sussex, 2000.
4. H.-J. Schneider, A Yatsimirsky, *Principles and Methods in Supramolecular Chemistry*, John Wiley & Sons, 2000.
5. J. D. Dunitz, *Pure Appl. Chem.*, 1991, 177.
6. C. B. Aakeröy, K. R. Seddon, *Chem. Soc. Rev.*, 1993, 397-407.
7. J.-M. Lehn, *Angew. Chem. Int. Ed.*, 1990, **27**, 1304.
8. J. Harrowfield, D. Matt, *J. Incl. Phenom.*, 2004, **50**, 133-150.
9. J.-M. Lehn, *Supramolecular Chemistry: Concepts and Perspectives*, Weinheim: VCH, 1995.
10. D. Braga, F. Grepioni, A.G Orpen, *Crystal Engineering: from Molecules and Crystals to Materials*, Kluwer Academic Publishers, Germany, 1999.
11. C. B. Aakeröy, *Acta Cryst. Sect. B*, 1997, **53**, 569-586.
12. G. R. Desiraju, *Angew. Chem. Int. Ed.*, 2007, **46**, 8342–8356.
13. G. R. Desiraju, *Angew. Chem. Int. Ed.*, 1995, **34**, 2311 - 2327.
14. G. R. Desiraju, *Crystal Engineering The Design of Organic Solids*, Elsevier, Amsterdam, 1989.
15. G. R. Desiraju, *The Hydrogen Bond*, Marcel Dekker, New York, 2004.
16. J.M. Dumas, L. Gomel, M. Guerin, *Interactions involving Organic Halides. In The Chemistry of Functional groups*, Wiley, New York, 1983.
17. F. J. Guthrie, *J. Chem. Soc.*, 1863, **16**, 239 - 244.
18. O. Hassel, *Science*, 1970, **170**, 497 - 502.
19. P. Metrangolo, G. Resnati, *Halogen Bonding*, Marcel Dekker, New York, 2004.
20. B. Sarma, L. Reddy, A. Nangia, *Cryst. Growth. Des.*, 2008, **8**, 4546-4552.
21. I. Dance, *π-π Interactions: Theory and Scope*, Marcel Dekker, New York, 2004.
22. J. S. O. Evans, *J. Chem. Soc., Dalton Trans.*, 1999, 3317–3326.
23. R. M. Hazen, C.T. Prewitt, *Am. Mineral.*, 1977, **62**, 309.
24. I.D. Brown, A. Dabkowski, A. McClearly, *Acta Cryst. Sect. B*, 1997, **53**, 750.
25. S. Haas, B. Batlogg, C. Besnard, M. Schiltz, C. Kloc, T. Siegrist, *Phys. Rev. B*, 2007, **76**, 1-5.
26. H. D. Young, R. A. Freedman, *University Physics*, Pearson Education, San Francisco, 2004.
27. A. L. Goodwin, *Nature*, 2010, **9**, 7-8.
28. H. Birkedal, D. Schwarzenbach, P. Pattison, *Angew. Chem. Int. Ed.*, 2002, **114**, 780-782.
29. T.A. Mary, J.S.O. Evans, T. Vogt, A.W. Sleight, *Science*, 1996, **90**, 272.
30. A.P. Ramirez, G.R. Kowach, *Phys. Rev. Lett.*, 1998, **80**, 4903.

31. G. K. White, C. L. Choy, *J. Polym. Sci. Polym. Phys. Edn.*, 1984, **22**, 835.
32. D. Das, T. Jacobs, L. J. Barbour, *Nature Mater.*, 2010, **9**, 36-39.
33. J. Bernstein, *Polymorphism in molecular Crystals*, Clarendon press, Oxford, 2002.
34. R. H. Blessing, *Acta Cryst. Sect A*, 1995, **51**, 33-38.
35. G. M. Sheldrick, *Acta Crystallogr. Sect A*, 2008, **64**, 112-122.
36. J. L. Atwood, L. J. Barbour, *Cryst. Growth. Des.*, 2003, **3**, 3-8.
37. L. J. Barbour, *J. Supramol. Chem.*, 2001, **1**, 189-191.
38. G. M. Sheldrick, *SHELX Manual*, **2010**.
39. F. H. Allen, *Acta Crystallogr. Sect B*, 2002, **58**, 380-388.
40. D. J. G. S.K Wolff, J.J. Mckinnon, D. Jayatilaka and M.A. Spackman, *Crystal Explorer 2.1*, University of Western Australia, Perth, 2007.
41. F. L. Hirshfeld, *Theor. Chim. Acta*, 1977, **44**, 129-138.
42. M. A. Spackman, D. Jayatilaka, *CrystEngComm*, 2009, **11**, 19-32.
43. J-F. Moulin, J. C. Kengne, R. Kshirsagar, M. Cavallini, F. Biscarini, S. Leon, F. Zerbetto, Gi. Bottari, D. A. Leigh, *J. Am. Chem. Soc.*, 2006, **128**, 526-532.
44. P. o. V. Team, *POV-Ray for Windows*, 2003-2004.
45. D. Schwarzenbach, S.C. Abrahams, H.D Flack, E. Prince, *Acta Cryst. Sect. A*, 1995, **51**, 565-569.
46. D. Britton, *Acta Cryst. Sect. E*, 2005, **61**, o187-o188.
47. J. McMurray, *Organic Chemistry*, 6 Edn., Thomson Books, Belmont, 2004.
48. S.C. Nyburg, C.H. Faerman, *Acta Cryst. Sect. B*, 1985, **41**, 274.
49. I. Csöregh, T. Brehmer, P. Bombicz, E. Weber, *Cryst. Eng.*, **4**, 343.
50. F. Zordan, L. Brammer, P. Sherwood, *J. Am. Chem. Soc.*, 2005, **127**, 5979-5989.
51. L. Brammer, E. A. Bruton, P. Sherwood, *Cryst. Growth. Des.*, 2001, **1**, 277.
52. F. van Bolhuis, P.B. Koster, T. Migchelsen, *Acta Cryst.*, 1967, **23**, 90.
53. C. L. Nygren, C. C. Wilson, J. F. C. Turner, *J. Phys. Chem. A*, 2005, **109**, 2586-2593.
54. F. H. Allen, W. D. C. Mortherwell, P. R. Raithby, G. P. Shields, R. Taylor, *New J. Chem*, 1995, 23-25.
55. O. V. Grineva, P. M. Zorky, E. S. Rostov, *Struct. Chem.*, 2007, **18**, 443-448.
56. D. Vujovic, L. R. Nassimbeni, *Cryst. Growth. Des.*, 2006, **6**, 1595-1597.
57. T. Threlfall, *Org. Process Res. Dev.*, 2003, **7**, 1017.
58. T. L. Threlfall, T. Gelbrich, *Cryst. Growth. Des.*, 2007, **7**, 2297.
59. T. N. Drebushchak, E. V. Boldyreva, M. A. Mikhailenko, *J. Struct. Chem.*, 2008, **49**, 84-94.
60. J. Maddox, *Nature*, 1988 **335**, 201.
61. J. D. Dunitz, *Chem. Commun.*, 2003, 545-548